Modelling the Mass and Energy Balance in a Compost Biofilter

A Thesis

Submitted in Fulfilment

of the Requirement for the Degree

of

Doctor of Philosophy in Chemical and Process Engineering

By

Milinda A. Ranasinghe

Department of Chemical and Process Engineering

University of Canterbury

March 2003

Biographical Details

Author: Milinda A. Ranasinghe

Undergraduate Studies:

Bachelor of Science in Chemical Engineering

University of Peradeniya, Sri Lanka

Postgraduate Studies:

Doctor of Philosophy in Chemical Engineering

University of Canterbury, Christchurch, New Zealand

Publications and Presentations:

Ranasinghe, M.A., Jordan, P.J., Gostomski, P.A. *Proceedings of the Air & Waste Management Association's 95th Annual Meeting & Exhibition,* Paper No 42108, Baltimore, MD, USA, 2002

Ranasinghe, M.A., and Gostomski, P.A. A Novel Reactor for Exploring the Effect of Water Content on Biofilter Degradation Rates, *Proceedings of the 2002 USC-TRG Conference on Biofiltration*, Newport Beach, CA, USA.

Ranasinghe, M.A., Jordan, P.J., Gostomski, P.A. Modelling the Mass and Energy Balance in a Compost Biofilter, poster presentation at the 9th APCHE Congress and CHEMECA 2002, 29th Sept- 3 Oct 2002, Christchurch, New Zealand.

Ranasinghe, M.A., and Gostomski, P.A. A Novel Reactor for Exploring the Effect of Water Content on Biofilter Degradation Rates, *Environmental Progress*, 22(2), 103, 2003.

This thesis is dedicated to my loving parents
Upali and Nanda Ranasinghe

Acknowledgements

I would like to express my sincere gratitude to my supervisor, Dr Peter Gostomski for his encouragement, motivation and guidance throughout this dissertation. The advice and knowledge imparted by Pete will always be remembered not only from a research perspective but also due to its pertinence in everyday life. I fervently hope that the academic and personal relationship that we built would be consolidated and extended as I pursue my Chemical Engineering career. My deepest appreciation also go out to my co-supervisor Dr Pat Jordan and to Dr Ken Morrison for providing time to discuss and clarify issues which greatly aided me in taking the research project in the right direction.

The moral support and valuable suggestions provided by my colleagues Nohemi Quispe Chavez, Nataliya, and Senti will be deeply admired. In particular, Nohemis' friendship in times of despair and happiness will be greatly treasured in times to come. I would also like to acknowledge the excellent technical assistance of Ron Boyce, Paul Tolson, David Brown, Bob Gordon and Warwick Earl for their valuable and timely assistance with the experimental set-up. Many thanks go out to Tony Allen for the hardware and software support. The keen enthusiasm and the excellent workmanship displayed by Paul Tolson in fabricating the experimental apparatus are immensely appreciated. The wealth of practical knowledge imparted by David Brown during informal discussions will always be valued and remembered. Particular mention is also made of Trevor Berry, whose patient explanations and assistance in time of need made the operation of the GC and other analytical apparatus very simple and uncomplicated. Also the assistance of Lene Steffensen from Ingeniørhøjskolen Odense Teknikum for her extensive and careful data collection is gratefully acknowledged.

The financial assistance provided by the Foundation for Research Science and Technology (FRST), New Zealand, under a Bright Future Doctoral Scholarship is gratefully acknowledged without which this work would not have materialised.

Finally and most importantly, I would like to thank my mom, dad and sister for being patient and providing a supporting role. If not for the love and encouragement of my family, this work would never have been successfully completed.

Table of Contents

List of Tables

List of Figures

Nomenclature

A	Fitting parameter
C	Gas phase concentration of the contaminant, g/m^3
C_i	Inlet gas phase concentration, g/m^3
C_o	Outlet gas phase concentration, g/m^3
C_p	Gas phase concentration within the pores, g/m^3
C_{pa}	Specific heat capacity of air, J/g K
C_{pb}	Specific heat capacity of the bed, J/g K
C_{pl}	Specific heat capacity of liquid water, J/g K
C_{ps}	Specific heat capacity of compost, J/g K
C_{pv}	Specific heat capacity of water vapour, J/g K
D_c	Micropore diffusivity, m^2/s
D_e	Effective diffusivity, m^2/s
D_{lT}	Diffusivity of toluene in the biofilm, m^2/s
D_m	Molecular diffusion of a binary mixture, m^2/s
D_p	Macropore diffusivity, m^2/s
E	Rate of evaporation, g water/m^{3}s
$g(s)$	Transfer function
h	Soil water pressure (tension), cm
h_c	Heat of combustion of toluene, J/g
h_e	Latent heat of vaporisation, J/g
K	Unsaturated hydraulic conductivity, cm/s
K_a	Thermal conductivity of air, W/m K
K_C	PI Controller gain, cm/g s or m^{3}cm/m^{3}s
K_{eff}	Effective thermal conductivity of bed, W/m K
K_{eqm}	Equilibrium adsorption coefficient, g of toluene/ (m^3 of compost) (g/m^3)
k_f	External film mass transfer resistance, m/s
K_g	Thermal conductivity of gas phase, W/m K
k_l	Liquid permeability, cm/s
K_l	Thermal conductivity of water, W/m K
K_{LDF}	Linear driving mass transfer coefficient into solid phase, 1/s
K_m	Half saturation constant, g/m^3
K_N	Half saturation constant in the Monod model for nutrient, g/m^3

k_0	Equilibrium coefficient at base case
K_p	First order gain, g s/cm or m^3s/m^3cm
k_{rl}	Relative conductivity of wetting phase
k_{rnl}	Relative conductivity of non-wetting phase
K_s	Thermal conductivity of compost, W/m K
K_S	Half saturation constant in the Monod model for substrate, g/m^3
K_{sat}	Saturated hydraulic conductivity, cm/s
K_{Tol}	Production of water from metabolism, g/g
K_v	Thermal conductivity of vapour, W/m K
L	Length of the biofilter column, cm
mX	Maintenance coefficient, g substrate/(m^3 compost)(s)
M	Saturated vapour concentration, g/m^3
M_f	Moisture Content Factor
M_w	Molecular weight of water g/mol
N	Nutrient concentration, g/m^3
P_s	Saturated vapour concentration, kPa
q	Solid phase concentration of contaminant, g/m^3compost
$q_{surface}$	Surface flux, cm/s
r	Rate of biodegradation in the biofilm, g substrate/(m^3biofilm)(s)
R	Universal gas constant, J/mol K
r_c	Microparticle radius, m
R_p	Particle radius, m
S	Substrate concentration, g/m^3
S_g	Fraction of the void volume occupied by the gas phase, m^3/m^3
S_w	Fraction of the void volume occupied by water, m^3/m^3
t	Time, s
T	Temperature within the biofilter, K
T_a	Temperature of inlet air, K
T_f	Temperature Factor
T_i	Initial temperature within the bed, K
U_l	Liquid velocity, m/s
U_g	Interstitial gas velocity, m/s

V Filter bed volume, m^3

V_m Maximum degradation rate, g substrate/(m^3 compost)(s)

X Biomass density, g dry cell/m^3 biofilm

Y Yield coefficient, g dry cells/g substrate

z Axial distance from gas inlet, m

Superscripts

* Equilibrium

Subscripts

a Atmospheric

f Factor

g Gas phase

i Spatial location

j Location in the time domain

l Liquid phase

m Fitting parameter for Eq. 3.28

n Fitting parameter for Eq. 3.28

p Particle

v Water vapour

Greek Letters

α, β, γ Fitting parameters for Eq. 3.31 & 3.32

ΔH Activation energy, J/mol

ε Porosity

θ Volumetric water content, m^3/m^3

θ_s Saturated volumetric water content, m^3/m^3

θ_r Residual volumetric water content, m^3/m^3

μ Specific growth rate, 1/s

μ_{max} Maximum growth rate, 1/s

ρ_b Density of bed, g/m^3

ρ_s	Density of wet compost, g/m^3
ρ_l	Density of liquid water, g/m^3
ρ_v	Density of air, g/m^3
τ	Tortuosity factor
τ_l	Reset time, s
τ_c	Time constant, s
Θ	Non - dimensional water content

Abstract

A biofilter model was developed using the mass and energy balances in the gas, liquid and solid phases, which related the biofilter performance to the water content in the packing material. A key simplification of the model was that the concentration gradients in the biofilm were neglected by treating the biofilm/water layer as well mixed and in instantaneous equilibrium with the gas phase. Thus, the biofilm geometry and density parameters were lumped into the overall degradation term. The solid phase was treated as a separate well-mixed layer but solid phase dynamics were accounted for by using the Linear Driving Force (LDF) mass transfer model. The mixed form of Richard's equation together with experimentally obtained unsaturated hydraulic conductivity and water retention curves for compost were used in the continuity equation for the liquid water phase. This approach produced a model where all parameters could be potentially independently determined.

The model was used to test suitable irrigation strategies for a biofilter system degrading toluene subject to different operational conditions. Under this approach both uni-directional and directionally switched biofilter configurations were tested for a 1 m long column. The unidirectional schemes incorporated both open and closed loop irrigation schemes, where the latter was based on commonly used on-line moisture measurement techniques. All schemes were evaluated based on the removal efficiency achieved and the leachate produced. Simulations under a constant irrigation rate of 5.46×10^{-2} g/m^{2}s for a mass loading range of 13-60 g/m^{3}h yielded removals ranging from 88%-26%. An order of magnitude drop in leachate under the high loading indicated severe drying in the system. For a high mass loading of 60 g/m^{3}h, directional switching with a one-day frequency yielded a removal of 33% Vs 26% in an upflow scheme with similar leachate rates. Feedback control on water content provided an improved removal of 84% as compared to 73% under constant irrigation, when both schemes were subjected to load and inlet air step disturbances from 13 g/m^{3}h to 62 g/m^{3}h and from 298 K to 283 K respectively. A sensitivity analysis indicated that the model was most sensitive to the relationship between moisture content and degradation, which was also reflected by the high sensitivity of the model to the kinetic parameters in the degradation term.

A novel batch recycle reactor was thus developed to investigate the effect of water content changes on the degradation rate in low water content systems such as biofilters. The reactor tightly controlled the water content of the unsaturated packing material by using the principle of a suction cell. Experimental runs were performed with toluene as the contaminant using unamended compost at a constant temperature of 30 °C. Matric potential in the compost was maintained at values between -6 and -36 cm H_2O and the gas phase was monitored by sampling/gas chromatography. A soil water retention curve relating matric potential to gravimetric water content was generated for the compost. Periodic dry weight analyses of reactor samples together with the water retention curve verified moisture content control. Degradation results demonstrated a biologically limited region followed by a non-linear region at lower concentrations. Elimination capacities were obtained along the wetting and drying curves and changes in the water content affected the removal rates in the linear region ranging from 155 g/m^3h to 24 g/m^3h over the matric potential range investigated. Repeatability studies indicated that moisture content was the most likely parameter that influenced the changes in performance. Batch scale experiments were also performed using microbially inhibited compost, which provided linear sorption isotherms for toluene on compost at concentrations between 0-1000 ppm_v and temperature values of 25 °C and 35 °C.

The simulation model developed here provides a useful tool to implement and evaluate various operational schemes under different irrigation strategies. This is achieved by way of greater flexibility in incorporating the various schemes into the base model and the comparatively low simulation time to obtain the relevant results.

Chapter 1: Gas Phase Biofiltration

1.1 Introduction

Biofiltration is a relatively modern technique for the elimination of low concentrations of volatile organic compounds (VOC) & Hazardous Air Pollutants (HAP) present in waste gas streams. Though originating from Europe, biofiltration has over the years found widespread applications in many fields and markets due to its cost effective nature in treating waste gas flows. Furthermore, this technology has evolved from rudimentary soil bed systems treating odours from sewage treatment plants to complex, enclosed multi storey systems treating toxics from a variety of industrial sources (Leson & Winer, 1991). The driving force for the rapid growth and development of gas phase biofilters could be primarily attributed to the high capital costs associated with meeting stringent air pollution legislation using conventional technology. Greater awareness of the detailed processes involved through diversified research has also created a favourable atmosphere for biofiltration (Devinny *et al.*, 1999).

The success of biofilters has predominantly centred on the ability to treat low concentrations ($\leq$ 1,000 ppm_v) of volatile organic compounds (VOC) present in high gas flow streams (1,000-50,000 m^3/h) by way of low operating cost and minimal by-products. The low pressure drop and the high removal efficiency attained for most compounds make this a very appealing technique. Research at various levels, complemented with mathematical modelling, has greatly revealed the intricate details of the various mechanisms involved in biofilter operation and has given this field an added impetus. Though various alternative technologies such as incineration, adsorption and wet scrubbing have been developed for waste gas elimination, their operational and capital costs are dependent on the relevant processing requirement. Furthermore, the potential for by-product formation under conventional waste gas control techniques has also promoted biofiltration as an eco-friendly yet successful way of treating VOCs.

1.2 Comparison with Other Technology

Biofiltration over the years has successfully competed with the more conventional waste gas elimination techniques mainly by way of low operating costs, smaller pressure drops and minimal by-products. According to Devinny *et al.* (1999), there is no universal waste gas treatment technology that could effectively and economically be applied to all commercial applications. Thus, in commercial applications, prior to selection the economic viability of available waste gas treatment schemes is assessed by way of a cost analysis (Leson and Winer, 1991). As seen in Fig. 1.1 techniques such as incineration, scrubbing and condensation are more suitable for handling high VOC concentrations, but suffer from various drawbacks, such as the production of nitrogen oxide during incineration and the generation of large quantities of wastewater.

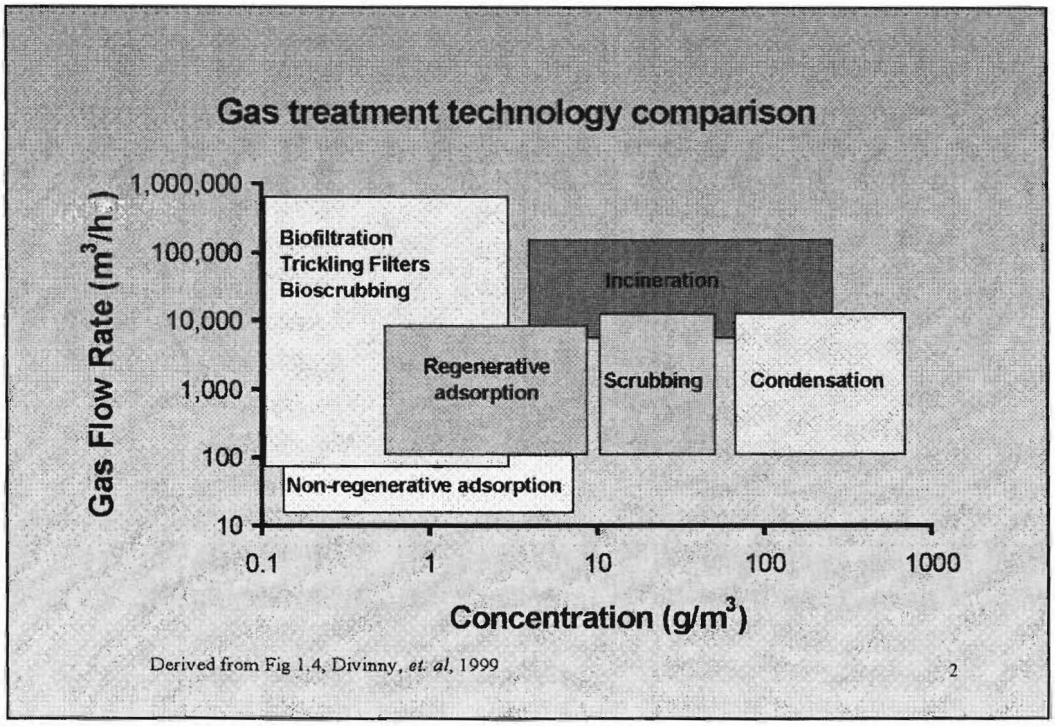

Figure 1.1 Comparison of various air pollution control technologies

The removal of VOC contaminants, through adsorption onto fixed or fluidised beds consisting of material such as Granular activated carbon (GAC) and Zeolite, has met with success in the past, particularly with VOCs with low vapour pressure and high molecular weights. However, the major drawback of this technique is the need to dispose of the bed material once it has reached saturation and this is aggravated due to the hazardous nature of the bed at this stage. Although an alternative to the above would be the regeneration of

the bed through desorption, using dry air or steam, the economic viability of this technique depends on whether the pollutant has recovery value and the free availability of steam.

1.3 Contaminants Treated and Industrial Applications

1.3.1 Global Applications

In a global context, biofilter applications fall into three main categories: odour treatment; VOC/HAP control; and the treatment of petroleum hydrocarbons. According to Devinny *et al.* (1999) odour control occupies a significant portion of biofilter usage, while treatment of VOCs from process industries and contaminated soil sites is gaining popularity. The contaminant subjected to biofiltration should be biodegradable and non-toxic (Swanson and Loehr, 1997) and greater removal could be obtained from organic compounds with low molecular weight and high solubility. Thus, alcohols, ketones, aldehydes and monocyclic aromatics have been successfully treated, while moderate to low removal are exhibited for chlorinated hydrocarbons and phenols (Leson and Winer, 1991). Commercial industries that use biofiltration are given in Table 1.1.

Table 1.1 Examples of successful biofiltration in Europe (Leson and Winer, 1991)

Adhesive production	Coffee roasting	Industrial wastewater treatment plants
Coating operation	Cocoa roasting	Residential wastewater treatment plants
Chemical manufacturing	Fish frying	Composting facilities
Chemical storage	Fish rendering	Landfill extraction
Film coating	Flavours and fragrances	Waste oil recycling
Investment foundries	Pet food manufacturing	Print shops

1.3.2 Biofilter Applications in New Zealand

In New Zealand, the application of biofiltration has predominantly focused on odour control. Preference for this technique has primarily been due to the high capital and operating costs associated with the more conventional odour control technology (Archer and Fullerton, 1992). Compost/soil based biofilters have successfully been applied in the treatment of odorous air (sulphides) from trickling filters used in municipal wastewater treatment plants. Biofiltration has also been utilised in meat rendering plants to treat off gas odour concentrations up to 1×10^6 OU m^{-3}, containing both organic and inorganic compounds (Luo and van Oostrom, 1997). Literature (Gostomski, 2000) indicates a gradual diversification of the industries utilising biofiltration for odour control. Enactment of legislation governing air pollution, such as the Resource Management Act (1991), could also result in more industries embracing biofiltration as an efficient yet cost effective, air pollution control technology.

1.4 Description of the Mechanism Involved

Biofilters normally consist of either organic (compost, peat) or inorganic (soil) porous media, which are conducive for the growth and attachment of the microorganisms. The microorganisms normally thrive in a biofilm (Fig 1.2) or in the liquid phase surrounding the porous media under favourable conditions.

These systems are also defined as fixed film bioreactors due to the very nature of the biofilm attachment onto the solid phase. Thus, contaminants from a humidified waste gas stream are simultaneously adsorbed/absorbed and biodegraded in a biofilter (Luo & Van Oostrom, 1998). The absorbed contaminant diffuses through an acclimated consortium of microorganisms, where degradation as a primary or cosubstrate maintains concentration gradients in the biofilm (Swanson & Loehr, 1997). The absorbed phase contaminant is subjected to adsorption onto the biofilm, organic matter and the solid surface.

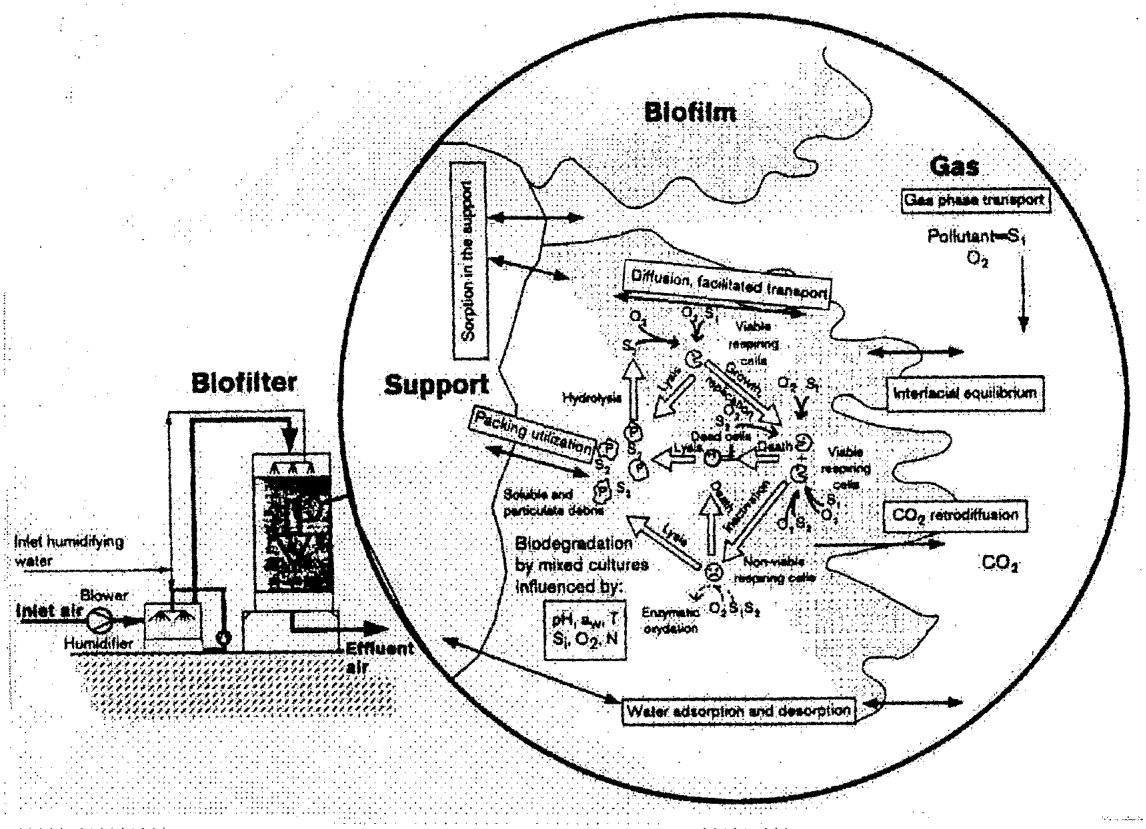

Figure 1.2 The biofiltration principle, the fate of pollutants and the physiological states of the process culture (From Deshusses, 1997)

Adsorption has been identified as the predominant form of contaminant removal at the initial stages of biofilter operation (Devinny & Hodge, 1995). This process is credited with reduced contaminant release during microbial acclimation. Biofilters often operate under transient conditions due to the fluctuating VOC emissions and intermittent operations and the adsorption capacity of the packing material acts as a buffer to attenuate the shock loadings (Baltzis & Androutsopoulou, 1994). The adsorption capacity of the media can be affected by external factors such as water and polymeric material present in the biofilm. The sorbed contaminant provides the necessary carbon and energy for microbial activities. The removal efficiency of a biofilter is either mass transfer (diffusion) or biologically limited, and depends on many factors, such as concentration, nature of the compound treated and biofilm characteristics.

1.5 Objectives of Research

The overall objective of this study is to develop a biofilter model to investigate the relationship between performance and the water content of the packing material. The governing equations developed are based on the mass and energy balances in the gas, liquid and solid phases. A number of assumptions are introduced in reflection of the model goals, ease of numerical solution and eventual experimental verification.

The compound selected for modelling purposes is toluene. This contaminant is highly volatile, hydrophobic and is a major constituent in automobile gasoline while also being used in substantial quantities as a feed material in process industries (Elmirini *et al.*, 2001; Hwang and Tang, 1997). Owing to its low solubility, toluene has become a source of concern with regard to subsurface soil and groundwater contamination, which has generated significant interest in the area of soil vapour extraction (SVE) of non-aqueous phase liquids (NAPL) (Wilkins *et al.*, 1995; van der Ham *et al.*, 1998; Sleep *et al.*, 1989)

In addressing the key objective, irrigation control strategies encompassing open and closed irrigation are implemented using the model for a variety of operating conditions, and evaluated based on removal efficiency and leachate produced. In the above exercise a sensitivity analysis on model parameters is also performed to explore the effect of assumptions made with regard to parameter estimation. A novel batch recycle reactor is also developed in this study and is used to investigate the effect of water content changes on the degradation rate in low water content systems such as biofilters. The adsorption isotherms of toluene on compost and their temperature dependence are also ascertained during this study using batch scale experiments.

Chapter 2: Literature Review

2.1 Biofilter Configurations

Biofilter systems originated as single bed open systems as depicted in Fig 2.1 (Leson and Winer, 1991). An excellent description of the different systems available and their relative merits/demerits is available in Swanson and Loehr (1997). Pre-treatment processes are carried out primarily to ensure optimal microbial activity and to prevent excessive moisture loss from media. Supplementary operations on the off-gases include removal of particulate matter (oils, fats), temperature regulation and pre-humidification. Biofilter systems may be operated as top or bottom loaded where the former scheme is deemed to be favourable for moisture control under high loading and also for facilitating a better drainage. Upward flow is suitable in the treatment of compounds, which produce acidic by-products, where pH drop in the active lower regions could be avoided using irrigation without affecting the pH of the entire bed (Devinny *et al.*, 1999). The above configurations could also vary, depending on whether the air distribution is performed as forced or induced draft.

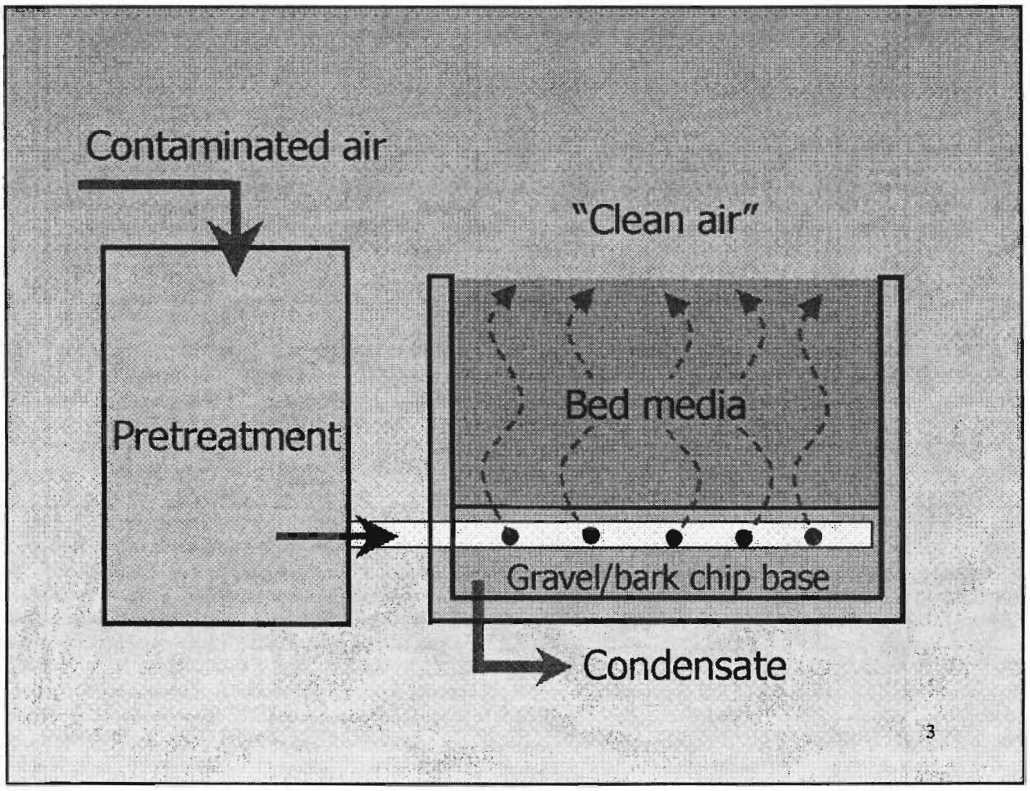

Figure 2.1 A typical forced draft upflow biofilter system

2.2 Internal Structure of a Biofilter

The following discussion focuses on some of the fundamental internal components (phases) of an air phase biofilter.

2.2.1 Water Phase

Biofilters may contain a standing water film outside the periphery of the biofilm, provided a net increase in the water content occurs. The water film could host a mobile array of microorganisms (Devinny *et al.*, 1999) and is normally regarded as stationary (Gostomski *et al.*, 1997). However, the exception to this could occur due to irrigation or condensation, where field capacity would have been reached, resulting in drainage. Experimental work performed by Hon (1999) had indicated smaller hydraulic conductivity in compost as compared to various sand types, which was subsequently attributed to the presence of larger pores and poor connectivity in the former medium. The transport mechanism would thus incorporate both a laminar liquid flow and a diffusional mass transfer of contaminant through the liquid layer.

2.2.2 Biofilm

Successful biofilter design/operation would be greatly enhanced by understanding the intricacies of the biofilm structure. Biofilms, by nature, host a thriving community of organisms (bacteria, fungi and actinomycete) that facilitate an efficient biodegradation process. The microbial ecosystem may also consist of protozoa, which effectively engage in a predatory role using processes such as phagocytosis. A common occurrence would be axial stratification of the heterotrophic microorganisms due to the disparity in the gas phase concentration along the column height (Devinny *et al.*, 1999). From a microbial perspective compost is preferred due to the indigenous consortium of microorganisms present (Cardenas-Gonzales *et al.*, 1999). Inoculating with a species grown on the target pollutant could minimise the acclimation time (Leson and Winer, 1991), although success may be temporary due to competition from native organisms (Bohn, 1992). Acclimation time in literature is defined as the time taken to reach 95% of maximum removal and the relative importance of it with respect to initial and restart is clearly stated in Swanson and Loehr (1997). Cellular acclimation has been defined as a process, whereby enzymes are synthesized through a complex interaction among the genes, Ribonucleic acids (RNA) and proteins. Experimental work performed by Webster *et al.* (1997) using compost and GAC biofilters for the treatment of hydrogen sulphide, indicated a gradual acclimation of

the microbial community to low pH conditions, which was depicted as stable populations under PLFA (phospholipids fatty acids) analysis of the ecosystems.

From a structural aspect, the biofilm geometry has been subjected to many studies. However, in Devinny *et al.* (1999) the biofilm has been defined as a uniform layer of cells enclosed in a polysaccharide gel, which is predominantly water. The biofilm could also consist of entwining channels that could conduct water. The water within the polysaccharide gel (in the periphery of the cell) would normally be regarded as stationary (de Beer *et al.*, 1994) and molecular diffusion advocated as the mass transfer mechanism. The planar one-dimensional biofilm concept used in modelling has been subjected to criticism (de Beer *et al.*, 1994), as experimental work had indicated that the biofilm geometry for fixed film reactors consists of cell clusters and interstitial voids (Fig 2.2). This was confirmed by confocal scanning laser microscopy, which indicated the existence of cell clusters of 300 μm diameter and pores (voids) of 20 - 40 μm in diameter. Thus, results from this work indicated that substrate transport to the biofilm was facilitated through the bulk phase and from the array of pores extending to the substratum (solid phase).

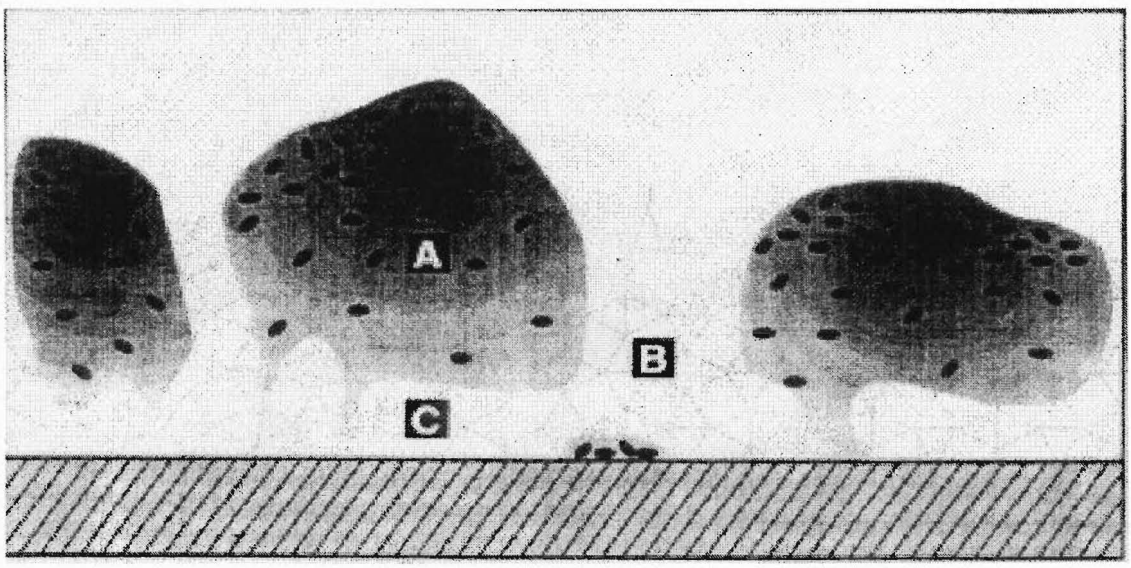

Figure 2.2 Conceptual model of biolfilm: (A) cell cluster, (B) pore, (C) conduit (From Debeer *et al.*, 1994)

2.2.3 Biofilter Packing Material

The selection of a suitable bed medium plays a pivotal role in the performance and operational cost of a biofilter system. The rapid growth in biofiltration has seen the use of both synthetic and organic material as bed media with varying success. The need for superior forms of packing stems from the need to attain higher removal efficiencies, which in turn is affected by crucial media characteristics such as water retention, specific surface area and internal pore structure. Typical biofilter media consist of organic material, inert bulking material, pH buffer and mineral salts, while the low cost media primarily consist of soil. Media properties expected from a packing material have been stated by Swanson and Loehr (1997) as follows:

- Optimal microbial environment.
- Large specific surface area.
- Structural integrity.
- High moisture retention.
- High porosity.
- Low bulk density.

Literature (Devinny *et al.*, 1999; Swanson and Loehr, 1997; Leson and Winer, 1991) indicates the widespread use of compost as a packing material in most air phase biofiltration processes. The high demand for compost occurs mainly due to its low cost and also due to the presence of an indigenous microbial consortium, which avoids the need for inoculation. Furthermore, the neutral pH and good water retention has made compost more attractive than other forms of packing material. However, compaction resulting from consolidation tends to increase the pressure drop and as a result various bulking agents need to be added to counteract this phenomenon. Peat is an alternative organic material but due to its hydrophobic (if dried), acidic nature is rarely used alone as a packing material, but is used in conjunction with other bulking agents (Devinny *et al.*, 1999). The need to inoculate a peat bed and the necessity to add nutrients also are a drawback to the extensive use of this material.

Soil is another common bed material which is relatively inexpensive and yet contains numerous microbes. Also, its potential to rehydrate as compared to organic media which display irreversible drying in the absence of sufficient irrigation is a plus factor in selecting soil. However, its low permeability can cause potential problems with regard to

channelling of the gas stream and loss of removal efficiency (Devinny *et al.*, 1999). Soil beds are therefore operated at high gas residence time in the treatment of slowly degrading compounds (Bohn, 1992).

Mineralization of organic mediums and the resulting bed compaction, severely affects the efficiency of a biofilter. Hence, organic media are normally supplemented with inert bulking agents that facilitate an increase in the useful life of the medium (Swanson and Loehr, 1997). Typical amendments added are wood chips, bark, polystyrene and GAC. Another type of bulking agent that is commonly used due to its ability to reduce the pressure drop and channelling is chaff (Tang *et al.*, 1996). In addition to improving the porosity and reducing pressure drop and compaction, these bulking materials also perform secondary tasks such as increasing the adsorptive capacity and pH buffering.

2.3 Moisture in Biofilters

2.3.1 Introduction

A major setback to successful biofilter operation is the inability to maintain the media water content at desired levels. According to Bohn (1992), with proper maintenance of water content, removal efficiencies in the range of 99-100% are possible. Moisture content has been singled out as the most important and sensitive parameter in biofilter operation (van Lith *et al.*, 1997). Water content in the media is significant as the microbial consortiums populating a biofilter bed depend on moisture for their metabolic activity. According to Bohn *et al.* (1999), organic media moisture content of 50-60% wet basis provides good performance. This corresponds to a water activity of 0.94-0.97 that is required by the common type of microorganisms found in a biofilter e.g. *Pseudomonas fluorescenes, Aerobacter aerogenes* etc (Cox *et al.*, 1996; Devinny *et al.*, 1999). Moist organic media tend to exhibit increased sorption capacity with respect to hydrophilic compounds (Hodge and Devinny, 1997; Leson and Winer, 1991), which has subsequently been attributed to increased partitioning of these compounds due to their greater water solubility.

Excess moisture in the medium causes:

- Increased pressure drops and reduced retention times due to the filling up of pore space by water.
- Reduced air/water interfacial area and the formation of anaerobic zones. Odour (hydrogen sulphide) emissions and poor performance could occur as a result.
- Loss of valuable nutrients and microbial species as leachate.
- The incurring of high costs in disposing the leachate produced.

A bed medium that is too dry causes:

- Retardation of microbial activity. The lack of moisture would hinder the formation of a wet 'biofilm' and thereby limit microbial growth (van Lith *et al.*, 1997).
- Bed contraction and subsequent channelling of gas due to the formation of cracks. The resulting low residence times could cause a loss of efficiency.
- Irreversible drying of hydrophobic media. Humidification and subsequent water addition does not rejuvenate the bed, but promotes channel formation (Cardenas-Gonzalez *et al.*, 1999).

Thus, it is imperative that the correct water content be maintained at all possible times to ensure suitable performance. Review papers indicate a wide range of optimum values for the moisture content, although the actual value would depend on media composition and physical characteristics of the compound treated (van Lith *et al.*, 1997). A moisture content of 40-60% wet weight was recommended by Leson & Winer (1991), while Pinnette (1995) indicated a moisture content below 40% wet weight as detrimental to performance. Based on practical experience, van Lith *et al.* (1997) recommended that the moisture content should be maintained around 40% wet weight for compact, poorly drained soils and at 60% wet weight for lighter, highly porous media.

2.3.2 The Difficulty in Controlling Moisture Content

Very few investigative studies have ascertained the mechanisms of water content change and the techniques available to counter this phenomenon. Influence of water content on the degradation of specific compounds has been observed in lab scale work. Microcosm experiments performed by Acuna *et al.* (1999) for toluene degradation in a peat medium indicated reduced degradation at low water contents, although a water activity sufficient to maintain the metabolism was said to prevail. A decrease in ethanol elimination capacity in a peat medium was observed by Auria *et al.* (1998) at low water contents and was attributed to the poor absorption capacity of the material together with low water activity at reduced moisture content. Experiments performed by Govind *et al.*(1993) for isopentane degradation on compost indicated an irreversible decline in performance below a water content of 0.58 g/g dry weight and a drop in removal efficiency for moisture contents above optimal values of 0.65 g/g dry weight. Furthermore, the recovery process of compost from a dried-out condition was also monitored experimentally by Yang and Allen, (1994) and Cardenas-Gonzalez *et al.* (1999).

A thorough analysis of the thermodynamics of biofilters by van Lith *et al.* (1997) identified five mechanisms for moisture content change. Moisture loss was dependent on factors such as contaminant loading, off gas temperature and external conditions, with rapid bed dry out possible at concentrations greater than 0.5 g/m^3 and at elimination capacities greater than 50 g/m^3h. Gostomski *et al.* (1997) carried out a mass and energy balance to identify three mechanisms for water content change and experimentally showed that microbial heat generation could cause drying and loss of activity in a pilot-scale compost biofilter treating toluene. Experiments by Cox *et al.* (1996) verified the presence of a water content gradient in a perlite medium treating styrene and also highlighted the influence of humidity and water content on microbial degradation.

Moisture loss mechanisms, which tend to complicate the maintenance of moisture, are:

- **Non-Saturated Air at Inlet**

  Unsaturated off gases, while propagating through the bed, tend to remove moisture until equilibrium between the two phases is reached (van Lith *et al.*, 1997). Experimental work by Cox *et al.* (1996) indicated that inlet air humidity had a significant influence on performance and the resulting drying fronts. This work complemented the work performed by Gostomski *et al.* (1997), who also observed moisture stripping by inlet air even at high inlet humidity.

- **Microbial Heat Generation**

  The exothermic metabolic activity of the microbial consortiums present in a biofilter generates heat. The heat released is compound specific and quite substantial in certain instances (Devinny *et al.*, 1999; van Lith *et al.*, 1997). Gostomski *et al.* (1997) and Strieberg *et al.* (2001) observed moving waves of degradation in biofilter beds, due to the evaporative moisture loss from consecutive sections of the bed, which eventually retarded activity throughout the bed.

- **Redistribution**

  Experimental work of Cox *et al.* (1996) indicated an uneven distribution of the water content which was attributed to the presence of different mechanisms. The resulting water potential gradient effectively initiated a water flow in the unsaturated media, as governed by Darcy's law. Moisture distribution by capillary gradients would influence the effects of other moisture loss mechanisms (Gostomski *et al.*, 1997). The importance of this mechanism would be seen during the addition of water to counter microbial drying and when manipulating the overall water content. The hydraulic gradient and the unsaturated hydraulic conductivity form the driving force for this mechanism. Experimental observations by Hon (1999) indicated that the unsaturated hydraulic conductivity of compost was of an order of magnitude lower than that of soil. These findings effectively nullified the common assumption of rapid redistribution of moisture in compost.

- **Media Degradation and Heat Loss to the Surroundings**

  Biofilters transfer heat with the surroundings, which causes temperature differences between the off gas and bed material, and results in moisture transfer (van Lith *et al.*, 1997). Gostomski *et al.*, (1997) experimentally indicated the existence of radial temperature gradients, which facilitated the evaporation of water from the active centralised parts of the reactor and caused condensation at the walls. Heat exchange with the environment tends to be greater in small-scale, poorly insulated biofilters as these would be easily susceptible to sudden changes in ambient conditions. Media degradation was identified as a source of moisture loss, although on a relative basis it was shown to be of low significance. The evaporative losses associated with this exothermic bio-reaction was said to depend on factors such as media composition, age and bed temperature.

2.3.3 Methods of Control

Numerous biofilter researchers have highlighted the maintenance of proper bed moisture as a key to successful performance over a sustained period of time. As discussed in the preceding section, the presence of moisture loss mechanisms tend to add some complexity to the process of maintaining appropriate bed moisture. Thus, any feasible technique should incorporate both monitoring and controlling of moisture content. Techniques available for moisture control are:

a) Pre Humidification

Industrial bioreactors commonly use humidification chambers located before the blower to prevent rapid bed dry out. Swanson and Loehr (1997) described various humidification designs where the selection of an appropriate type would depend on the location and cost (Devinny *et al.*, 1999). However, prehumidification would only minimise the rate of drying and hence supplementary irrigation schemes need to be implemented.

b) Direct Irrigation

Irrigation systems commonly use a variety of systems such as overhead sprinklers, soaker hoses or pressure compensated irrigation hoses (Devinny *et al.*, 1999). An effective irrigation system would require periodic monitoring and control, the accuracy of which would need to increase with the contaminant load (van Lith *et al.*, 1997). Monitoring of bed moisture content was categorised into two sections, namely automatic and manual, by van Lith *et al.* (1997) and four common monitoring and controlling strategies discussed. The suitability of the various techniques was dependent on the degree of moisture loss and level of maintenance performed. A similar classification and the relative merits/demerits of the systems currently available, was provided in Devinny *et al.* (1999).

2.4 Temperature

Biofilters consist of microbial consortiums, and hence, long-term temperature effects on the ecosystem would be quite different as compared to a single species environment (Devinny *et al.*, 1999). Owing to the diversified structure, the microbial ecosystem tends to be more resilient to temperature variations, which is indicated by the rapid recovery exhibited (Leson and Winer, 1991). According to Pinnette *et al.* (1995) biofilter operations rely on mesophilic temperatures (25-35 °C) due to the prevalent high microbial diversity. Increased temperature would result in lower solubility/sorption capacity in the medium (Bohn, 1992), which could have an adverse impact on performance. The most common type of temperature control arises from the need to cool off-gases entering at high temperature. While humidification would indirectly aid this process, an accurate control over the final temperature attained is not possible. Thus, this reduction in off-gas temperature could be facilitated through the use of heat exchangers or by dilution with ambient air to reach the desired entry temperature. The selection of the latter technique would ultimately depend on whether the cost of installing a heat exchanger exceeds the cost associated with the extra medium required to ensure a low empty bed residence time (EBRT) with diluted air (Swanson and Loeher, 1997)

2.5 Biofilter Terminology

2.5.1 Empty Bed Residence Time (EBRT)

In literature EBRT has been defined as the ratio between empty bed filter volume and the volumetric airflow.

EBRT= Volume of biofilter bed/Air flow rate [Eq. 2.1]

The EBRT tends to overestimate the actual residence time, as the pore volume available for airflow is significantly reduced, due to a substantial fraction of the bed volume being occupied by the packing material. Hence, the true residence time would reflect the actual volume available within the filter bed for airflow and provide a realistic quantification of the residence time. The impact of the above parameter on biofilter performance is that a high residence time correlates to a higher removal efficiency, but is not always feasible as this would amount to a larger filter bed and hence higher start-up costs. Typical values for EBRT in biofilter operation tend to vary between 15 s to 1 min for high VOC concentration (Swanson and Loeher, 1997).

2.5.2 Surface/Mass Loading

Surface loading reflects the volume of air being treated per unit area of filter material. Normalisation of the above parameter facilitates the comparison between different biofilters. High surface loads characterise higher flows, shorter EBRT, low removal efficiency and are restricted due to the potential of drying (Swanson and Loehr, 1997). The pressure drop associated with high surface loading could also impose a limitation on the volume of air to be treated, although loads as high as 500 m^3/m^2h were used for optimised filter material mixtures (Leson and Winer, 1991). Typical values for surface loading range from 50-200 m^3/m^2h.

Mass loading is defined as the mass of contaminant applied to the biofilter per unit volume of filter material. Owing to the plug flow nature of the bioreactor, the contaminants tend to decrease in the axial direction and the mass loading reduces accordingly along the length of column. Furthermore, as it is a function of both the concentration and volumetric flow rate, bioreactor performance could vary for identical mass loadings (Swanson and Loeher, 1997).

2.5.3 Removal Efficiency/Elimination Capacity

Removal efficiency and elimination capacity are indicators of performance within a biofilter system. The removal efficiency (RE) indicates the fraction of contaminant removed, while elimination capacity (EC) represents the contaminant removed, per unit volume of filter bed per unit time. These parameters are of vital importance as the optimisation of these should be the final objective of any design/operation strategy to meet increasingly stringent regulatory requirements.

$$RE = \left(\frac{C_i - C_o}{C_i} \right) \times 100\% \qquad \text{[Eq. 2.2]}$$

$$EC = \left(\frac{C_i - C_o}{V} \right) \times Q \qquad \text{[Eq.2.3]}$$

Literature indicated a high RE in the range of 95-99% with respect to aromatic compounds. Although RE is a very convenient indicator of performance, the major drawback of this parameter is its variation with inlet concentration, air flow and biofilter volume. Thus, in order to make realistic comparisons between two different systems the normalised approach of EC is used. EC tends to vary with concentration, EBRT and mass loading, while typical values for EC range from 10-300 g/m^{3}h (Devinny *et al.*, 1999)

2.6 Past Studies on Biofilter Modelling

2.6.1 Introduction

Biofilters have often been treated as black boxes due to the complex interaction of various chemical, physical and biological processes in biofiltration. Thus, the need for fundamental knowledge is imperative to facilitate the development of design criteria based on experimental results obtained, which otherwise is dependent on empirical evidence. Development and subsequent validation of biofilter models therefore provides a useful tool to elucidate the complexity of the processes involved and would greatly enhance the ability to predict performance while paving the way for sound biofilter designs.

Transient and steady state biofilter models constructed in the past have primarily attempted to explore performance under different operating conditions and also the sensitivity of performance to biofilm parameters. While model simulations have greatly increased the awareness of the detailed processes involved and provided an insight into the interaction of the complex activities at microscopic scale, the nature of certain simplifications and parameter estimations made in the development of models casts a sense of doubt into their actual usefulness. In particular, the models that tend to incorporate biofilm dynamics pursue an approach of fitting column data to evaluate the relevant biofilm parameters instead of using independent experimental techniques. Most dynamic models constructed have ignored the coupled mass and energy balance relationship present in a biofilter and have assumed an isothermal operation coupled with a uniform moisture content. These inherent weaknesses in existing models curtail their usefulness when required to ascertain the implications of, water addition rates, propagation of drying fronts, water movement through the bed material and leachate production. Only one other model (Mysliwiec *et al.*, 2001) in addition to the current

model developed in this study incorporates a combined mass and energy balance approach to address the above issues, which are commonly encountered in full-scale biofilters.

2.6.2 Diffusion Type Models

Amanullah *et al.* (1999) presented a comprehensive review of recent biofilter models and categorised them into detailed diffusion models and LDF (Linear Driving Force) approximation models. The diffusion models, which use relatively realistic biofilm geometries, have progressed to become mathematically elegant. However, the parameters associated with the biofilm geometry (e.g. - thickness, percent coverage, density) are difficult to validate independently and are often used as fitting parameters.

A brief review of some diffusion type models available in literature is given below.

- **Ottengraf *et al.*, Model**

  Ottengraf *et al.*(1983), with their pioneering biofilter modelling, provided the background for the development of subsequent models. The steady state model developed, incorporated a plug flow type behaviour for the gas flow. The mechanism advocated for pollutant removal was inter-phase mass transfer followed by degradation in the biolayer as zero order kinetics. The governing equations were analytically solved for both reaction and diffusion limited scenarios under zero order kinetics. Continuous and batch scale studies using a mixture of compost and peat were presented to verify the above, using toluene, butanol, ethyl acetate and butyl acetate.

- **Shareefdeen *et al.*, Models**

  Shareefdeen and Baltzis (1993) developed a biofilter model for the removal of methanol vapour. This model based on principles similar to that of Ottengraf's, introduced several novel, yet practical concepts. In formulating the reaction kinetics, the authors introduced oxygen and substrate limitations. Oxygen limitation was modelled by a Monod relationship, while substrate inhibition kinetics was modelled on an Andrews's type relationship. Furthermore, the concept of an effective biofilm thickness, which was determined by the depletion of one of the components before the biofilm/solid interface, was also introduced. The use of numerical methods for the

solutions had avoided the simplification into first and zero order kinetics, which previous models had extensively relied on. The model advocated diffusion and degradation of contaminants in the biofilm, while axial dispersion in the gas phase was neglected. The model parameters in this case were determined both by literature surveys and through suspended cell experiments. The model was validated using experimental data from "separated" and "non-separated" columns. This model was subsequently used to model the biofiltration of hydrophobic compounds such as benzene and toluene using different kinetic expressions for the specific compounds (Shareefdeen *et al.*, 1994a). This steady state model was also used to analyse and compare performance with the models of Ottengraf (Zarook *et al.*, 1997). The above model was also extended to the biofiltration of toluene vapour under transient conditions, while incorporating concepts such as partial biofilm coverage of the solid media and adsorption into the solid surface (Shareefdeen *et al.*, 1994b). The adsorption of toluene into the solid media was modelled using a Freundlich isotherm. The resulting analysis indicated that for hydrophobic compounds oxygen limitation was not as significant as it was for hydrophilic compounds. Sensitivity analysis performed on kinetic parameters in the degradation term invalidated previous claims, which advocated simplified biodegradation (first or zero order kinetics) to obtain analytical solutions. The main drawback to this model was the estimation of certain model parameters by fitting column data, which introduced a certain discrepancy to the predicted results.

- **Deshusses *et al.*, Model**

  Deshusses & Dunn (1995) developed a biofilter model based on the elimination of a binary mixture of methyl ethyl ketone (MEK) and methyl isobutyl ketone (MIBK). This model was intended to provide an insight into transient (dynamic) responses and to binary contaminant loading. In this novel approach to modelling, the actual biofilter was divided into 10 finite sections (layers) and mass balances written for the pollutants in each of the subdivisions in a layer. Each layer contained a gas phase, biofilm and sorption volume. The biofilm contained four subdivisions, which were well mixed. Oxygen limitation was excluded based on experimental evidence. A competition inhibition constant in the rate expression accounted for substrate competition. Contaminants were subjected to diffusion, biodegradation in the biofilm

and finally storage in the sorption volume. The sorption volume contained the excess water content dispersed in the bed and was intended to act as a buffer for fluctuations in contaminant concentrations. Model simulation depicted the concept of competition between the contaminants, where MIBK was deemed to be more sensitive to competition than MEK. The existence of diffusion and reaction controlled regimes was indicated in the parametric sensitivity. In this model, adsorption of contaminants onto the solid surface was neglected, which prevented the estimation of contribution by different filter material to performance. Furthermore, as stated by Tang *et al.* (1997) the use of the sorption volume to buffer transients could underestimate the adsorption of hydrophobic compounds by different filter material.

- **Abumaizar *et al.*, Model**

  Abumaizar *et al.*(1997) developed a steady state biofilter model for the elimination of benzene, toluene, ethylbenzene and *o*-xylene (BTEX). The unique feature of this model was the introduction of a dual media concept to assess its feasibility on contaminant removal. The gas flow was assumed to be plug flow while the medium was comprised of compost and GAC. In this model, the degradation kinetics followed a Monod relationship, which subsequently reduced to either first or zero order depending on the contaminant concentrations. The contaminants were subjected to diffusion/oxidation in the biofilm and to adsorption by activated carbon. Biodegradation in the adsorbed phase was treated as instantaneous and the rate-limiting factor was treated as the zero order adsorption rates. Model parameters were obtained from column studies and literature. Simulation results were validated using columns containing varying GAC content, which also highlighted the effect of mixed media composition, on BTEX removal.

2.6.3 Linear Driving Force (LDF) Models

The lumped LDF approach has found widespread applications in fixed bed adsorption work due to its ability to approximate accurately the solution from the differential equation pertaining to diffusional mass transfer into the solid phase (Yang, 1997; Ruthven, 1984). Recent biofilter models have incorporated the LDF concept to model the dynamics in a combined solid/liquid phase. The LDF approach lumps the interfacial and diffusional mass transfer resistance in the solid phase into an overall mass transfer rate coefficient, which simplifies the mathematics by eliminating the biofilter geometry and the associated differential equations (Amanullah *et al.*, 1999).

Hodge & Devinny (1995) developed a biofiltration model, which incorporated a LDF approach in modelling the interphase and diffusional mass transfer. This model incorporated an axially dispersed plug flow behaviour for the gas phase, while mechanisms such as adsorption, absorption and degradation, were also included. The key parameters were determined through both continuous flow columns and batch scale experiments. The model was experimentally validated using ethanol and bed material consisting of compost, activated carbon and a mixture of compost/diatomaceous earth (Hodge and Devinny *et al.*, 1994). The fundamental difference in this model was that the solid and the biofilm were treated as one single phase with an average concentration. A first order degradation was selected to represent substrate degradation in the unified phase. Amanullah *et al.* (2000) developed a similar LDF model for the degradation of MEK on compost and GAC. In this case, the LDF model was extended with success for non-linear isotherms for MEK adsorption into GAC. The biodegradation of MEK was described by an expression of the form of Michaelis-Menten kinetics. Breakthrough column experiments had provided the key parameters in the model. The reaction rate parameters were evaluated using transient to steady state biofilter response for a range of contaminant loading.

2.6.4 The Volume Averaged Model of Mysliwiec *et al.*, 2001

Most biofilter models (of either type) assume an isothermal operation coupled with a uniform moisture distribution profile. Mysliwiec *et al.* (2001) developed a comprehensive non-isothermal model detailing the moisture and energy balance in an upflow biofilter treating toluene. This transient model relied extensively on the concept of volume averaging to spatially smooth, phase specific microscopic equations to produce equations that were valid within the entire porous media. The hierarchal structure present in a porous media, presents disparities in the length scales, which were smoothed out using the concept of volume averaging in this work (Whitaker, 1999). The phases involved in the porous media were regarded as a continuum at points within the medium occupied. This rigorous technique was very useful in analysing a complex structure such as a porous medium, where at a microscopic scale the surface configurations and the boundary conditions were quite difficult to estimate independently. Hence, by transforming the problem to a macroscopic one, the microscopic scale parameters that were difficult to quantify through independent experimental means were eliminated. This approach transformed the model from a detailed diffusion type model to an LDF type model (Mysliwiec, 2000). In the transformation, each phase was regarded as a continuum in the entire domain and averaged values of phase variables taken over a Representative Elementary Volume (REV) centred at points in the continuum. A spherical REV was selected in the model and by traversing through the entire porous domain with a moving REV, macroscopic parameters that were functions of spatial coordinates were obtained.

In the model, the growth term was described using a double Monod relationship to depict the functional dependence on substrate and nutrients, and was complemented with expressions for moisture, temperature and biofilm density. The evaporation term was modelled on the basis of laminar gas flow and the corresponding mass transfer coefficient accounted for pore size and moisture content. Biomass desiccation was included in the model to account for the transfer of bound water in the biofilm to the free liquid water. The resulting two-phase system was modelled by writing the gas and liquid permeability as functions of effective saturation. The model parameters were either estimated through literature analysis or from experimental work. This model highlighted the relative importance of varying bed permeability (hydraulic conductivity) on local moisture content and performance under water addition.

Chapter 3: Model Development

3.1 Introduction

The objective of this modelling exercise was to develop an effective transient biofilter model to investigate the relationship between performance and the water content of the packing material. The governing equations were based on conventional mass balance techniques combined with mass transfer theory, which coupled the gas phase to the liquid/biofilm. The key assumption was that diffusion in the biofilm was neglected. This was based on the fact that, due to the difference in the length scales of the biofilm and solid phase, the time scale of activity in the biofilm was two orders of magnitude lower than that of the solid phase. Therefore, the biofilm was assumed to be in instantaneous equilibrium with the gas phase and the degradation within the biofilm was directly a function of the gas phase concentration similar to traditional solid-phase catalysis. Thus, under this approach biofilm dynamics were ignored and greater emphasis was placed on the solid phase dynamics. Hence, the uncertainty associated with the biofilm parameters (biofilm thickness, specific surface area, coverage etc) in the detailed diffusion models was transferred into a lumped degradation term under this model. The solid phase dynamics were modelled using a LDF (Linear Driving Force) approach. In this approach the solid phase was treated as consisting of well-mixed layers (individual particles in the layer treated as well mixed continuous stirred tank reactors (CSTR)). Furthermore, under this conceptual model, since mass transfer dynamics were relegated to the inert solid phase, a biologically limited scenario was modelled (Ottengraf, 1983). These assumptions and structures produced a dynamic biofilter model where all parameters potentially could be independently validated. For modelling purposes, toluene was selected as the model compound.

A number of assumptions were introduced in reflection of the model goals, ease of numerical solution and eventual experimental verification. These are listed below:

3.2 Assumptions in Model Development

1. Ideal plug flow behaviour for the gas. The Peclet number is normally ≈ 300-600 in most biofilters, which indicated plug flow (Amanullah *et al.*, 1999).
2. Change in local water content in the compost column had little effect on the overall gas porosity and therefore the gas phase velocity (permeability) was treated as constant (Gostomski *et al.*, 2001).
3. Gas/liquid biofilm was in equilibrium at the interface according to Henry's law.
4. For absorption, the mass transfer resistance in the liquid biofilm was neglected and local instantaneous equilibrium with the gas phase was assumed. This was based on the assumption that the characteristic time scale of the biofilm dynamics was significantly smaller than that of the solid phase.
5. Oxygen limitation was assumed not to occur over the toluene concentrations of interest (Acuna *et al.*, 1999, Baltzis, 1997).
6. Constant biomass density.
7. Sorption in the solid phase was a reversible process and was modelled as an isothermal, single transition, single mass transfer (LDF) resistant process. Adsorption characteristics were obtained through isotherms generated from experiments.
8. The material diffusing into the intraparticle voids was not available to the organisms due to the difference in length scales of pores and voids compared to typical microbe dimensions. Hence the microbial degradation effect in the solid phase was negligible.
9. The hysteresis effect in the wetting and drying curve was assumed to be negligible. Therefore the relation between matric potential and volumetric water content was unique.
10. For the overall packed bed model (Fig. 3.1), a thin "bark layer" provided air distribution and ensured proper drainage of the leachate produced but did not participate in the degradation process. This assumption permitted the boundary condition for volumetric water content at the bottom of the active bed to be less than saturated.
11. The liquid water density was independent of the concentration and its spatial variation was regarded as negligible.

12. The compost medium was assumed to be homogeneous and isotropic.
13. In the temperature range considered, the heat capacities and thermal conductivities of air, water and water vapour were constant with the exception of those of compost.
14. The biomass and toluene present in the liquid phase (water) did not affect the saturated vapour pressure of water given by the TRC database (TRC k-5969, 1987).
15. Ideal gas behaviour assumed for the gas phase and gravitational effects were neglected.
16. Complete degradation of toluene to CO_2 and H_2O. No degradation of compost.
17. The gas phase consisted of dry air and water vapour. The gas-phase contaminant had a negligible effect on heat transfer coefficients.
18. Local thermal and moisture equilibrium in the gas, liquid and solid phase.
19. Pseudo-homogeneous structure for the packed bed with regard to heat transfer.
20. The gas phase was assumed to be continuous.
21. The biofilter was well insulated (adiabatic) at the wall. In full-scale biofilters, the small surface to volume ratio present and the low thermal conductivity of the bed medium gives approximately adiabatic operation (Gostomski *et al.*, 1997). Thus, the system modelled consisted of only axial heat conduction.
22. The changes in water content over time were assumed to have negligible effect on the bulk heat capacity.
23. In the normal temperature range of biofilter operation, as ρ_a and ρ_v were of similar magnitude, the gas pressure was assumed to remain at atmospheric throughout the column.
24. The gas phase was saturated with water vapour and hence was in (instantaneous) equilibrium with the liquid phase. Thus, the evaporation was regarded as instantaneous and dynamics associated with mass transfer were neglected.

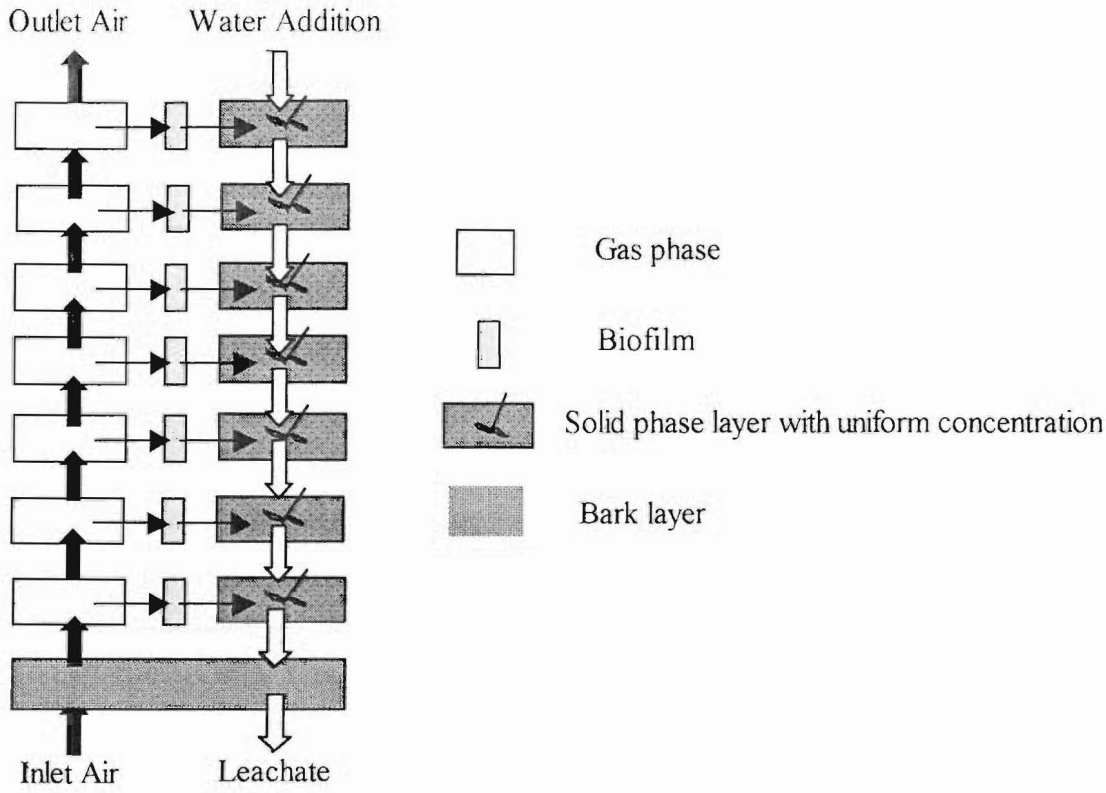

Figure 3.1 Conceptual diagram for the biofilter model, depicting the three phases present. The vertical and horizontal arrows indicate the direction of air/liquid flow and the coupling of the phases respectively.

Mass Balance Equations for the System

3.3 Gas Phase

The Mass Balance Equation for Toluene in the Gas Phase

$$\frac{\partial(CS_g)}{\partial t} = -U_g \frac{\partial(CS_g)}{\partial z} - \left(\frac{1-\varepsilon}{\varepsilon}\right) K_s (q^* - q) - (-r)\left(\frac{1-\varepsilon}{\varepsilon}\right) \qquad \text{[Eq. 3.1]}$$

The change in gas phase concentration of toluene (C) was driven by the axial convection gas flow rate (U_g), the transfer rate of contaminant to the solid phase K_s (q^*- q) and the biological degradation rate ($-r$) of toluene. Owing to the plug flow assumption no axial dispersion term was included. The two-phase nature of the system resulted in the inclusion of the gas phase saturation (S_g) as an integral part of the above equation.

The initial and boundary conditions were,

$t = 0, z = 0, C = 0,$ [Eq. 3.2]

$t = 0, 0 < z \leq L, C(z, 0) = 0,$ [Eq. 3.3]

$t > 0, z = 0, C = C_i$ [Eq. 3.4]

For initialising purposes of the model S_g ($0 < S_g < 1$) was set at a value to reflect the moisture content at the start of simulation.

3.3.1 Degree of Saturation

In the analysis of soil water phenomena, the concept of degree of saturation had been well defined. Literature (Bear, 1972) on unsaturated flow in porous media indicated that water content alone was sufficient to characterise the media, as air was deemed to be stationary. However, in the case of a biofilter with a two-phase flow of immiscible fluids (i.e. gas and liquid) the degree of saturation had to be included. Thus, the liquid phase saturation (S_w) could be defined as the fraction of the void volume occupied by the liquid phase and gas phase saturation (S_g), the fraction of the void volume occupied by the gas phase in a representative elementary volume.

$S_w = 1\text{-}S_g$ [Eq. 3.5]

$\theta = S_w \varepsilon$ [Eq. 3.6]

In the preceding sections the derived equations contained the degree of saturation (S_w) as an integral part of the volumetric water content (θ) instead of as a separate entity.

3.3.2 Biodegradation Kinetics

The traditional biodegradation rate modelling in biofilms have consisted of both an active growth term as well as a maintenance component (Eq. 3.7).

$$(-r) = \mu \frac{X}{Y} + mX$$ [Eq. 3.7]

A double Monod type relationship (Eq. 3.8) was initially assumed for the specific growth rate of biomass, taking into account the nutrient limitation imposed on the organisms (Cherry and Thompson, 1997).

$$\mu = \mu_{\max}\left(\frac{S}{K_s + S}\right)\left(\frac{N}{K_N + N}\right) \qquad \text{[Eq. 3.8]}$$

The packing material compost consisted of organic material, which facilitated the release of nutrients during the degradation of the substrate. However, it was assumed that in the absence of a nutrient supply a fully developed biomass with no further net growth ($\mu = 0$) would occur. Nevertheless, substrate utilisation for maintenance kinetics would still take place, so (Eq. 3.7) was simplified to $-r = mX$.

The maintenance term (mX) was a lumped term combining a specific microbial degradation rate (m) and the biomass concentration (X). The biodegradation rate (maintenance) was a function of contaminant concentration, water and temperature (Eq. 3.9). The concentration relationship was based on kinetic data for toluene degradation in a peat medium (Shareefdeen, *et al.*, 1994b) using a Monod-type model (Eq. 3.10). Furthermore, the half saturation constant (K_m) and maximum degradation term (V_m) were obtained by converting the corresponding constants in the above reference to a gas phase concentration for consistency with the biofilm assumptions. The resulting lumped maintenance term was expressed as mass of toluene degraded per unit volume of packing material per unit time. This approach facilitated independent verification of the key parameters in the degradation term.

$$(-r) = f(C) M_f T_f \qquad \text{[Eq. 3.9]}$$

$$f(C) = \frac{V_m C}{K_m + C} \qquad \text{[Eq. 3.10]}$$

$$V_m = 1.17 \times 10^{-1}\ \text{g/m}^3\text{s},\ K_m = 2.97\ \text{g/m}^3 \qquad \text{[Eq. 3.11]}$$

The temperature dependence on degradation (Fig. 3.2A) was modelled using data available in literature (Acuna, *et al.*, 1999).

$$T_f = -35.7T^2 + 215.4T - 323.9 \qquad \text{[Eq. 3.12]}$$

for $298\ \text{K} \leq T \leq 318\ \text{K}$.

In model simulations for $T > T_{max}(313K)$, $T_f = 0$ reflected the upper limit of the mesophilic operating range. Although experimental data existed in the literature for the water content effect on toluene degradation in peat, very little data were available for Organix[1, 2] compost (Acuna, *et al.*, 1999). Since the data of Acuna *et al.* (1999), when converted to volumetric water content, were outside the residual water content for Organix compost, the moisture content effect was modelled using hypothetical data that provided a relationship analogous to that in above reference (Eq. 3.13).

$$M_f = \frac{2.04(\theta - 0.44)}{0.210 + (\theta - 0.44)} \qquad \text{[Eq. 3.13]}$$

for $0.44 \leq \theta \leq 0.64$

In model simulations (Eq. 3.13) for $\theta > 0.64$, $M_f = 1$ which indicated approaching pore saturation (Fig. 3.2B). Furthermore, degradation was assumed to be zero below $\theta = 0.44$ (residual water content, see "Section 3.5.3") even though a water activity sufficient for microbial metabolism could have prevailed. However, according to the experimental findings of Cox *et al.* (1996), the degradation depended on the water content irrespective of the water activity. Hence, near residual water content, the effect of water content surpassed that of water activity to essentially stop any degradation.

[1]Organix compost was used for this study, as extensive data pertaining to the hydraulic properties (unsaturated conductivity, water release curves) for this compost type was available within the research group.

[2] Organix compost consisted of pig manure and sawdust starting material and was supplied by Parkhouse Garden Supplies™, Christchurch, NZ.

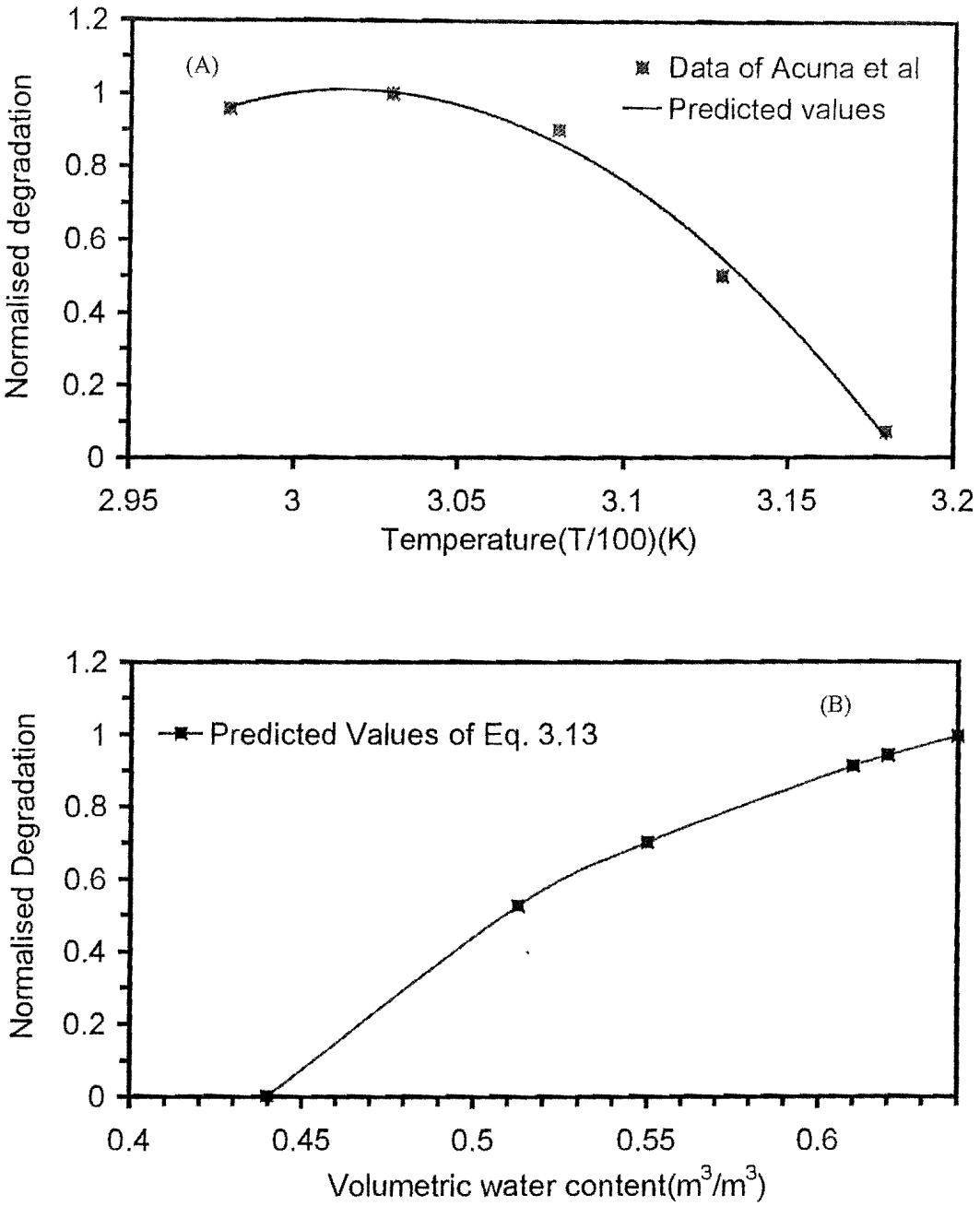

Figure 3.2 Temperature effect on degradation (A), Water content effect on degradation (B).

3.3.3 Oxygen Effect on Biodegradation Kinetics

Modelling work by Shareefdeen *et al.* (1994) on toluene and toluene/benzene removal demonstrated that the Monod kinetic constant for oxygen had little effect on model performance. In a subsequent article by Baltzis (1997), it was also pointed out that oxygen was present in excess in the biolayer, when treating hydrophobic compounds. Experimental work by Acuna *et al.* (1999) also indicated the negligible effect of oxygen concentration on toluene degradation. Hence, the oxygen dependence on the degradation kinetics for this system treating toluene was neglected.

3.4 Solid Phase

Traditionally, solid phase dynamics have been modelled using a differential equation (Eq. 3.14) describing diffusional mass transfer into a spherical porous pellet (Yang, 1999). The mass balance for the bulk gas phase, the continuity expression at the pellet surface and Eq. 3.14 are simultaneously solved to obtain the solution.

$$\frac{\partial q}{\partial t} = D_e\left(\frac{\partial^2 C_p}{\partial R_p^{\,2}} + \frac{2}{r}\frac{\partial C_p}{\partial R_p}\right) \qquad \text{[Eq. 3.14]}$$

However, due to the intense numerical computational effort involved in the solution of Eq. 3.14 a simplified expression was developed, which related the uptake rate in the solid phase to the gas phase concentration. This approach known as the LDF (Linear Driving Force) approach lumps the interfacial and diffusional mass transfer resistance in the solid phase into an overall mass transfer rate coefficient (K_{LDF}), which provides a much simplified expression (Eq. 3.15). In the resulting expression the solid phase is treated as consisting of well-mixed layers (individual particles in the layer treated as well mixed CSTR). Literature on fixed bed adsorption indicated close agreement between the LDF and the traditional diffusion model under linear equilibrium isotherms (Yang, 1999; Ruthven, 1984). Therefore, due to the above fact and the numerical convenience afforded, the LDF concept was used to model the absorption mass transfer into the solid phase.

Mass Balance for the Solid Phase

$$\frac{\partial q}{\partial t} = K_{LDF}(q^* - q) \qquad \text{[Eq. 3.15]}$$

$q^* = K_{eqm}C$, for a linear equilibrium isotherm [Eq. 3.16]

Initial conditions,

$$q(z,0) = 0 \qquad \text{[Eq. 3.17]}$$

Batch scale experiments using microbially inhibited compost gave linear sorption isotherms for toluene on compost at concentrations between 0-1000ppm$_v$ and temperature values of 25°C and 35°C. Furthermore, in the absence of data relating the water content effects on toluene sorption and also due to related work by Acuna *et al.* (1999), which indicated no significant influence of moisture on toluene sorption in a peat bed, the moisture aspect with respect to sorption was neglected. The temperature effect on the sorption capacity of the bed tended to be slightly more pronounced at the higher headspace concentration values, which was consistent with observations reported in literature (Apel *et al.*, 1994) for gasoline adsorption onto an organic medium. The temperature effect on the bed sorption capacity was modelled using an Arrhenius type relationship. The final sorption isotherm derived was as follows,

$$q^* = k_0 e(-\Delta H / RT)C \qquad \text{[Eq. 3.18]}$$

k_0= 0.577 g of toluene/m^3 of compost/ g/m^3, ΔH = -10.5×10^3 J/mol

The Mass Transfer Resistance in an Equivalent LDF Model,

The LDF mass transfer coefficient (K_{LDF}) is related to the external mass transfer resistance, macropore and micropore diffusional resistance of a porous particle through equation 3.19.

$$\frac{1}{K_{LDF}K_{eqm}} = \frac{R_p}{3k_f} + \frac{R_p^2}{15\varepsilon_p D_p} + \frac{r_c^2}{15K_{eqm}D_c} \qquad \text{[Eq. 3.19]}$$

Experimental and modelling work (Amanullah *et al.*, 2000) was able to show that the mass transfer in porous GAC particles was controlled by diffusion in macropores and this was also extended to compost particles with success. Experimental work (Hon, 1999) performed on compost indicated that a significant proportion of intraparticle space consisted of macropores. Furthermore, the assumption of instantaneous equilibrium in the biofilm resulted in negligible mass transfer resistance in the biofilm. In addition, molecular diffusion was assumed to drive the transport of contaminant in the intraparticle pores (macropore diffusion). Thus Eq. 3.19 simplified to,

$$\frac{1}{K_{LDF}K_{eqm}} = \frac{R_p^{\,2}}{15\varepsilon_p D_p} \qquad \text{[Eq. 3.20]}$$

Owing to the random orientation of the pores and the variation in pore diameter, the pore diffusivity (D_p) tends to be smaller than that in a straight cylindrical pore. This is accounted for by the tortuosity factor (τ), which is used in the expression relating pore diffusivity to molecular diffusion, given by $D_p = \frac{D_m}{\tau}$ (Ruthven, 1984).

$$\frac{1}{K_{LDF}K_{eqm}} = \frac{R_p^{\,2}}{15\varepsilon_p \frac{D_m}{\tau}} \qquad \text{[Eq. 3.21]}$$

The effect of biomass concentration on the effective diffusivity of a compound within a biofilm has been experimentally explored (Fan *et al.*, 1990). However, in the current study it was explicitly assumed that the pores were filled with water and hence the diffusivity of toluene was taken as that in pure water. Since $\frac{\varepsilon_p}{\tau}$ was a physical (geometric) parameter of compost, a similar value to that used by Amanullah *et al.* (2000) was assumed.

3.5 Liquid Phase (Water)

3.5.1 Unsaturated Flow in Porous Media

Although many similarities exist in the study of unsaturated flow of water in soil and biofilter packing material, one of the fundamental differences is the presence of the moving gas phase in biofilters. Nielsen *et al.* (1986) developed a two-phase flow model, which considered the simultaneous flow of both liquid and gas. However, due to the nature of the system and assumptions made in their model, their equations were not used although the influence of the gas phase on system dynamics was adequately recognized.

Work performed by soil physicists pertaining to the analysis of liquid flow in unsaturated media, has concentrated on the selection of an appropriate form of the unsaturated flow equation and the subsequent numerical solution of the relevant equation (Hillel, 1980; Marshall & Holmes, 1979). However, due to the nature of the typical soil system considered, a combined approach encompassing gas flow and microbial activity has been ignored. Several forms of defining media moisture content exist as stated in Stephens (1996). However, in this case the mass balance equation for liquid water used the volumetric water content (θ) to represent the moisture in the porous media.

Mass Balance Equation for Liquid Water

$$\frac{\partial(\theta\rho_l)}{\partial t} = -\frac{\partial(\rho_l U_l)}{\partial z} - E + K_{Tol}(mX)(1-\varepsilon) \qquad \text{[Eq. 3.22]}$$

The change in water content in the system (θ) was driven by the water addition rate (U_l), the evaporation rate (E) and the water produced by toluene oxidation $K_{Tol}(mX)$. The liquid velocity (U_l) was expanded using Darcy's law for unsaturated media and was written as a function of the hydraulic gradient $\partial h/\partial z$ and the unsaturated hydraulic conductivity (K). The evaporative rate (E) term was expanded to reflect the effect of saturated vapour pressure variations with temperature on moisture content change giving an expanded version of the water balance in Eq. 3.23.

$$\frac{\partial \theta}{\partial t} = \frac{\partial}{\partial z}\left[K\left(-\frac{\partial h}{\partial z}+1\right)\right] - \frac{\varepsilon S_g U_g}{\rho_l}\frac{\partial M}{\partial z} + \frac{K_{Tol}(mX)}{\rho_l}(1-\varepsilon) \qquad \text{[Eq. 3.23]}$$

Equation 3.23 indicated that the liquid water velocity in the axial direction was equal to the volumetric water content plus evaporative moisture removal offset by water produced by metabolic oxidation of toluene. Furthermore Eq. 3.23 minus the evaporative and biological activity is commonly identified in soil physics as the mixed form of Richards' equation for a porous medium (Celia *et al.*, 1990).

Initial condition, $t = 0,\ 0 < z < L,\ \theta = 0.5$ [Eq. 3.24]

Boundary conditions are,

$t \geq 0, z = 0, \frac{\partial \theta}{\partial z} = 0$ (Gravitational drainage assumed) [Eq. 3.25]

$$t \geq 0,\ z = L,\quad q_{surface} = K_{20}\left[-\left.\frac{\partial h}{\partial z}\right|_{20} + 1\right] \qquad \text{[Eq. 3.26]}$$

This boundary condition represented the water flux imparted at the top of the column as g/m^2s, where the subscript 20 referred to the position 100 cm from the bottom of the column.

The vertical direction (z) was assumed positive upwards. The negative sign in the capillary component of the advective term indicated that tension (h) was substituted positive during the simulation process. In this case the modelling focused on situations where the volumetric water content was predominantly above the residual saturation (vadose zone) and thus flow was driven by a hydraulic gradient (convective transport).

Soil scientists/modellers tend to use the Richards' equation to predict the infiltration of water in soil columns with either a constant flux or water content at the surface. In Celia *et al.* (1990) both the h-based and mixed form of Richards' equation were numerically evaluated using finite difference/finite element techniques coupled together with a Picard iteration scheme using the constitutive relationships of Van Genutchen *et al.* (1980) and those reported by Havercamp *et al.* (1977) for unsaturated hydraulic data. The results of this work was able to indicate the superiority of the mixed form over the h-based form, in

conserving the global mass over the domain concerned, where the latter form's inferiority stemmed from the time derivative term. This adequately displayed the mass conservation property of the mixed form under increasing time steps (more diffuse front), whereas the h-based form yielded a significant under-prediction of the infiltration depth under the same test.

Havercamp *et al.* (1977) solved the *h*-based form of the Richards' equation with six different numerical models using explicit/implicit schemes with explicit/implicit linearisation of the non-linear terms. The numerical solutions were compared to experimental results and the respective schemes evaluated using execution time and mass balance in the above reference. Most schemes were said to provide good agreement with the measured data, although the stability of the explicit schemes tends to be compromised with the introduction of large time steps. Thus, due to these findings, it was decided to use a modified form of the mixed equation in the current work.

3.5.2 Relative Conductivity

In the two-phase immiscible fluid flow, the conductivity (permeability) of a porous medium with respect to a certain fluid will be reduced due to the presence of the other fluid. The relative permeability of the medium would depend on the nature of the porous medium and on the degree of saturation.

$$k_{rl} = \frac{k_l}{K_{sat}} \qquad \text{[Eq. 3.27]}$$

A rapid drop in k_{rl} of wetting phase conductivity and rise in k_{rnl} of the non-wetting phase could be attributed to the emptying of larger pores during drying (Bear, 1972). Relative conductivity is also affected by the hysteresis phenomenon. van Genuchten *et al.* (1980) using the statistical model of Mualem *et al.* (1976) developed an expression to predict the unsaturated hydraulic conductivity of the wetting phase, by defining a suitable equation for the soil water retention curve. The relationship relating the pressure head (capillary pressure) to the effective water content (effective saturation) was,

$$\Theta = \left[\frac{1}{1+(\alpha h)^n} \right]^m \qquad \text{[Eq. 3.28]}$$

On further simplification the above expression becomes,

$$h = \frac{1}{\alpha}\left[\frac{1}{\Theta^{1/m}} - 1 \right]^{1/n} \qquad \text{[Eq. 3.29]}$$

where $\Theta = \dfrac{\theta - \theta_r}{\theta_s - \theta_r}$

The expression derived by van Genuchten *et al.* (1980) for the unsaturated hydraulic conductivity as a function of soil water pressure (h) is given in (Eq. 3.30). In order to obtain a closed form expression the algebraic condition m=1-1/n had been used.

$$k_l = \frac{K_s \left\{ 1 - (\alpha h)^{n-1} \left[1 + (\alpha h)^n \right]^{-m} \right\}^2}{\left[1 + (\alpha h)^n \right]^{m/2}} \qquad \text{[Eq. 3.30]}$$

An important aspect of this expression was that it was far more accurate than those based on Burdine's model in terms of agreement with experimental data (van Genuchten *et al.* 1980). Mualem *et al.* (1976) also concluded that, based on a numerical approximation for the soil water retention curve, "Burdine" based expressions were not accurate on an overall basis with regard to the average of the mean square deviation of the unsaturated hydraulic conductivity computed.

3.5.3 Water Retention Curves

In the application of soil models to compost, work done by Hon (1999) indicated negligible hysteresis between the wetting and drying curve for several types of compost media (Biomix, Organix and Envy). This was subsequently attributed to the presence of a uniform pore size distribution and consolidation that occurred in compost.

Thus, in the model development the hysteresis effect was neglected. The constitutive relationships of van Genuchten *et al.* (1980) were not used for model simulation purposes, as the compost data could not be adequately fitted to both expressions (i.e. $K(h)$ and $\theta(h)$). Instead, the constitutive relationships (Havercamp *et al.*, 1977) given by (Eq. 3.31, 3.32) provided the relationship between volumetric water content and matric potential and unsaturated hydraulic conductivity and matric potential. Matric potential is defined in soil physics as the force acting on the soil water from the attractive forces of the solid matrix and the adjoining water molecules (Stephens, 1996). It is a thermodynamic property, which at equilibrium relates to the relative humidity of the vapour phase (Papendick, 1980). Furthermore, matric potential consists of both capillary and adsorptive water and is negative as referenced to free water at zero potential (Hillel, 1980).

The parameters in Eq. 3.31 & 3.32 were obtained experimentally for Organix compost (Fig. 3.3 & 3.4).

$$\theta(h) = \frac{\alpha(\theta_s - \theta_r)}{\alpha + h^{\beta}} + \theta_r \qquad \text{[Eq. 3.31]}$$

$$K(h) = K_s \frac{A}{A + h^{\gamma}} \qquad \text{[Eq. 3.32]}$$

Table 3.1 Parameter values

Relationship	Organix Compost
$\theta(h) = \frac{\alpha(\theta_s - \theta_r)}{\alpha + h^{\beta}} + \theta_r$	$\alpha = 631$ $\beta = 2.34$ $\theta_s = 0.64$ $\theta_r = 0.43$
$K(h) = K_s \frac{A}{A + h^{\gamma}}$	$K_s = 1.28 \times 10^{-1}$ cm/s $A = 50.5$ $\gamma = 4.7$

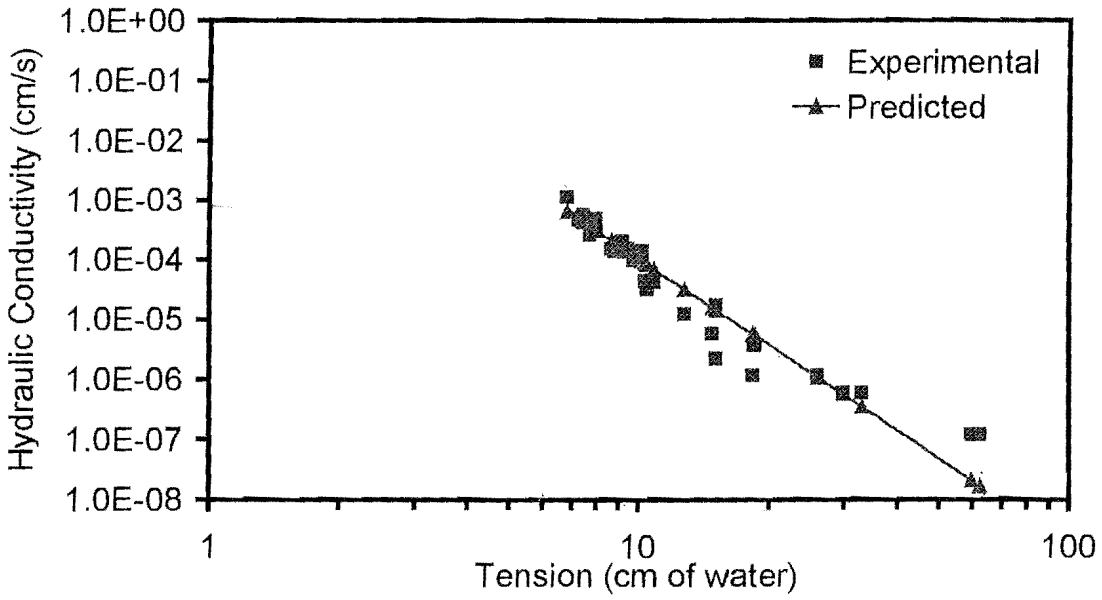

Figure3.3 Unsaturated hydraulic conductivity of compost (Adapted from Hon, 1999).

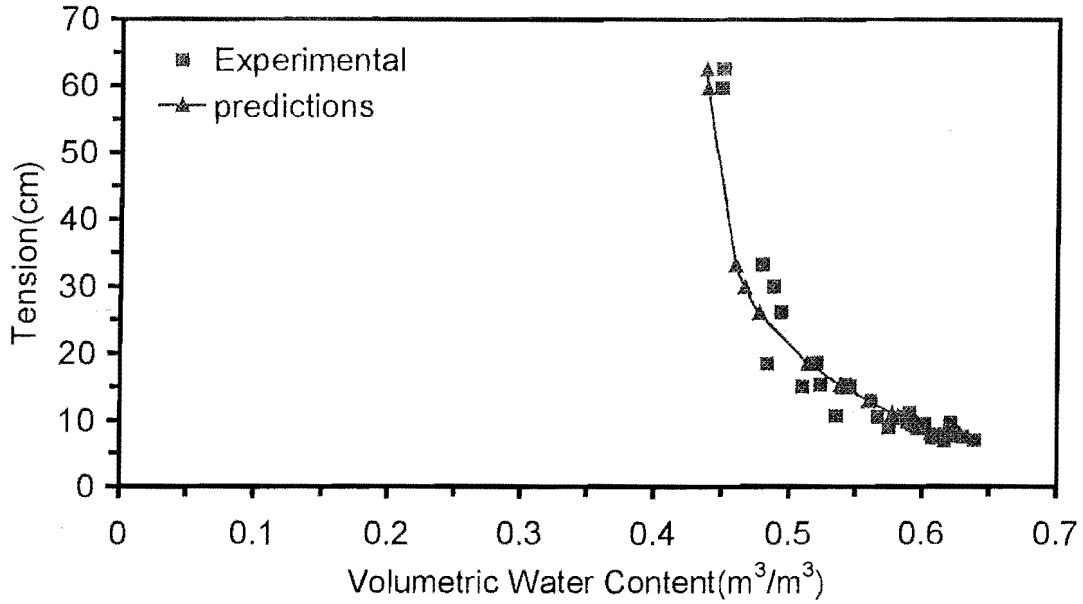

Figure 3.4 Soil water retention curve (Adapted from Hon, 1999).

3.5.4 Evaporative Mass Transfer

Based on the assumption that the gas, liquid and solid phase were in equilibrium in regards to water content, evaporative mass transfer was driven by the change in saturated vapour pressure with temperature. The relevant saturated vapour pressure (P_s) data were obtained from the TRC database (TRC k-5969, 1987) and were converted to mass per unit volume by,

$$M = \frac{P_s M_w}{RT} \qquad \text{[Eq. 3.33]}$$

The data obtained from Eq. 3.33 were represented by a polynomial for the operating temperature range of (20 °C – 40 °C) to obtain a relationship between M and T (Eq. 3.34). Owing to the small spatial step size and the resulting low temperature variations in the cells, the change in specific volume of air was ignored.

$$M = 0.0382T^2 - 21.496T + 4883.4 \qquad \text{[Eq. 3.34]}$$

Thus, the expression for evaporative mass transfer can be written in relation to gas phase properties with changes being driven by temperature changes. The effect of velocity on moisture removal was reflected by the inclusion of the interstitial velocity term, while the vapour pressure gradient represented the temperature effect on evaporation.

$$E = \varepsilon S_g U_g \frac{\partial M}{\partial Z} \qquad \text{[Eq. 3.35]}$$

As the saturated vapour concentration was a function of temperature, the dynamics in the vapour phase closely matched the temperature dynamics (Eq. 3.36).

$$\frac{\partial M}{\partial t} = \left(\frac{\partial M}{\partial T}\right)\left(\frac{\partial T}{\partial t}\right) \qquad \text{[Eq. 3.36]}$$

Complete degradation of toluene was assumed as stated earlier, which was governed by the following stoichiometric equation.

$$C_7H_8 + 9O_2 \rightarrow 7CO_2 + 4H_2O$$

Hence from the above K_{Tol} = 0.783 g of water/g of toluene degraded

3.6 Energy Balance

3.6.1 Theory and Governing Equations

The energy balance for biofiltration was conceptually similar to solid-state fermentation. However, often in solid-state fermentation literature, large temperature variations tend to dominate the biological activity as compared to moisture content changes in the solid phase (Ghildyal *et al.*, 1994; Mitchell & von Meien, 2000). Thus, modifications were required to account for the bed moisture, which was of paramount importance in biofilters. The biofilter energy balance incorporated a transient heat component, liquid/gas convection in the axial direction, conduction in the axial direction, heat released due to metabolism and latent heat which was the major mechanism for heat removal in a packed bed under forced aeration.

The energy balance used a pseudohomogeneous bed assumption compared to a heterogeneous one. Under this concept, global parameters (mass weighted average properties) of the constituents were used and the bed was assumed to behave as a single medium (Sangsurasak *et al.*, 1998). These equations were also defined as one-equation models as they made no distinction in the temperature of the solid, liquid and gas phase. The principal criteria required for a pseudohomogeneous assumption were those of thermal and moisture equilibrium. Since saturated air is used for aeration purposes in biofilters and also due to the assumption that the moisture adsorption into the solid phase was deemed negligible, the system could be considered to be in moisture equilibrium (Sangsurasak *et al.*, 1998). However, the vapour pressure of the saturated air would vary with temperature (Coulson & Richardson, 1996) and hence equilibrium was maintained by evaporation/condensation.

Owing to the assumption of moisture equilibrium between the gas/liquid phases, these phases could be assumed to be in equilibrium with respect to temperature. Using thermal sterilisation theory (Bailey & Ollis, 1986), the time taken for a spherical compost particle to reach the external temperature was found to be one to two orders of magnitude smaller than the typical residence time of a biofilter (Appendix A). Hence, the solid phase reached the relevant external temperature instantaneously and the three phases were assumed to be in thermal equilibrium.

The energy balance equation for the system was,

$$\frac{\partial\left(\rho_b C_{pb} T\right)}{\partial t}+\left[\left(\varepsilon S_g U_g\left(\rho_g C_{pg}+h_e \frac{\partial M}{\partial T}\right)+\rho_l C_{pl} U_l\right)\frac{\partial T}{\partial z}\right]=K_{eff}\frac{\partial^2 T}{\partial z^2}+h_c m X(1-\varepsilon)$$

[Eq. 3.37]

- The transient temperature term used the bulk heat capacity for the bed ($\rho_b C_{pb}$), which was determined as the mass weighted average for all the components.

- The terms $\rho_g C_{pg}$ and $\rho_l C_{pl}$ accounted for heat transfer by convection in the axial direction by the gas and liquid phases respectively.

- The term $h_e \frac{\partial M}{\partial T}$ indicated the evaporative heat removal by the saturated air and was lumped with the heat capacity of air to reflect the increase of the apparent heat capacity of air with temperature (Sangsurasak *et al.*, 1998).

- The term $K_{eff} \frac{\partial^2 T}{\partial z^2}$ represented the axial heat conduction term.

- The term $h_c m X(1-\varepsilon)$ represented the exothermic bioreaction. The energy generated from the oxidation of toluene was released as heat.

- Heat transfer by convection in the radial direction was neglected due to the adiabatic assumption at the walls.

Boundary Conditions,

$z = 0,\ t > 0,\ T = T_a$ (Relative Humidity (RH) 100%) [Eq. 3.38]

$$z = L,\ \frac{\partial T}{\partial z} = 0 \qquad \text{[Eq. 3.39]}$$

(No enclosure losses and hence there does not exist external cooling of exhaust air at the top of the bed. The air stream leaves at the same temperature as that of the bed at the point considered with no release of moisture back onto the bed.)

Initial Condition,

$t = 0,\ 0 \le z \le L\ ,\ T = T_i$ [Eq. 3.40]

The weighted average heat capacity (bulk heat capacity) for the bed,

$$\rho_b C_{pb} = \rho_s C_{ps}(1-\varepsilon) + \rho_l C_{pl}\varepsilon S_l + (\rho_v C_{pv} + \rho_a C_{pa}) S_g \varepsilon \qquad \text{[Eq. 3.41]}$$

This expression was simplified further by assuming the gas phase to be at atmospheric pressure,

$$\rho_b C_{pb} = \rho_s C_{ps}(1-\varepsilon) + \rho_l C_{pl}\theta + \rho_a C_{pa} S_g \varepsilon \qquad \text{[Eq. 3.42]}$$

The weighted average heat capacity for the gas phase,

$$\varepsilon S_g \rho_g C_{pg} = \varepsilon S_g (\rho_v C_{pv} + \rho_a C_{pa}) \qquad \text{[Eq. 3.43]}$$

Assuming the gas phase to be at atmospheric pressure and neglecting the presence of vapour phase Eq. 3.43 was simplified to,

$$\varepsilon S_g \rho_g C_{pg} = \varepsilon S_g \rho_a C_{pa}$$

The weighted average (effective) thermal conductivity for the bed,

$$K_{eff} = K_s(1-\varepsilon) + K_l S_l \varepsilon + K_g \varepsilon S_g \qquad \text{[Eq. 3.44]}$$

The effective thermal conductivity (K_{eff}) as discussed in section 3.6.3 was assumed to be constant.

3.6.2 Specific Heat Capacity

The specific heat capacities with the exception of C_{ps} had negligible variations within the temperature range considered. The value of C_{ps} in the literature tends to vary significantly with the moisture content ($\approx 11\%$)(Haug, 1993). Hence the correlation was adapted to Organix compost by a modification using the compost physical properties obtained by Hon, 1999. The resulting polynomial fit was,

$$C_{ps} = -15.8\theta^2 + 12.5\theta + 0.2 \qquad \text{[Eq. 3.45]}$$

3.6.3 Thermal Conductivity

The thermal conductivity (K_{eff}) for Organix compost varied only by 5% over the system's operating moisture range and hence was assumed to be constant. The term (K_{eff}) was calculated using a correlation for the moisture content effect on compost thermal conductivity (Haug, 1993). The values for C_{ps} & K_s were take from above reference as the material was very similar to the compost used in the experiments. The parameter values used in the energy balance of the model are listed in Table 3.2. It was assumed that the density of air and water would remain constant over the entire bed length.

i.e. $\rho_l = 1000$ kg m^{-3}, $\rho_a = 1.2$ kg m^{-3}, $\rho_s = 620$ kg m^{-3}

Table 3.2 Parameter values used in the energy balance[3]

Parameter	Numerical Value	Units
C_{pl}	4.18	J/g K
C_{pa}	1.05	J/g K
C_{pv}	1.88	J/g K
h_c	42.44	kJ/g
h_e	2.3	kJ/g
K_{eff}	0.58	W/m K
K_l	0.616	W/m K
K_v	61×10^{-2}	W/m K
K_a	2.62×10^{-2}	W/m K

3

3.7 Numerical Methodology

3.7.1 Numerical Technique

In the model, the governing dimensioned partial differential equations (PDEs) were spatially discretised using the numerical technique known as Method of Lines (Hyman, 1977) (semi discretisation). The 80 state variables were solved from simultaneous ordinary differential equations (ODEs) obtained from a 20-point discretisation of equations 3.1, 3.15, 3.23 and 3.37 along the bed length. The spatial derivatives of the resulting ordinary differential equations (ODEs) were approximated by the 2nd order correct explicit central difference scheme in order to minimise the local truncation error associated with derivative approximation. Boundary condition involving derivatives were also handled by a 2nd order correct approximation (Ozisik, 1994).

These equations were written in the dimensional format in order to make meaningful comparison of simulated results with observed data. The step length in the spatial direction was halved to obtain 40 points to ascertain any possible truncation errors. Subsequent simulation indicated no significant change in results, which indicated that a grid independent solution was obtained with a 20-point spatial discretisation.

[3] The parameter values in the table, with the exception of K_{eff}, were obtained from Perry (1973). The parameter K_{eff} was calculated using compost data obtained from Haug (1993).

The flux term (advective term) in the continuity equation required an explicit finite difference (Staple *et al.*, 1966; Havercamp *et al.*, 1977). This scheme involved the application of a 2^{nd} order correct central difference approximation to both the capillary and the gravitational component of the expanded advective term. Furthermore, in the original scheme the interblock conductivity was evaluated using the arithmetic mean of adjoining cells and this was mapped over for the evaluation of conductivity in the present work. In Zaidel and Russo (1992) the arithmetic mean for interblock conductivity computations was said to cause smearing of the wetting (attenuating the steepness) front. Several alternatives, including the use of geometric mean, were proposed for interblock conductivity, and the schemes evaluated using the constitutive relationships of van Genutchen *et al.* (1980) and Havercamp *et al.* (1977). However, these simulations for infiltration with alternative schemes indicated that no universal weighting scheme (interblock calculations) exists to predict accurately the wetting front and that the numerical error associated with these could be minimised using a finer spatial grid. Thus, these findings coupled together with the accurate description of the wetting front of Havercamp *et al.* (1977) using an explicit finite difference scheme coupled with arithmetic mean for interblock computations, prompted a similar scheme to be used for the interblock conductivity in the current work. The stability of the scheme as stipulated by Staple (1966) required the adjustment of the time step size at each integration step in the time domain according to the stability criteria laid out. However, the use of a multi order, multi step numerical integration algorithm (ODE15S), which continuously varied the time step size according to the rate of change of the state variables, alleviated the need to change the step size manually, while providing the desired numerical accuracy. This was confirmed by the close agreement that existed between the simulation of the mixed form of Richards' equation (explicit scheme) and the experimentally obtained water content profiles for infiltration into a sand column by Havercamp *et al.* (1977).

The spatially discretised PDEs were simulated using the Simulink® toolbox in Matlab® by representing the ordinary differential equations (ODEs) in block diagram notation (Appendix C). The principal advantage of using Simulink® was that the system dynamics were graphically animated while the simulation was in progress. This facilitated a better understanding of the system behaviour, while providing the ability to manipulate critical variables simultaneously in order to ascertain the impact of such modifications. Time

domain discretisation was generated with a variable-step ODE solver. The advantage of using a variable-step solver was that it continuously varied the integration step size in the time domain, according to the dynamics of the state variable in order to satisfy error control criteria, and hence minimised possible time truncation errors. Due to the stiff nature of the system, a multi step, variable order (order 2 selected to maintain stability) numerical integration algorithm (ODE15S) was preferred, which decoupled the integration step size from the time interval for output points, while providing the required numerical accuracy. These solvers, based on numerical differential formulas, possessed extra logic to capture the rapid transients present in stiff systems and were also described as being more efficient than those based on Gear's method (Dabney, 1998). Simulations were performed with an Intel® Pentium III, 733 MHz workstation and the CPU time required was generally between 1 and 1.5 hours, which depended on the final integration time, solver selected and error control criteria used.

The discretised forms of the equations were as follows,

Mass Balance for Toluene in the Gas Phase,

$$\left(\frac{dC}{dt}\right)_{j,i} = -U_g \frac{\left(C_{j,i+1} - C_{j,i-1}\right)}{2\delta z} - \frac{(1-\varepsilon)}{\varepsilon}\frac{K_{LDF}}{S_g}\left(q^*_{j,i} - q_{j,i}\right) - \left(\frac{V_m C_{j,i}}{K_m + C_{j,i}}\right)\left(\frac{1-\varepsilon}{\varepsilon}\right) \times \frac{\left(T_f\right)_{j,i}}{S_g} \times \left(M_f\right)_{j,i} \qquad \text{[Eq. 3.46]}$$

Where,

$$T_f = -35.7T^2 + 215.4T - 323.9 \quad , M_f = \frac{2.04(\theta - 0.44)}{0.210 + (\theta - 0.44)} \qquad \text{[Eq. 3.47]}$$

Mass Balance for Toluene in the Solid Phase,

$$\left(\frac{dq}{dt}\right)_{j,i} = K_{LDF}\left(q^*_{j,i} - q_{j,i}\right) \qquad \text{[Eq. 3.48]}$$

Energy Balance for the System,

$$\left(\rho_b C_{pb}\right)_{j,i}\left(\frac{dT}{dt}\right)_{j,i}+\left[\left(\varepsilon S_g U_g\left(\rho_a C_{pa}+h_e\left(0.07T_{j,i}-21.5\right)\right)+\rho_l C_{pl}\left(U_l\right)_{j,i}\right)\frac{\left(T_{j,i+1}-T_{j,i-1}\right)}{2\delta z}\right]$$

$$=K_{eff}\frac{\left(T_{j,i+1}-2T_{j,i}+T_{j,i-1}\right)}{\left(\delta z\right)^2}+h_c\left(\frac{V_m C_{j,i}}{K_m+C_{j,i}}\right)(1-\varepsilon)\times\left(T_f\right)_{j,i}\times\left(M_f\right)_{j,i} \qquad \text{[Eq. 3.49]}$$

Continuity Equation for Liquid Phase (water),

$$\left(\frac{d\theta}{dt}\right)_{j,i}=-\left(\frac{K_{j,i+\frac{1}{2}}\left(h_{j,i+1}-h_{j,i}\right)-K_{j,i-\frac{1}{2}}\left(h_{j,i}-h_{j,i-1}\right)}{\delta z^2}\right)+\left(\frac{K_{j,i+\frac{1}{2}}-K_{j,i-\frac{1}{2}}}{\delta z}\right)+$$

$$K_{Tol}\frac{(1-\varepsilon)}{\rho_l}\left(\frac{V_m C_{j,i}}{K_m+C_{j,i}}\right)-\left(\frac{\varepsilon S_g U_g}{\rho_l}\right)\left(0.07T_{j,i}-21.5\right)\left(\frac{T_{j,i+1}-T_{j,i-1}}{2\delta z}\right) \qquad \text{[Eq. 3.50]}$$

where :

$K_{j,i+1/2}=(K_{j,i}+K_{j,i+1})/2$,

$K_{j,i-1/2}=(K_{j,i}+K_{j,i-1})/2$

The constant flux boundary condition at the upper surface resulted in an algebraic loop at that point, since the tension (h_{20}) evaluated as the output was simultaneously used as an input to the block considered. This problem was addressed using the algebraic constraint block available in Simulink®, where the entire boundary condition was fed as an input signal to the block, which produced an output signal corresponding to the variable concerned (i.e. h_{20}) by constraining the input signal to zero. This essentially involved an iterative numerical technique, where convergence and efficiency of the iteration was dependent on the initial estimate of the variable that was provided to the block.

3.7.2 Inventory Check for Liquid Water and Gas phase Toluene

The numerical accuracy of the simulations was verified by performing a mass balance (inventory check) on the water and toluene on day 4 using the model parameters listed in chapter 5. The mass balance for water calculated the final mass of water on day 4 in the compost bed using the initial mass of water, mass of water added, water drained off, water produced by metabolic activity and mass of water evaporated. This value was compared with the mass of water provided by the water content profile on day 4. The toluene mass balance was also performed in a similar fashion. The water balance error was 0.05% for the upflow mode and 0.01% for the downflow mode while the toluene discrepancy was 0.45%. These values were well within the accepted limits for simulations (Staple, 1966).

The data for the above mentioned calculations consisted of both rate terms as well as terms expressed on a bulk volume basis. Thus, the data required for the inventory check were obtained through integration of the relevant rate terms with respect to time and subsequently in the spatial direction using the Simpson's rule within the Simulink® toolbox in Matlab® software. The latter calculation permitted the evaluation of total quantities of the respective variables along the bed depth. The aforementioned mass balance was performed for a base case (Case 2) and it was assumed that the inventory check for both water and toluene would hold for any point in time under the various boundary conditions simulated.

Chapter 4: Apparatus and Experimental Procedures

4.1 Introduction

The majority of the experimental work performed to ascertain the moisture content effect on degradation has lacked a robust moisture control strategy to regulate the moisture in the material during the progression of the experiment. Thus, moisture content changes in the medium during the degradation process could have influenced the final results. Sensitivity analysis (discussed in chapter 5) indicated that the model was highly sensitive to the shape of the characteristic equation, which correlated the water content effect to microbial activity. Furthermore, during the sensitivity analysis the model performance was also found to be very sensitive to the kinetic parameters in the degradation term. Hence, to investigate the relationship between water content and performance, a batch scale biofilter system coupled together with an accurate moisture control strategy was developed to control water content rigorously during the course of the experiment.

4.2 Biofilter Configuration

The batch recycle bioreactor system (Fig. 4.1 & 4.2) consisted of a stainless steel (SS) reservoir (5 L) and a SS reactor (ID = 79.6 mm, volume = 0.215 L) coupled together with a diaphragm pump (107CD18 - 198A, Thomas Pumps, WI, USA) using a Teflon diaphragm liner. The reactor (Fig. 4.3) consisted of two chambers separated by a ceramic plate permeable to water but not to air. The toluene-laden air recirculated through the top chamber and water was maintained in the bottom chamber at a reduced matric potential. A water reservoir connected to the bottom chamber of the reactor acted as a source and sink for changes in water content of the compost. A 5 mm thick, semipermeable ceramic plate (porous ceramic-0600 series, bubble point pressure 0.5 bar, Soil Moisture Equipment Corp. Goleta, CA, USA) supported the compost in the top chamber of the reactor and provided hydraulic contact between the water in the compost and the water in the lower chamber. Internal sealing was achieved by the use of Viton seals at three different positions in the reactor. Two seals on the top and bottom of the ceramic plate prevented air and water from bypassing the ceramic plate. A metal insert applied the appropriate pressure on these two seals. A third seal on the reactor lid limited gas exchange with the environment.

Moisture content in the compost was regulated based on the principle of a suction cell (Klute, 1986). This was achieved by changing the elevation of the water reservoir with respect to the ceramic plate. When the reservoir was placed below the level of the ceramic plate in the reactor, water did not drain from the lower chamber into the reservoir since the ceramic plate was not permeable to air and therefore the absolute pressure in the water in the chamber was below atmospheric pressure. The principle is the same as water being unable to drain from a vertical tube when the upper end is closed. The lower the reservoir was below the ceramic plate, the greater the vacuum applied to the water in the lower chamber.

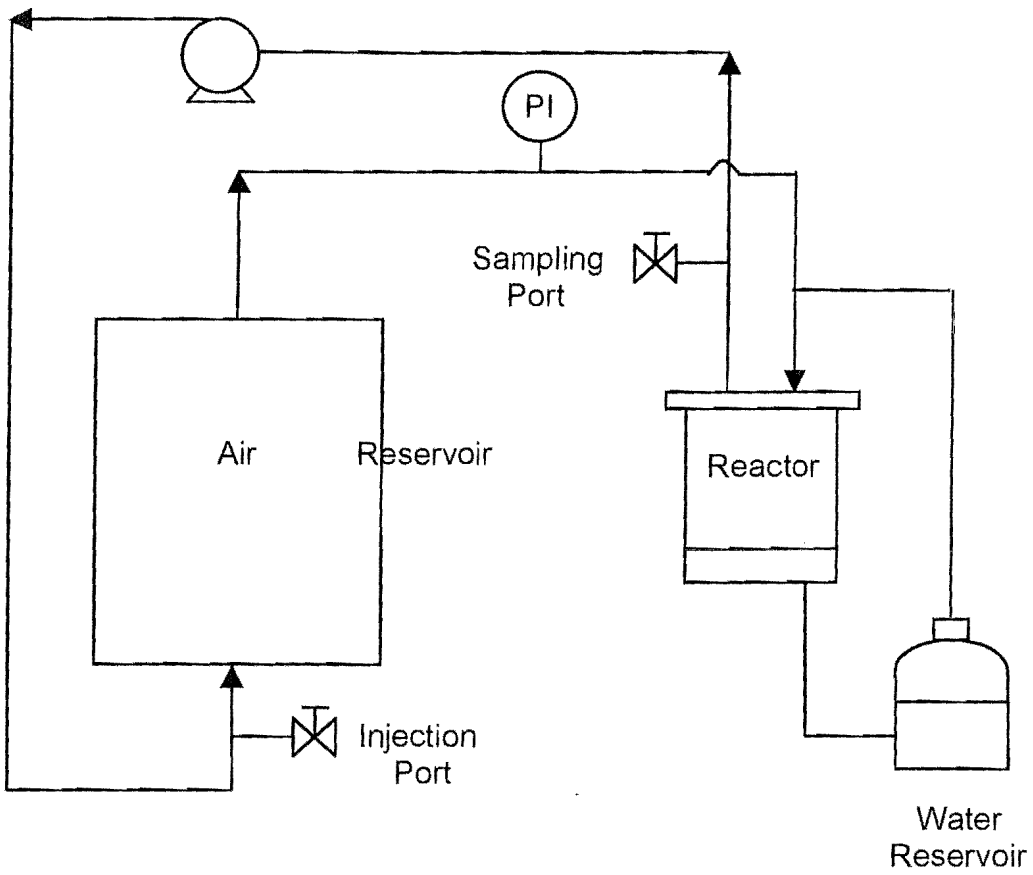

Figure 4.1 Schematic diagram of the batch biofilter system used for rigorous moisture control. PI is a water manometer used for both pressure indication and as a pressure relief valve.

Since the water associated with the compost was in equilibrium with the water in the chamber by way of the ceramic plate, increased vacuum caused a lower matric potential in the compost and thus lowered the water content. In addition, the water chamber compensated for changes in water content in the compost. Excess water deposited in the compost drained away and drying caused water to flow from the water chamber into the compost. This mechanism thus ensured that medium moisture content was maintained at the value corresponding to the matric potential applied as governed by the water release curve for Organix compost (see "Section 4.4.3"). The headspace of the water reservoir was connected to the reactor headspace to alleviate minor pressure changes in the recycle system. Slight changes in the reactor pressure effectively changed the matric potential applied to the compost if not coupled to the water reservoir headspace.

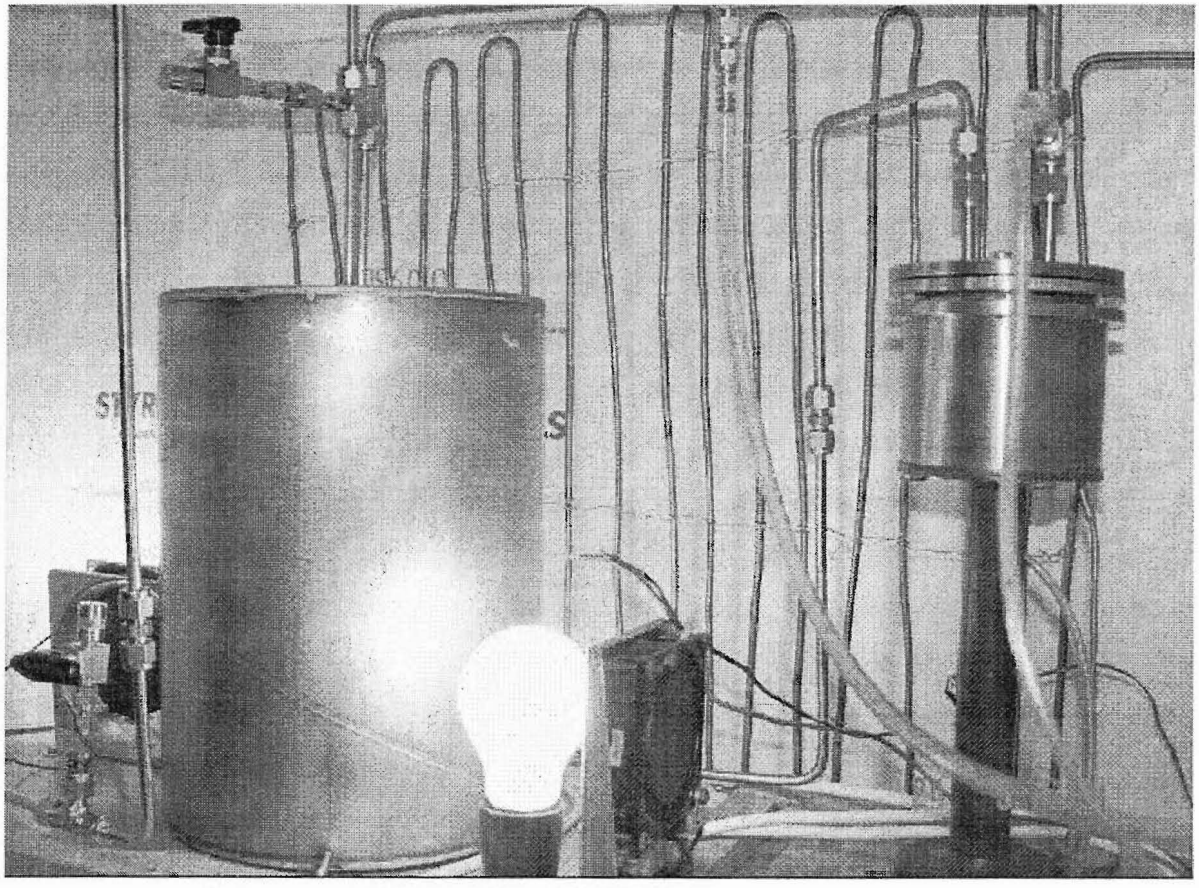

Figure 4.2 Digital image of the experimental set-up

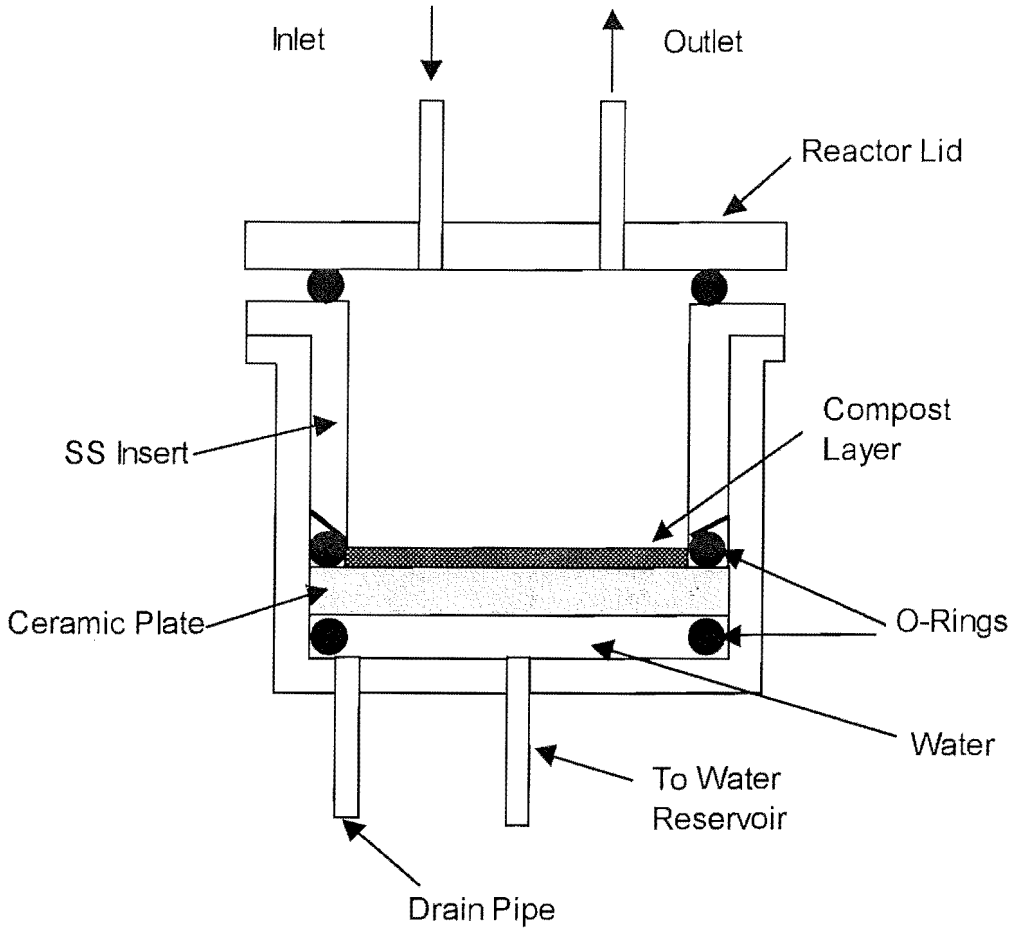

Figure 4.3 Detailed diagram of the reactor shown in Fig. 4.1, which controlled moisture content in the compost using the suction cell principle

The reactor, vessel and the pump were connected together using 1/4" SS tubing and appropriate pipe and compression fittings. The injection and sampling ports were isolated with a ball valve (Swagelok, B-41S2) to minimise septum degradation by toluene. Both ports also contained 1/8" SS septum injector nuts (Valco Instrument Co. Inc.). The apparatus was isolated from the lab atmosphere using an insulated box. Low-pressure water at a flow rate of 15 ml/s flowed through a copper coil located at the back of box to provide the required cooling. Temperature within the box was regulated with a temperature controller (Shinohara Electrical Inst. Works Ltd) coupled together with two 100 W bulbs to 30 ± 0.5 °C. The cooling load on the system made it less susceptible to external temperature changes coupled with the heat from the fans. The internal

temperature was monitored using a thermocouple. Two rotary fans were used ensure a uniform distribution of temperature within the closed box. A water manometer located adjacent to the reservoir on the pipeline served both as a pressure relief mechanism and as a leak detector. An additional manometer was attached to the reactor inlet to monitor reactor headspace pressure.

4.3 Batch Recycle Operation

A batch recycle operation with a high recycle flow rate (high mixing) and a small reactor volume with respect to the total volume of system, ensured a minimal conversion per pass in the reactor (Smith, 1981). The resulting uniform temperature and composition provided a differential type operation and facilitated the calculation of a point reaction rate valid within the reactor (Carberry, 1964, Govind *et al.*, 1997). A similar differential biofilter was used by Deshusses (1994) to determine the kinetic parameters for MEK and MIBK degradation while a differential bioreactor was also used to ascertain the biodegradation kinetic parameters for methanol and α-pinene by Mohseni and Allen (2000). The advantage of selecting a gradientless reactor was the ease in interpreting experimental data in the absence of temperature and composition changes (Borman *et al.*, 1994). The turbulence created by the high flow rate (22.6 litres/min) facilitated a negligible external and inter-particle mass transfer resistance.

Govind *et al.*, (1997) used a differential micro-biofilter to obtain the biokinetics for five substrates. A micro-bioreactor was selected over a suspended cell experiment due its compatibility with full-scale reactors in terms of the immobilised nature of the biomass. In this case an experimental set-up incorporating a reservoir, peristaltic pump and a jacketed micro-biofilter with provisions for nutrient supply and piping was used. Packing material (Celite) from a large-scale biofilter unit, under steady state operation was used as the bed medium.

4.4 Control Tests

4.4.1 Leak Testing

The initial system consisted of ¼" copper tubing connected together with brass compression fittings. However, due to the ductile nature of copper coupled together with frequent assembling/dissembling, the tubing was subjected to wear and tear. This potentially caused leaks along the lines, which required the tubing to be replaced quite often. Hence, for subsequent operation SS tubing was substituted. At the initial stages the reservoir in the system consisted of a glass vessel of 10 L volume, which contained an additional inlet that was sealed using a Teflon liner. Control studies involving pressurising indicated the vessel to be a source of leak, which resulted in its replacement with a SS cylindrical reservoir. Furthermore due to the low pressure nature of the application the original piston pump (607CD22, Thomas Pumps, WI, USA) was subject to leak and hence was replaced.

Extensive leak testing was thus performed to detect the presence of leaks on the differential biofilter system. An approach where the different components were separated and leaks isolated was pursued. Thus, the system was separated into three parts comprising of the tubing, reservoir and pump and each individual unit subjected to pressurising and subsequent application of Snoop (Nupro Company, Ohio, USA). Once preliminary testing was completed each of the above units were also pressurised and submerged in a water tank to detect any possible leaks. In each instance the in-house compressed air supply was used for pressurising purposes. Creating a leak-free system was more difficult than expected for this low-pressure application.

4.4.2 Abiotic Losses

A toluene control test was carried out without compost, to identify any non-biological loss that could occur in the system. The system was initially charged to a concentration of 1000 ppm_v and 0.5 ml samples were taken using a 1 ml gas syringe (SGE, Australia). Sampling was performed at intervals of 3-4 hours for a period of 70 hours and analysed using gas chromatography, which indicated no loss of toluene. Independent sorption experiments using microbially inhibited compost indicated that the mass of toluene sorbed to the compost represented only 1% of the initial mass loaded for each run.

4.4.3 Moisture Content Controls

An independently generated soil water retention curve for compost (wetting curve only) related the matric potential to the physical water content. During degradation experiments, dry weight analysis of the reactor compost was performed using a moisture analyser (Sartorius, MA-30). Comparison of the results from the destructive test and those from the water retention curve for a specific matric potential indicated that the difference was within the measurement error for dry weight analysis (± 2-5 %). This confirmed that the moisture content corresponding to the matric potential applied was maintained during the course of the experiment.

4.4.4 Oxygen Limitation

The oxygen content within the system declined with each run (Appendix B). However the final concentration profile for toluene was always obtained within 4-5 runs when the O_2 concentration had not significantly changed. However, if the system were to be operated at a higher initial concentration for extended runs, the supplemental oxygen addition would have to be considered.

4.5 Operational Procedure

The experiments used "Organix" compost (Parkhouse Garden Supplies™, Christchurch, NZ), based on pig manure and sawdust starting material. The compost was sieved to eliminate particles greater than 3 mm. Addition of nutrients or inoculation with microbial cultures was not performed. The compost depth was limited to a 2 mm layer of compost (≈ 3 g) to ensure uniform water content and to minimise toluene concentration profiles within the compost layer. Distilled/de-aerated water minimised the formation of air bubbles at the water/ceramic interface in the lower chamber.

Initially, the water reservoir was lowered 60 cm below the ceramic plate and a syringe was connected to the drainpipe and used to pull water into the lower chamber of the reactor from the reservoir. The sieved compost (moisture content 1.44 g H_2O/g dry compost) was added onto the surface of the ceramic plate and lightly compacted to give good contact with the plate and between the particles to facilitate water movement. Thereafter, the water reservoir was raised to obtain the required matric potential and the system was allowed to equilibrate for 2-5 days. Equilibrium moisture contents

corresponding to the matric potential applied (-6, -16, -26, -36 cm H_2O) were obtained by adjusting the water reservoir to the appropriate height in relation to the compost layer in the reactor. A 30 °C controlled temperature environment was used, due to the temperature dependence of the water retention curve and microbial activity (Devinny *et al.*, 1999; Liu *et al.*, 1993; Hopman *et al.*, 1986). Liquid toluene was injected into the system using a 100 µl syringe (SGE, Australia) to give a gas phase concentration of 1000 or 250 ppm_v.

Degradation profiles for toluene were thereafter obtained for a range of tension values by sampling the headspace at various time intervals. Initially for the -16 cm H_2O matric potential, the starting gas phase concentration was 1000 ppm_v. However, potential inhibitory effects on the microorganisms and possible oxygen limitation under a high loading prompted the use of 250 ppm_v concentrations in subsequent runs. The microorganisms in fresh compost took 4-5 days to acclimate to toluene. During the experimental runs, water was flushed through the lower chamber of the reactor every 2-3 days to purge any air bubbles formed between the ceramic-water interface. This procedure was performed as the dissolved air in water tended to cause poor hydraulic contact between the ceramic plate and the bulk water in the lower chamber by the formation of an air layer beneath the ceramic plate.

4.6 Gas Chromatography Analysis

Toluene concentrations in the gas phase were measured using a Varian Star 4800 gas chromatograph/workstation (Varian-Chromatograph Sys, Walnut Creek, CA, USA), which contained a capillary column (Alltech, head pressure 20 psi, 60 m), injector (1078 universal capillary injector, split/splitless) and a flame ionisation detector. The gas chromatograph (GC) was operated under a column temperature of 150 °C, injection temperature of 280 °C, detector temperature of 280 °C and in the split-less mode. For optimum performance of the detector, dry air pressure was maintained at 80 psi, helium pressure at 70 psi and hydrogen pressure at 50 psi. A calibration curve (Fig.4.4) was prepared, which consisted of concentrations of 1000, 750, 500, 250, 100, 50 and 10 ppm_v respectively. In this case, 0.5 ml gas samples from Teflon bags (Alltech, IL, USA) containing equilibrium concentrations were injected into the chromatograph using a 1 ml syringe (SGE, Australia).

This exercise was repeated until a consistent result was obtained with regard to the area counts from each bag. In order to maintain the accuracy with regard to actual concentrations achieved within the bags, the liquid syringe was weighed before and after the injection and concentration achieved within the bags computed using the ideal gas law.

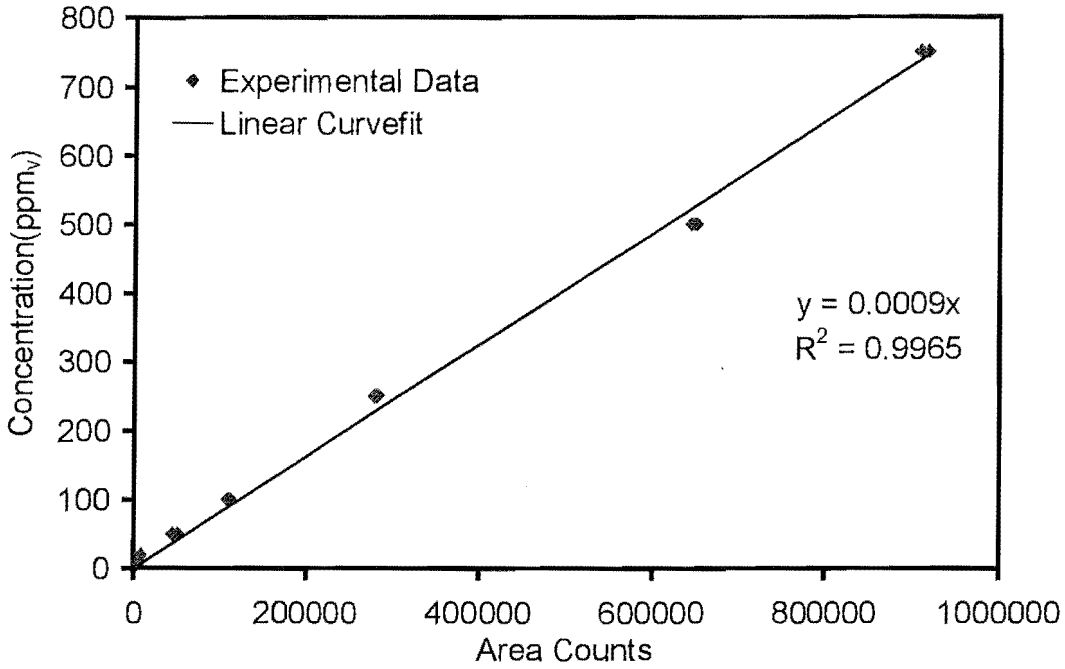

Figure 4.4 Calibration curve for toluene.

4.7 Adsorption Experiment

The adsorption isotherm of toluene on compost was obtained using batch scale studies. For these studies, the microbial consortium present in the compost was deactivated using mercuric chloride ($HgCl_2$) as opposed to using steam sterilisation. Literature (Wolf *et al.*, 1989) revealed that a major drawback in using autoclaving was the alteration of soil physical and chemical properties. These variations encompass the changes associated with the surface area and cation exchange capacity/pH respectively. Thus, as the aforementioned changes could give rise to erroneous results in terms of adsorption capacity of the bed media, it was decided to use 500 μg of $HgCl_2$/g of compost to effectively eliminate the microbial population in compost (Apel *et al.*, 1993). The moisture content of the compost was ascertained using a moisture analyser (Sartorius MA 30) where the drying temperature was set to 105 °C. Prior to the experiments the bottles and the caps were autoclaved at 120 °C for 15 minutes in an autoclave (Type AC-48, New

Brunswick Scientific, Edison NJ, USA). The samples with $HgCl_2$ were left for a period of 24 hours prior to the addition of toluene, to ensure that all microbial activity was effectively eliminated. A destructive test approach was taken to ascertain the isotherm for a particular concentration. A batch of 24 ml serum bottles closed with silicon septa faced with Teflon and plastic screw-on caps were filled with 1 g of the deactivated compost. The required liquid toluene was injected using a 1 µl syringe (SGE, Australia). The bottles were kept in a constant temperature water bath. Single headspace samples were taken at different time intervals (1, 3, 5 hours) from each of the bottles to ascertain whether equilibrium has been reached. Only one sample was taken from each bottle and the bottle then removed from the bath. Samples were subjected to GC analysis to determine the toluene concentration in the headspace. This procedure was repeated for contaminant concentrations reaching $1000ppm_v$. In order to satisfy the safety guidelines associated with using a toxic compound, the water bath containing samples was kept inside a fume cupboard (Smoothflow, Calibre Plastics Ltd, Auckland NZ) for the entire duration of the experiment. Furthermore, to ensure a uniform temperature distribution profile inside the bath the liquid water was stirred using a variable speed stirrer (Gallenkamp, 10 speed).

Chapter 5: Open Loop Model Performance

The model developed in this study was applied to explore moisture control, in a generic biofilter set-up subject to different operating conditions. The system was simulated with gas flow upwards and hence the 0 cm level corresponded to the bottom and 100 cm to the top of the column respectively. Open loop irrigation strategies (constant water addition rates) were implemented and performance under each scheme was evaluated in terms of removal efficiency and leachate produced. A sensitivity analysis was also performed to determine parametric sensitivity under steady state behaviour.

5.1 Case 1: Performance Under High Loading (Low Water Flux)

This simulation incorporated a high toluene loading (60 g/m^3h) with a constant water flux of 0.0546 g/m^2s. This flux value was chosen to maintain the bed moisture content near start up values and also ensure dynamic equilibrium of the system around day 10 when the system was operated at a lower loading (Case 2). This also ensured that Case 1 and Case 2 were performed under similar flux values.

Table 5.1 Parameter values for Case 1.

Parameter	Value	Units
Length	1	m
Diameter	0.05	m
EBRT	1.45	min
Interstitial Gas Velocity	4.7	m/min
Inlet Toluene Concentration	1.5 (400 ppm_v)	g/m^3
Toluene Loading	60	g/m^3h
Inlet Temperature	298	K
Bed Porosity (ε)	0.645	-
Gas Phase Porosity (εS_g)	0.145	-
Initial Moisture Content	0.5	m^3/m^3
Initial Gas Phase Concentration	0	g/m^3
Initial Solid Phase Concentration	0	g/m^3

The relatively high mass loading (60 g/m^{3}h) caused a drying front to originate at the column inlet (left side of Fig. 5.1). The exothermic bioreaction increased the local temperature, which increased the absolute humidity of the surrounding air. The humidity increase stripped water from the solid phase. Water was added from the top continuously and the moisture content rose slightly at the top of the bed (right side of Fig. 5.1). However, the water flow was insufficient to redistribute through the bed rapidly, and the bottom half of the bed experienced continued moisture loss until the system reached an equilibrium after 25 days.

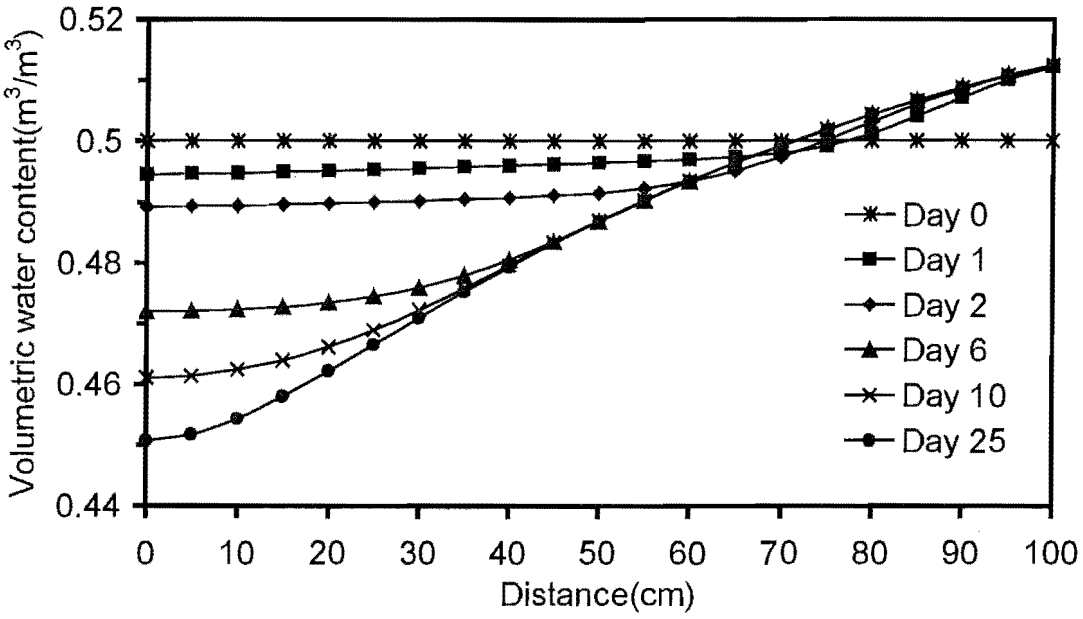

Figure 5.1 Variation of water content along bed depth for Case 1

The effect of the dynamics of water content changes on gas phase toluene concentration was quite evident in Fig. 5.2. Initially the removal efficiency was 32% but as the compost medium started to lose water from the gas inlet region of the column, the local biological activity was retarded and as the simulation progressed, the inlet region's microbial activity tended to decrease. An increase in the gas phase toluene concentration in that region and an overall decrease in the removal efficiency occurred as a result and at day 25 the efficiency was 26%.

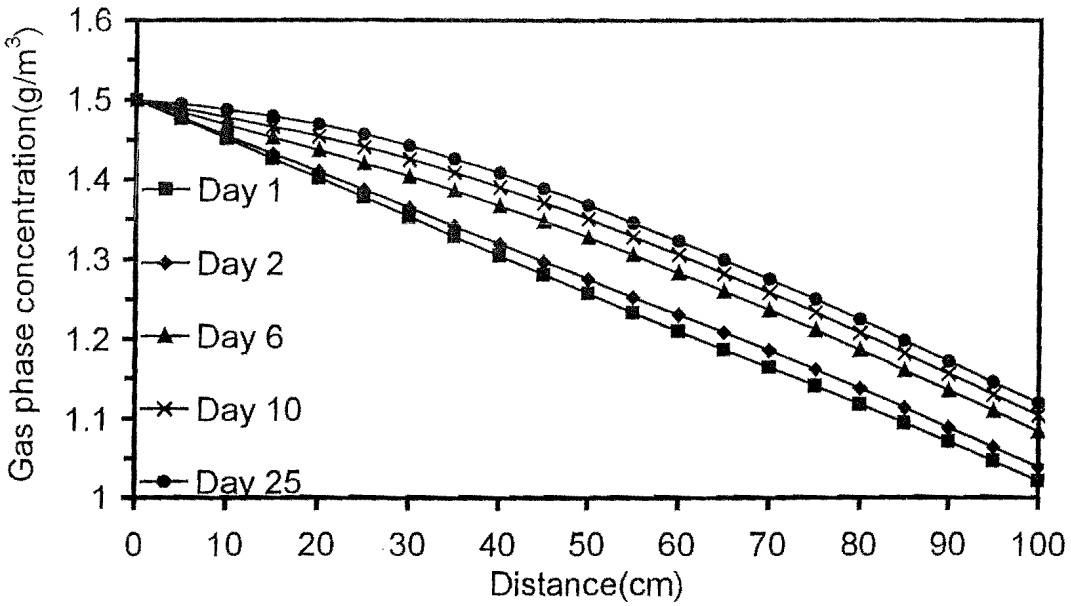

Figure 5.2 Concentration profile of toluene along the bed length for Case 1.

The temperature gradient across the bed decreased with time (data not shown). The upper regions of the bed initially experienced an increase in temperature, which was predominantly due to heat generation in the lower regions of the column. However, the loss of moisture and subsequent retardation of microbial activity in the inlet region of the bed limited the exothermic heat release and caused the temperature profiles across the bed to decline.

There was a close relationship between the water content and microbial degradation in the column. At the initial stages of the simulation run (day 1), the microbial activity was uniformly distributed along biofilter bed. However, as a consequence of the moisture loss, the activity in the inlet region decreased and by day 6 the cumulative loss of moisture in the inlet region forced the bulk of the activity to occur in the upper regions of the column, which yet contained substantial moisture (Fig. 5.3). The outlet region eventually achieved a higher specific degradation rate due to the higher contaminant concentration present from the lower activity of the inlet region. The simulation reached dynamic equilibrium around day 25 and the bulk of the degradation occurred in the upper region of the column.

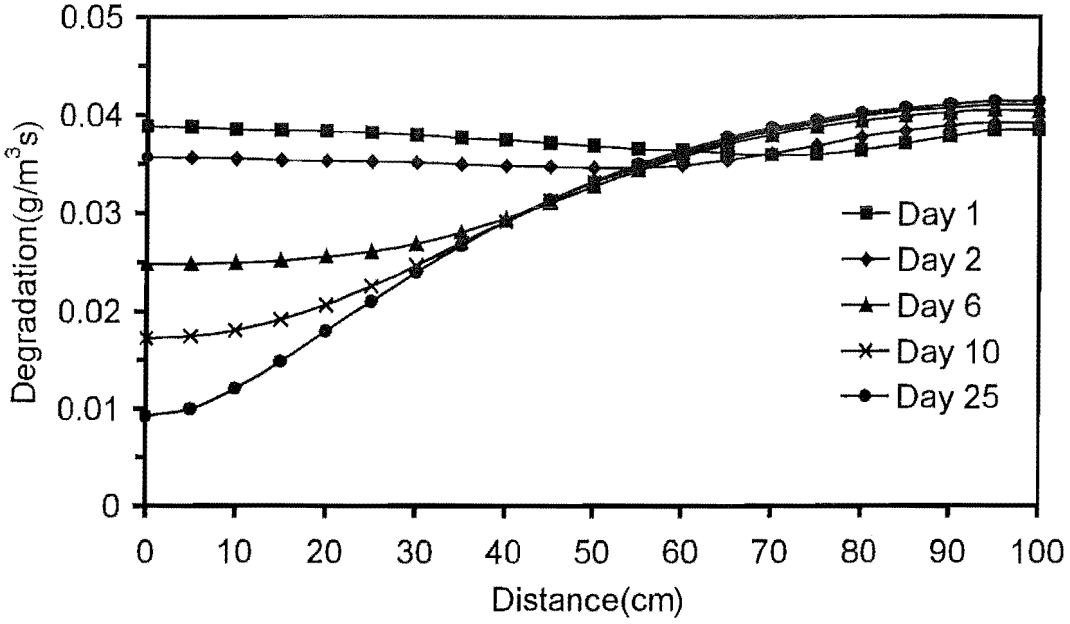

Figure 5.3 Degradation profile of toluene along bed length for Case 1.

A similar pattern of behaviour for a moving moisture and degradation front was observed experimentally (Gostomski *et al.*, 1997; Striebig *et al.*, 2001). The eventual shift in microbial activity to the upper regions was attributed in both cases to the evaporative moisture losses arising from microbial activity and, thus agreed with the model results. Model simulations by Mysliwiec *et al.* (2001) using a 1 m long, low hydraulic conductivity bed with controlled irrigation also demonstrated drying. In this case, a high mass loading of toluene (80 g/m^3h) at 100% RH resulted in the permanent drying of the first 20% of the bed with a complete loss of microbial activity. However, further drying was eliminated due to the addition of water.

The liquid velocity profile was strongly influenced by the local moisture content in the bed. As the inlet region of the bed dried up, the liquid velocity declined and, around day 10, the water in the inlet became essentially stationary (Fig. 5.4). Furthermore, propagation of the drying front and subsequent loss of moisture caused the middle regions of the bed also to experience a reduction in the local velocity. In this case the top of the bed had the highest liquid velocity because of constant water addition. A similar observation regarding the close relationship between local moisture content and liquid velocity was made by Mysliwiec *et al.* (2001).

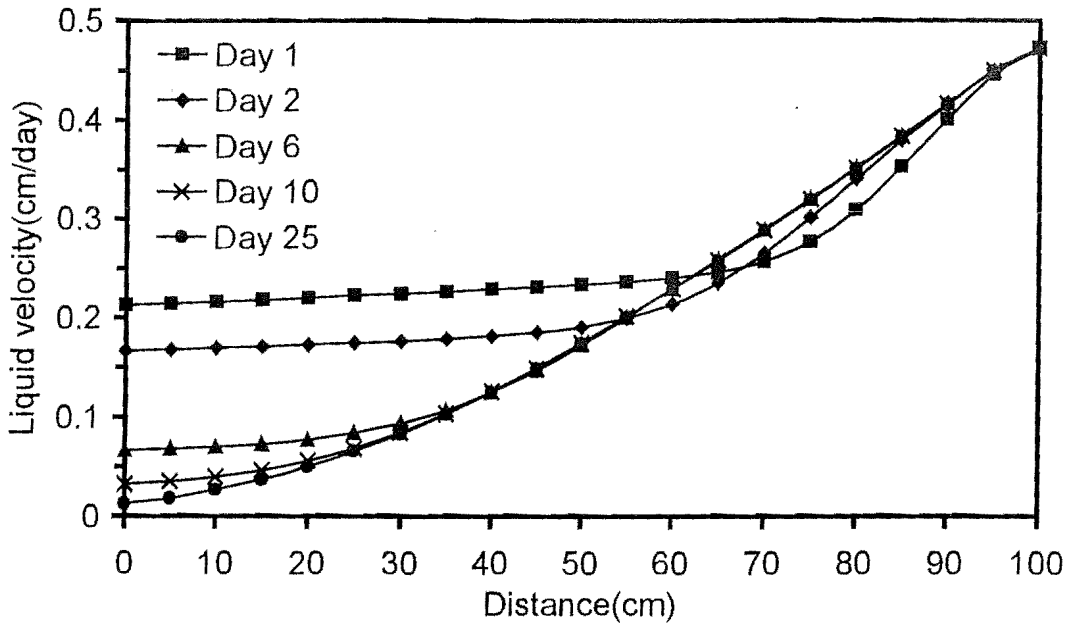

Figure 5.4 Liquid velocity profile along the bed length for Case 1

5.2 Case 2: Performance Under Low Loading (Low Water Flux)

Case 2 used a lower organic loading than Case 1 as might be generated by increasing the residence time by using a larger biofilter for the same air stream. Thus, the mass loading was lowered by a factor of five to 13g/m^{3}h (Table 5.2).

Table 5.2 Parameter values for Case 2.

Parameter	Value	Units
Length	1	m
Diameter	0.1	m
EBRT	6.8	min
Interstitial Gas Velocity	1	m/min
Inlet Gas Concentration	1.5 (400 ppm$_v$)	g/m^3
Gas Loading	13	g/m^{3}h
Inlet Temperature	298	K
Bed Porosity (ε)	0.645	-
Gas Phase Porosity (εS_g)	0.145	-
Initial Moisture Content	0.5	m^3/m^3
Initial Gas Phase Concentration	0	g/m^3
Initial Solid Phase Concentration	0	g/m^3

In this scenario during the initial stages (day 1 & 2), a drying front propagated from the inlet region (Fig. 5.5). However, in marked contrast to the previous case, the wetting front counteracted the drying front and the water content at the air inlet began to recover by day 10 after initial losses but was still less than the original water content. The system reached a steady state by day 10 compared to day 25 for Case 1 and overall this case indicated little water content change over time. Therefore, no shifting of the microbial activity from the air inlet region occurred over time. Thus, at steady state the system achieved a removal efficiency of 88% (Fig. 5.6). The higher removal as compared to Case 1 was attributed to the increased residence time (lower interstitial velocity), which resulted in a lower evaporative moisture removal. Hence, the resulting greater bed moisture content, which prevailed at steady state, coupled together with the sensitivity of Eq. 3.9 to moisture and concentration, permitted a higher removal to be attained.

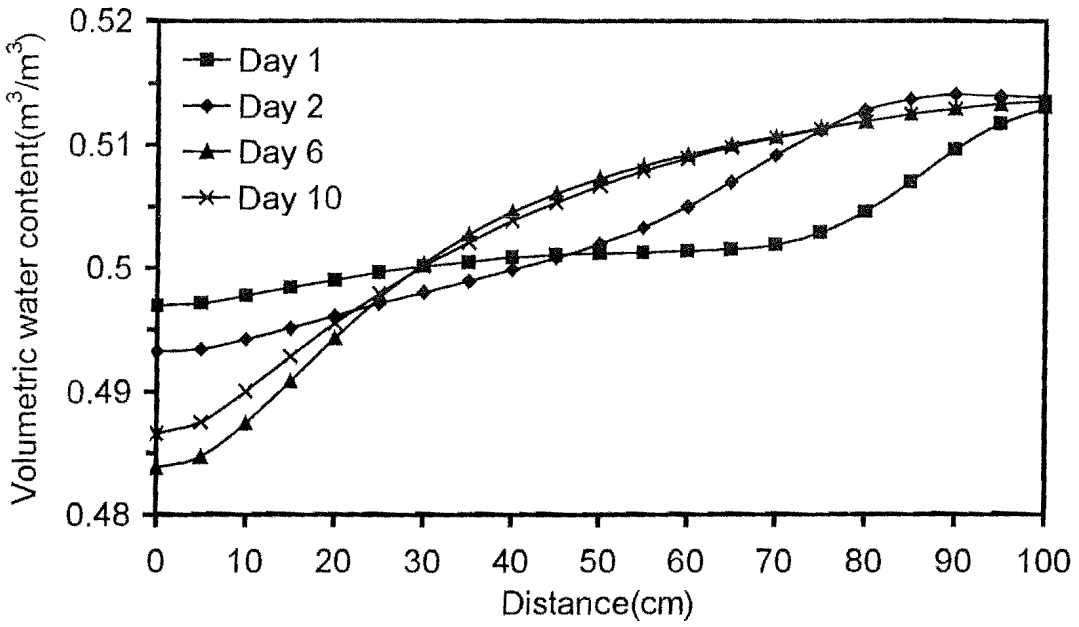

Figure 5.5 Variation of water content along the bed length for Case 2

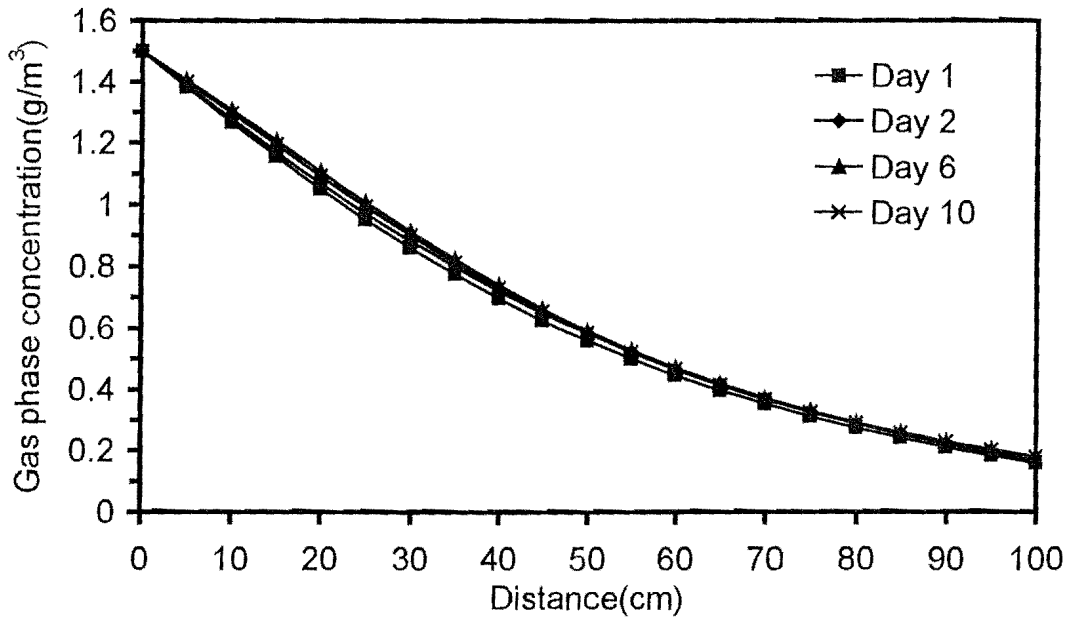

Figure 5.6 Concentration profile of toluene along the bed length for Case 2

The evolution of the temperature profile for the bed over time is depicted in Fig. 5.7. The upper half of the bed initially experienced condensation due to the cooler compost present. However, the upper regions of the bed increased in temperature due to the removal of heat from the metabolically active lower regions of the column and by day 10 there was a 10 °C increase at the gas outlet.

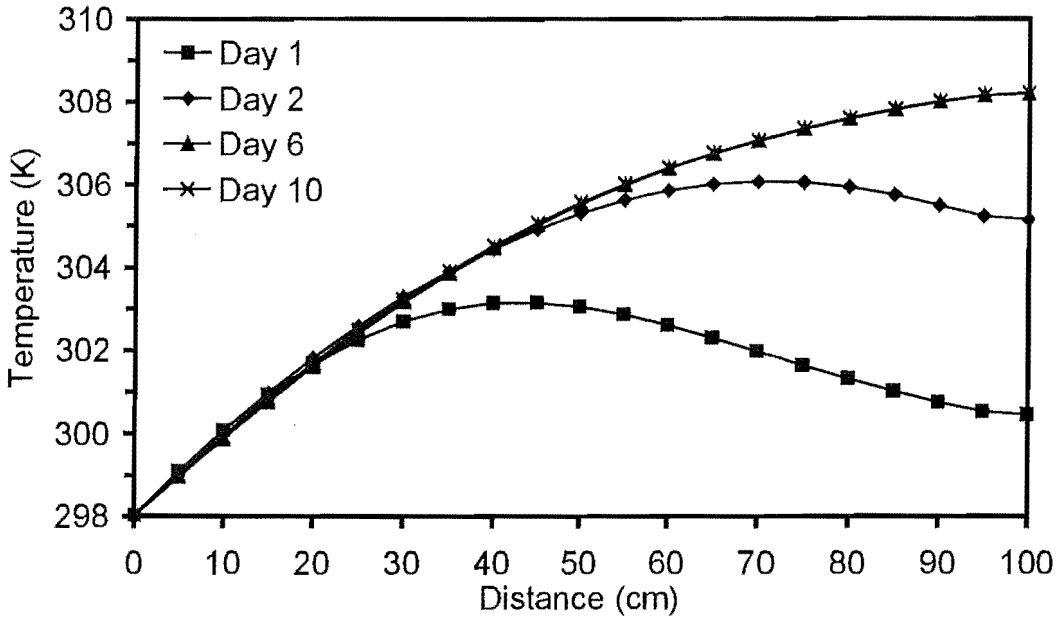

Figure 5.7 Temperature profile along the bed for Case 2

5.3 Case 3: Performance Under Low Loading (High Water Flux)

Case 3 tested the effect of higher water addition rate by raising the flux by an order of magnitude (0.821 g/m^2s). The parameters and initial values were the same as Case 2 except the higher water addition rate. Analysis of the water content profile (Fig. 5.8) indicated a wetting front that moved quickly through the column. This was attributed to the presence of large capillary gradients (high surface flux) in the upper regions of the column. Although a slight drying front developed in the inlet region, it did not propagate into the bed as in earlier cases (Case 1 & 2). Therefore, the higher liquid addition rate was successful in counteracting the moisture loss from evaporation. A significant aspect of this case was that the bed equilibrated to a higher water content (0.58 m^3/m^3) on day 6, which results in a higher removal efficiency of 97%. However the leachate rate was approximately twenty times more than in Case 2. This excess leachate could be a

hazardous waste in some biofilter applications, and it could strip valuable nutrients from the biofilter medium.

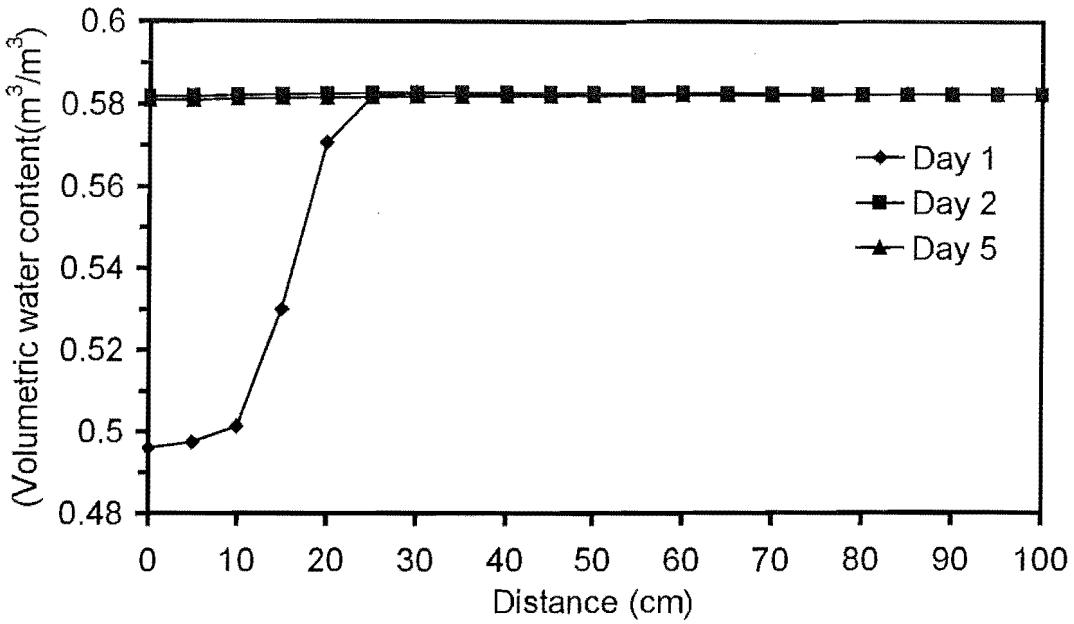

Figure 5.8 Variation of water content along the bed length for Case 3

5.4 Sensitivity Analysis

This model structure allowed all the parameters to be determined independently and contained no fitting coefficients. However for the purpose of this work, some parameters were assumed and some were less accurately known than others. To explore the effect of these assumptions, a sensitivity analysis of the various parameters on the steady state removal efficiency was performed, using the lower loading as the base case for comparison (Table 5.2). This included both quantitative and qualitative analysis of parameter effects on removal efficiency. All model parameters were investigated in this study but only parameters with known significance or those particularly difficult to measure are discussed in this chapter.

5.4.1 Moisture Content Effect on Microbial Activity

The model was very sensitive to the variations in the biological degradation parameters in Eq. 3.10. Doubling the maximum degradation rate (V_m), increased the removal efficiency from 88% to 99%. A decrease in the above parameter by 75% and 50% resulted in removal efficiencies of 40% and 65% respectively. Doubling the half saturation constant (K_m) caused the removal efficiency to drop from 88% from 68%. An increase in the removal efficiency to 99% from that of the base case value of 88% was observed for a 75% decrease in the above parameter. Since microbial activity was the driving force for the system, the sensitivity of the parameters describing the specific activity was unsurprising.

The water content effect on microbial activity probably contained the least defensible assumptions due to the extrapolation of the available quantitative data (Acuna *et al.*, 1999). Changing the structure of the relationship from sigmoid (Eq. 3.13) to Langmuir or exponential showed the model was very sensitive to the actual form of the function (Fig. 5.9). In this case the Langmuir-type relationship provided an 8% increase in removal efficiency, while the exponential correlation provided a 60% decrease in performance from that of the base case. Unsurprisingly, adjusting the parameters of the sigmoid relationship had an equally large effect. Also, increasing the initial bed moisture content (S_w) by 14% increased the removal by 11%, however the absolute value of initial moisture content was somewhat arbitrary and the outcome was related to the form of Eq. 3.13. Thus, the moisture content effect was an extremely important parameter for model performance and was subsequently, experimentally verified (Sec. 8.3).

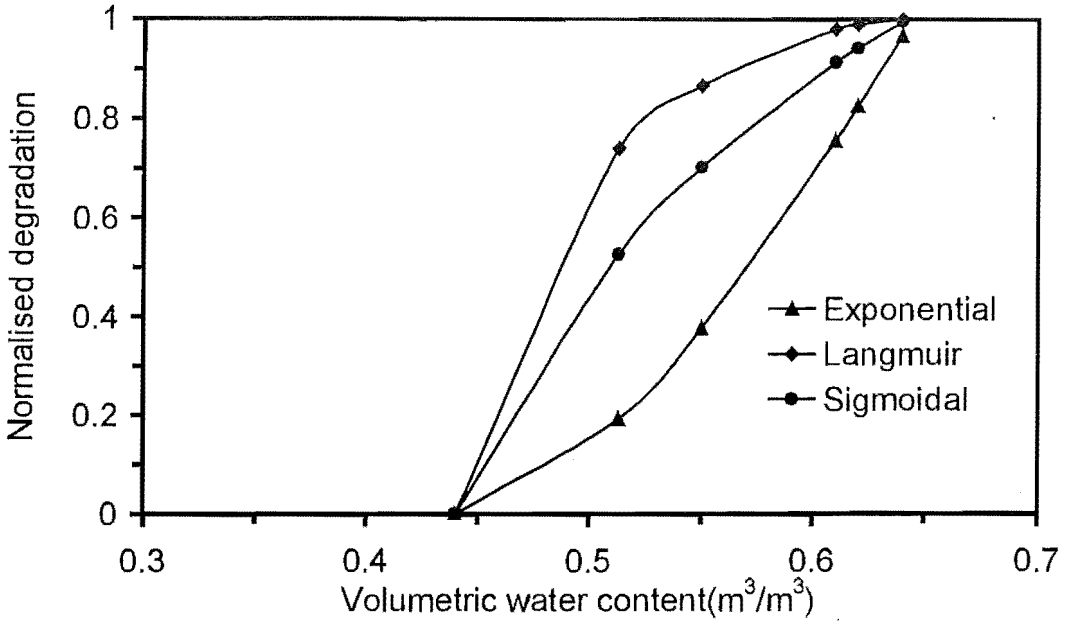

Figure 5.9 The characteristic curves correlating the moisture content to degradation

5.4.2 Unsaturated Hydraulic Conductivity

Contrary to expectation, increasing the unsaturated hydraulic conductivity by an order of magnitude (which might be obtained by changing compost type or bulking agent) yielded no significant change (0.5%) in removal efficiency. This indicated that a change in the compost medium does not necessarily result in a rapid redistribution and subsequent increase in local water content required for attaining higher removal efficiencies. This was undoubtedly due to the highly non-linear relationship between matric potential and hydraulic conductivity common to most porous media, including compost (Fig. 3.3)

5.4.3 Temperature Effect on Microbial Activity

The establishment of temperature profiles from convective and evaporative heat transfer influenced the local degradation rates in the model, which contained a temperature dependence term. However, comparison of degradation along the column indicated that temperature affected bed performance very little. Eliminating the temperature dependency on microbial activity *(T_f)* increased the removal efficiency from 88% to 90%. Therefore using literature correlations was reasonable.

5.4.4 Effective Thermal Conductivity of Bed

In order to ascertain the influence of the effective thermal conductivity (K_{eff}) on model performance, the above parameter was varied by 50%, 200% and 400% from the base case value. For the larger parameter values there was no change in both the steady state and transient response of the system. A slight decrease of steady state RE (1%) was observed for the smaller values and was attributed to minimal contribution of conduction at this stage to heat transfer. This effectively resulted in a local temperature rise that retarded the degradation. The implication from this was that conduction played a very minor role and that heat transfer within the bed was governed mainly by evaporative and convective heat removal.

A summary of the sensitivity analysis performed on key model parameters is given in Table 5.3.

Table 5.3 Model sensitivity to key parameter values

Property	% Change in parameter[1]	Sensitivity as measured by removal efficiency of model[2]
Maximum degradation rate (V_m)	100	99
	-75	40
	-50	65
Half saturation constant (K_m)	100	68
	-75	99
Moisture content effect on microbial activity[3]	Langmuir	96
	Exponential	28
Water content effects at start-up (S_w)	14	99
Temperature effect on microbial activity[3]	Ignored the temperature dependence	90
Effective thermal conductivity (K_{eff})	200	88
	400	88
	50	87
Unsaturated hydraulic conductivity (K)	1000 (Order of magnitude)	88.5

[1] The percentage change in parameter from that of the base case was recorded.
[2] Provides the removal efficiency of the system under the parameter change introduced. The base case removal efficiency was 88%.
[3] A qualitative change in the parameter was performed.

5.5 Case 4: Performance under Downward Flow (Low Loading)

Although the bulk of full-scale biofilters tends to operate in an upflow mode, literature (Devinny, 1999) indicates certain benefits associated with the down flow mode of operation. A particular benefit arising from down flow operation is better moisture control. This effect could be quite influential in the performance of a biofilter as this option would help to achieve higher removal through better moisture control in the more biologically active air inlet region.

A downflow biofilter operation was simulated with the same parameters and water flux as in Case 2. In this case the 0 cm level corresponded to the water and gas inlet (top of the column) while the 100 cm level referred to the bottom of the column. Analysis of the moisture distribution profile (Fig. 5.10) on days 1-2 indicated a slight increase in local water content in the lower half of the bed, which could be attributed to local condensation caused by the cooler compost.

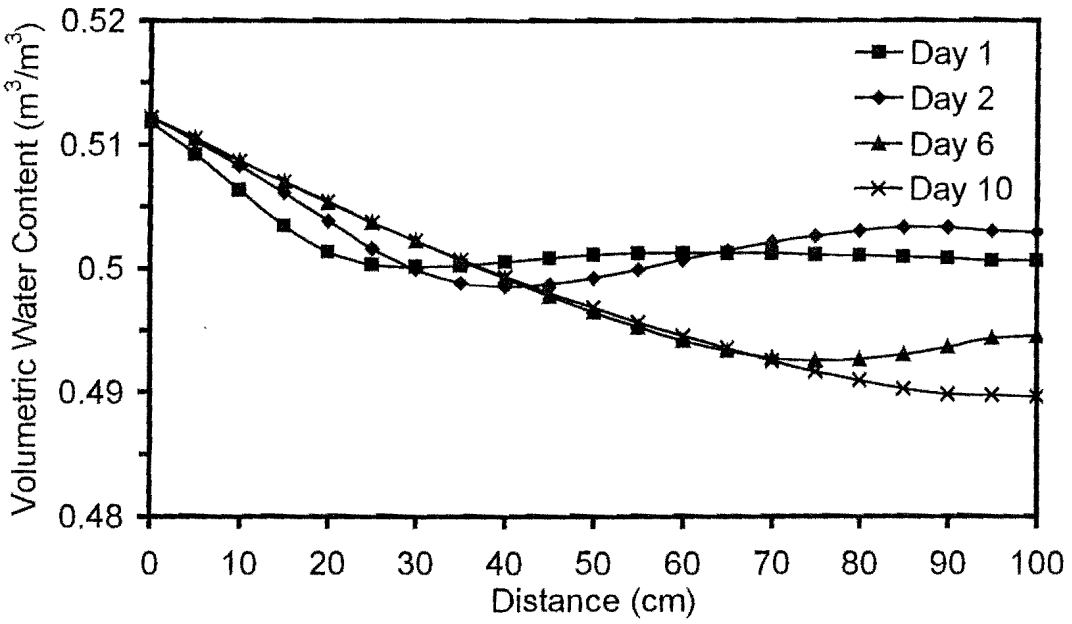

Figure 5.10 Variation of water content along the bed length for Case 4

However, subsequent warming up of these regions from convective and evaporative heat, resulted in the evaporation of this excess moisture and a decrease in the local moisture content was observed on days 6-10 as a result. This system also reached steady state with respect to the key variables around day 10. The temperature profile for the bed depicted a similar pattern of behaviour as in Case 2 with the second half of the bed experiencing an initial lower temperature. However, this was subsequently followed by an increase in temperature that was attributed to the warming effect from convective and evaporative heat removed from the metabolically active upper regions of the bed.

5.5.1 Comparison of Upflow Vs Downflow

For the majority of mass loading no significant difference in EC was observed between upflow and downflow modes of operation (Fig 5.11).

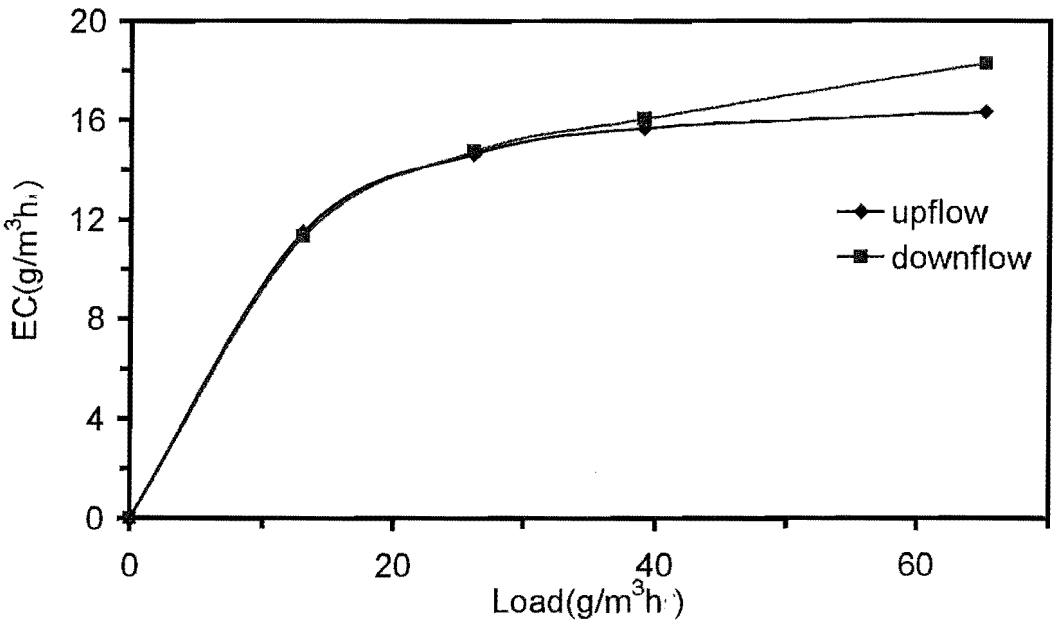

Figure 5.11 The variation of EC with load.

This was attributed to the fact that, although the inlet attained a higher degradation rate under downflow mode due to better moisture control, the local degradation rates and concentrations (Fig. 5.12) along the bed were very much similar to the upflow operation due to similar moisture distribution patterns exhibited.

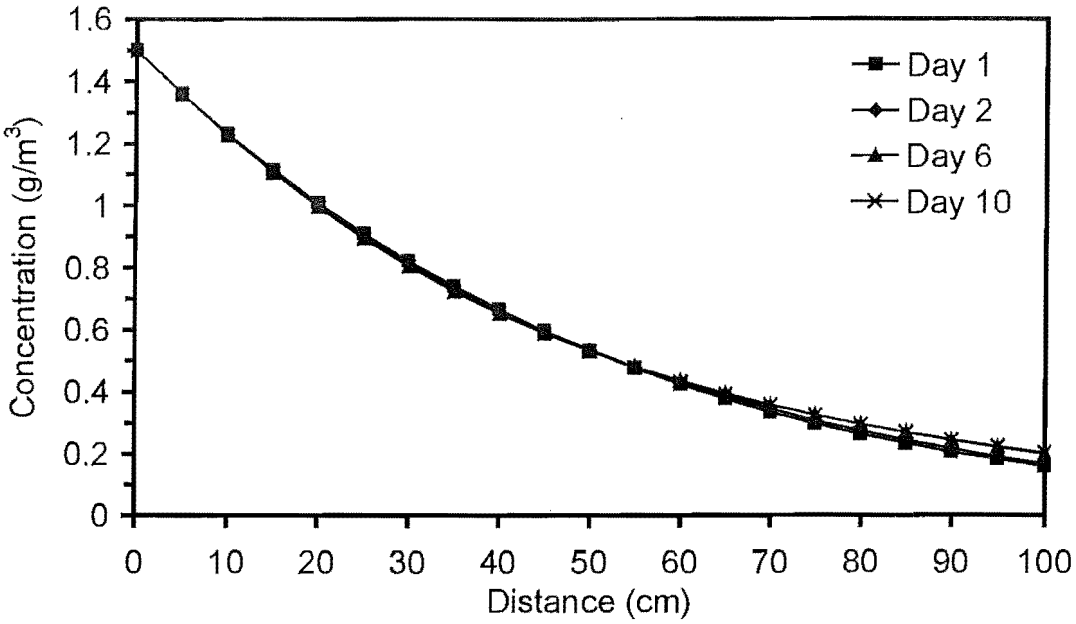

Figure 5.12 Concentration profile along bed length for Case 4

However, at higher loading values a slightly lower elimination capacity was exhibited by the upflow mode. This was associated with the drying in the inlet region and the difficulty in compensating for the moisture loss through water addition, due to the slow rate of redistribution in the media. A higher leachate production was observed for the downflow operation (on an average basis 0.3 g/h) and was attributed to the local condensation that occurred during the initial stages. Higher loadings (65 g/m^3h) had an inhibitory effect on both systems as exhibited by the lower removal efficiency (25-28%), which could directly be correlated to the loss of moisture and subsequent retardation of biological activity. These simulated results confirm the experimental observations made by Krailas (2000) for the removal of humidified (RH 95-99%) methanol vapour using packed columns with compost/Pall rings, and intermittent water spraying.

5.6 Case 5: Performance Under Varying Inlet Air Temperature (Low Loading)

The typical biofilter operation is subjected to the influence of external disturbances (e.g. varying inlet contaminant concentration and the feed gas temperature). However, a typical scenario is where the inlet temperatures vary in relation to diurnal conditions. Fluctuations in feed gas temperature affect the moisture content in well-insulated biofilters. Literature (van Lith *et al.*, 1997) clearly demonstrates the implications of fluctuating off gas dry-bulb temperature on biofilter performance. In Devinny *et al.* (1999) the monitoring of inlet air temperature has been stressed in order to prevent extremes in temperature, which could adversely affect the microbial activity through inhibition or cell death. Variations in feed temperature could be attributed to a multitude of factors ranging from the nature of the feed source, environmental conditions, time scale of operations, etc.

Thus, for the case study considered the average inlet temperature selected was 21°C (294 K) and a sinusoidal component added to reflect the daily variation (Fig.5. 13). Therefore, over a one-day period the inlet air (RH 100%) was above the initial bed temperature of 298 K for a period of 0.4 days and below the initial bed temperature for the rest of time.

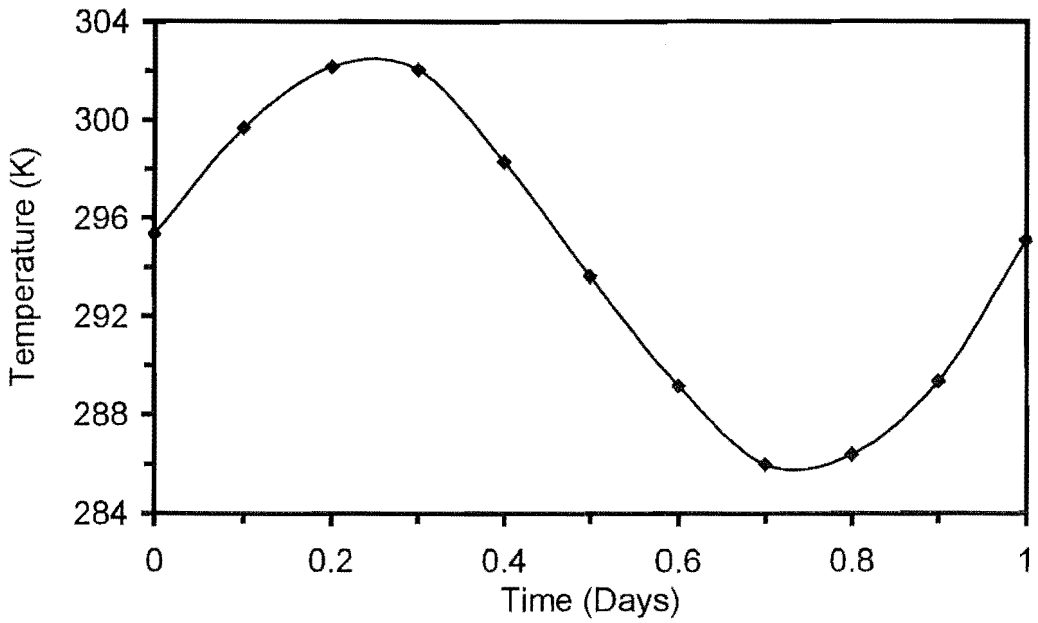

Figure 5.13 The daily variation of inlet air temperature for Case 5.

The maximum and minimum inlet temperature thus achieved was 302 K and 286 K respectively.

The scenario for Case 5 therefore simulated an industrial situation where the air stream temperature was changing over a 24-hour period. The parameters, initial values and the water addition rate were the same as Case 2. The temperature profile for the bed (Fig. 5.14) indicated that the daily variation in inlet air temperature influenced the evolution of the bed temperatures. However, the effect of inlet air temperature changes was more pronounced in the first 20-30% of the bed. Owing to the time lag associated, a delayed response occurred in the upper the regions to the influent temperature changes (i.e. these regions did not instantaneously respond to the variations in temperature at the inlet).

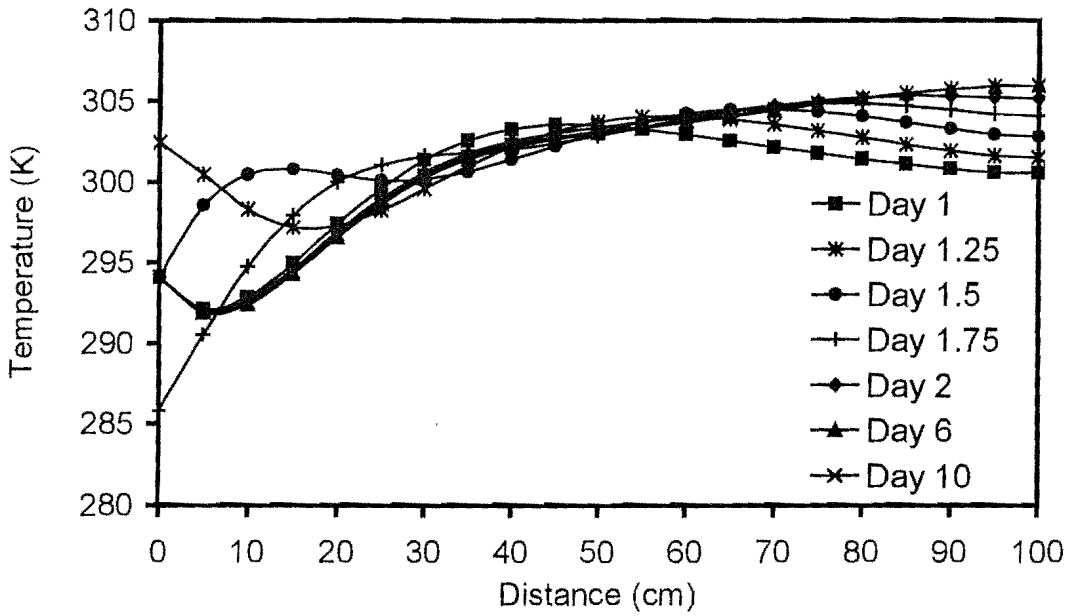

Figure 5.14 Temperature profile along the bed for Case 5

Thus, on day 1 the region closest to the inlet was affected by the second half of the temperature cycle while the upper regions responded to the first half of the cycle. On days 1.25 and 1.5 the inlet region underwent the first half of the cycle and was depicted as a local minimum and maximum respectively in the temperature profile. During this time period the upper regions of the column were subjected to the second half of the cycle although its effect was muted due to the increase in local temperatures from evaporative

and convective heat. On day 1.75 the inlet region exhibited a decrease in temperature as it underwent the second half of the cycle before progressing to day 2. This process repeated itself due to the continuous propagation of the inlet temperature variation within the bed. This was clearly manifested in the temperature profiles for days 1, 2, 6, 10 which displayed a similar local minimum for the time frames considered.

The general trend for the water content profile (Fig. 5.15) was similar to that of Case 2, with moisture stripped from the solid phase due to the biological activity. But, the oscillatory nature of inlet local temperatures during a daily cycle as depicted in Fig. 5.14 gave rise to unanticipated condensation/evaporation in the inlet region. Thus, when compared with Case 2 on days 1, 2, 6, and 10 on an overall basis this yielded a slightly higher drying in the inlet region. However, the variation in local moisture was marginal as compared to Case 2 and hence this system also attained dynamic equilibrium on day 10 with a removal efficiency of 88%, while producing leachate comparable to Case 2.

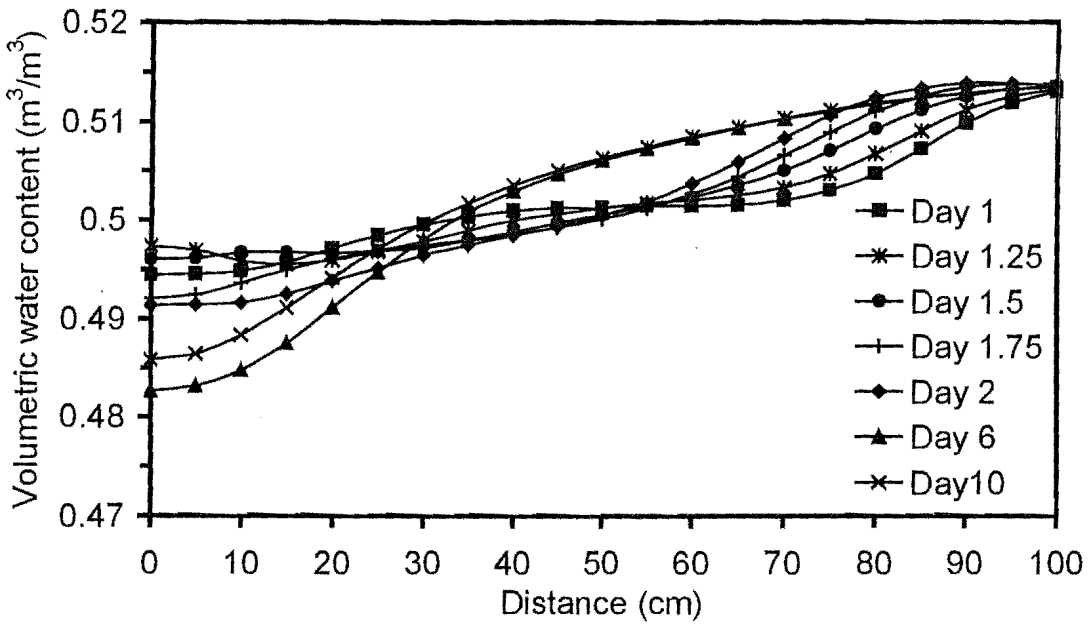

Figure 5.15 Variation of water content along the bed length for Case 5

The degradation profile for the bed (Fig. 5.16) reflected the effect of varying inlet temperature on the system performance. The temperature dependence of the degradation term given by Eq. 3.9 meant that the local temperature variations affected the degradation rates. This was clearly demonstrated in the quarterly variation of the degradation rates in the inlet region within days 1-2, which closely followed a similar trend exhibited by the local temperatures. The activity in the inlet region characterised by a local minimum on days 1, 2, 6 and 10 was due to a similar temperature drop observed in the temperature profile (Fig. 5.14). The shift from a minimum on day 1 to a local maximum on days 1.25, 1.5 and 1.75 was also due to a similar temperature variation in the aforementioned regions from the propagation of the inlet temperature oscillations. The loss of moisture caused the local degradation rates to decrease in the inlet region at the initial stages (days 1, 2, 6), which however was reversed later due to the advection of water. Thus, the degradation in the inlet experienced an increase after day 6 from increased local water content through redistribution.

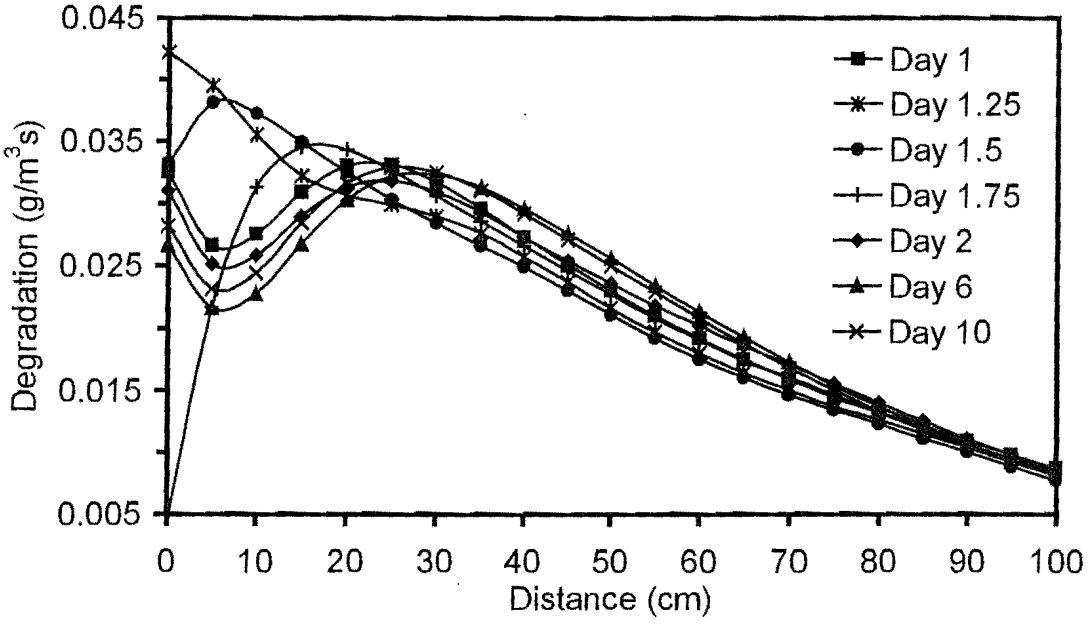

Fig. 5.16 Degradation profile along bed length for Case 5

The effect of higher water addition rate on Case 5 was explored by raising the flux by an order of magnitude (0.821 g/m^2s). Analysis of the water content profile (data not shown) showed a wetting front moving quickly through the column, which was similar to that of Case 3. Although a slight drying front developed in the inlet region, it did not propagate into the bed as in earlier cases. Therefore, the liquid addition rate was successful in counteracting the moisture loss from evaporation. In this case also, the inlet temperature dynamics had a direct influence on the inlet degradation rates. However, rapid distribution and subsequent increase in local moisture on day 2 promoted a more vigorous activity in the above region. This system attained dynamic equilibrium on day 6 with a removal efficiency of 98%, while producing leachate comparable to Case 3.

Chapter 6: Closed Loop Model Performance

6.1 Irrigation Strategies Based on Feedback Control

The simulations in chapter 5 (and common industrial practice) indicate that for successful biofilter operation, water addition is of paramount importance. In simple biofilter systems, the water flow rate could be manipulated to maintain the required moisture content without producing excessive leachate. However, systems with external disturbances, as depicted in Case 5, prove too complex to be controlled by a simple constant water addition rate. A constant irrigation flow rate is not sensitive to the changes in spatial moisture content introduced by external disturbances. Hence, the maintenance of an optimum moisture content to achieve the dual criteria of high removal and low leachate would not be possible.

Feedback control was investigated as a technique for maintaining adequate moisture control and minimising leachate production. For feedback control, a continuous estimate of the biofilter moisture content is required. Literature indicated that the options for on-line measurement of moisture content were limited and included techniques such as total bed weight using load cells or point measurements using time domain reflectometry or tensiometer-based measurements (Devinny *et al.*, 1999; Gostomski *et al.*, 1997; Cook *et al.*, 1999). For this exercise two measurements were investigated, overall bed weight and the average of moisture content measured at three points distributed axially along the bed.

Industrial scale biofilter units commonly use load cells that measure the changes in bulk moisture content by weighing the packing material (van Lith *et al.*, 1997). The readings obtained are processed in a control unit, which determines the rate of irrigation to maintain the desired moisture content. Although this technique has drawbacks such as being limited to fully enclosed systems and the need to recalibrate periodically, its practicality over the alternative spot techniques has prompted greater use.

There are many commercial probes on the market that measure moisture content using various technologies. These probes can be inserted in the bed and provide a local moisture content (Cook *et al.*, 1999). By measuring the bed moisture content over

multiple points, the spatial moisture distribution is measured rather than an average moisture content in the bed as generated by total bed weight.

6.2 Controller Tuning

To facilitate controller tuning, a simple first-order plus time delay model of the system relating the water addition rate to the moisture content was developed for the system and cast in Laplace transfer function form (Eq. 6.1). This approach, defined as "approximate process modeling", was implemented by using the model to generate simple input/output responses between the water addition rate and the set point variables (overall bed weight, average moisture content) (Ogunnaike, 1994).

$$g(s)=\frac{K_p e^{-\theta s}}{1+\tau_c s} \qquad \text{[Eq. 6.1]}$$

The parameters in the transfer function (Eq. 6.1) were ascertained by implementing a step input in the flow rate and monitoring both the transient and steady state response of the controlled variable.

A PI (proportional + integral) controller was selected to regulate the water addition due to its ability to eliminate steady state offset and rapidly reject disturbances (Eq. 6.2).

$$g(s)=K_C\left(1+\frac{1}{\tau_I s}\right) \qquad \text{[Eq. 6.2]}$$

The parameters in the PI controller were determined using IMC (internal model control) approximate model tuning rules. In designing the controller, the filter parameter (λ) was selected to satisfy the recommended choice (i.e. $\lambda > 0.2\tau_c$) (Morari, 1989).

$$K_C=\frac{\tau_c}{\lambda K_p},\ \tau_I=\tau_c \qquad \text{[Eq. 6.3]}$$

The values of the controller parameters for controlling total bed weight are listed in Table 6.1.

Table 6.1. Parameters used in the PI controller for set point using bed weight

Controller Parameter	Bed Weight
K_p	7.75×10^{6} g s/cm
τ_c	103,680 s
K_C	6.45×10^{-7} cm/g s
τ_I	103,680 s

Although control theory generally considers both set point changes and disturbance rejection, this discussion will focus on the latter topic as it is frequently encountered in practical biofiltration operation. The systems simulated comprised of gas flow upwards. The model parameters used (Table 6.2) were identical to those of Case 2, with the exception of inlet air temperature and inlet concentration.

Table 6.2 Parameter values used in the model under feedback control

Parameter	Value	Units
Length	1	m
Diameter	0.1	m
EBRT	6.8	min
Interstitial Gas Velocity	1	m/min
Bed Porosity (ε)	0.645	-
Gas Phase Porosity (εS_g)	0.145	-
Initial Moisture Content	0.5	m^3/m^3
Initial Gas Phase Concentration	0	g/m^3
Initial Solid Phase Concentration	0	g/m^3

6.3 Disturbance Rejection

Practical biofilter operation is subjected to external disturbances that could affect the moisture content (see Chapter 5). However, in a feedback control system the controller would counteract any such disturbances in order to maintain the variable at its desired set point. In order to explore this control mechanism, two set point criteria, bed weight and average moisture content, were analysed. The set point selection for both criteria was based on an open loop system where removal and leachate were optimal. This was achieved in a system subjected to a load of 13 g/m^3h and a constant water flux of 0.158 g/m^2s, which yielded a 96% removal with a steady state leachate flow of 0.12 g/m^2s. Thus the average moisture content of 0.538 m^3/m^3 and the corresponding bed weight of 5951 g from the above system were selected as the set points. In order to emphasise the capability of schemes using feedback control in maintaining adequate moisture control, comparison was made with the above open loop case. For this study the temperature effect on microbial activity *(T_f)* was ignored. This was due to the fact that the step change in temperature under external disturbance required the extrapolation of Eq. 3.12 outside the data range available in literature. However, sensitivity analysis indicated, elimination of Eq. 3.12 would have negligible influence on model performance.

The following two types of external disturbances were used in the simulations.

Variation in Inlet Concentration

Variable feed concentrations are also common in industrial biofiltration (Swanson and Loehr (1997); Devinny *et al.*, 1999). Literature indicates that to ensure optimal microbial activity, a constant feed stream is required (Devinny *et al.*, 1999). However, survival of the microbial population during shutdown has also been documented and is enhanced through periodic aeration of the biofilter (Leson and Winer, 1991). Contaminant concentration in the off-gas is directly affected by the variations in the process facility (source). These variations in the inlet concentration are attributed to changes in product line, weekend shutdowns and transient operation of batch processes. Furthermore, the frequency of these variations is industry specific and could range from diurnal to weekly variations.

The simulations in this chapter were based on a scenario similar to an industrial ink drying process, where VOCs are volatilised during the drying process. In this study the biofilter system was subjected to a step increase in toluene concentration from 1.5 g/m^3 to 7 g/m^3, which reflected a shift to a new product line and hence subsequent increase in contaminant concentration in the off-gas (Fig. 6.1). Hence, as a result a five-fold increase in the mass loading to the system occurred (13-62 g/m^3h).

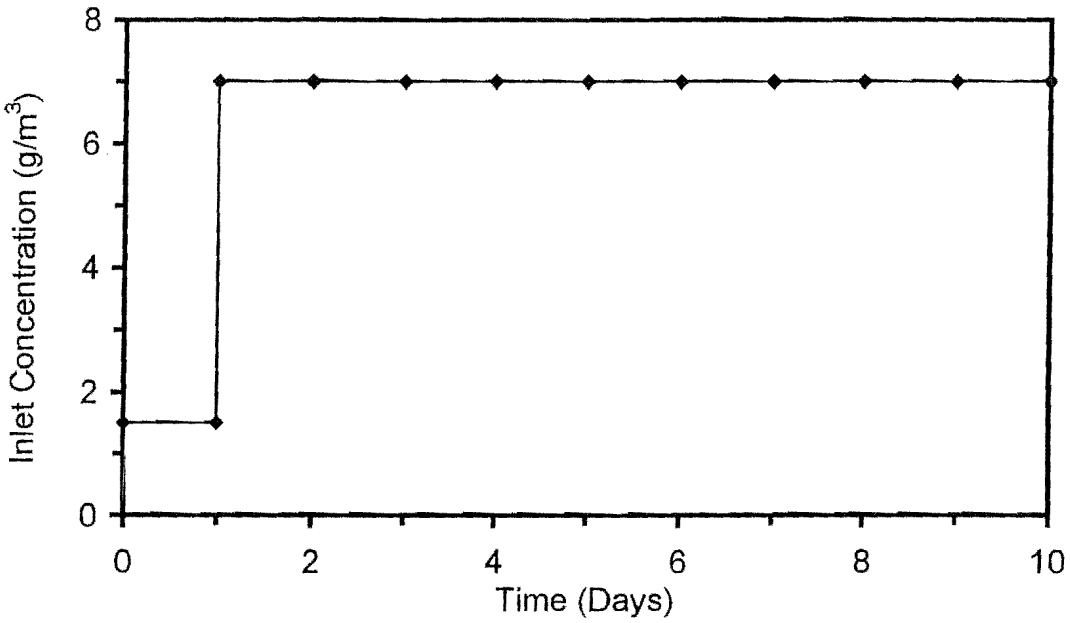

Figure 6.1. Variation of inlet toluene concentration with time

Variation in Inlet Air Temperature

As stated in section 5.6, fluctuations in feed gas temperature affect the moisture content in well-insulated biofilters. Variations in feed temperature could be attributed to a multitude of factors ranging from the nature of the feed source, environmental conditions, time scale of operations, etc, while the frequency of variations could range from daily to weekly. In this exercise, a scenario where the inlet air temperature varied from warmer to cooler conditions was emulated. The transition in the inlet air temperature encompassed the product line change under which the new ink product required less drying. In order to emulate this scenario the off-gas temperature (RH 100%) was decreased from 25 °C (298 K) to 10 °C (283 K) using a step transformation (Fig.6.2).

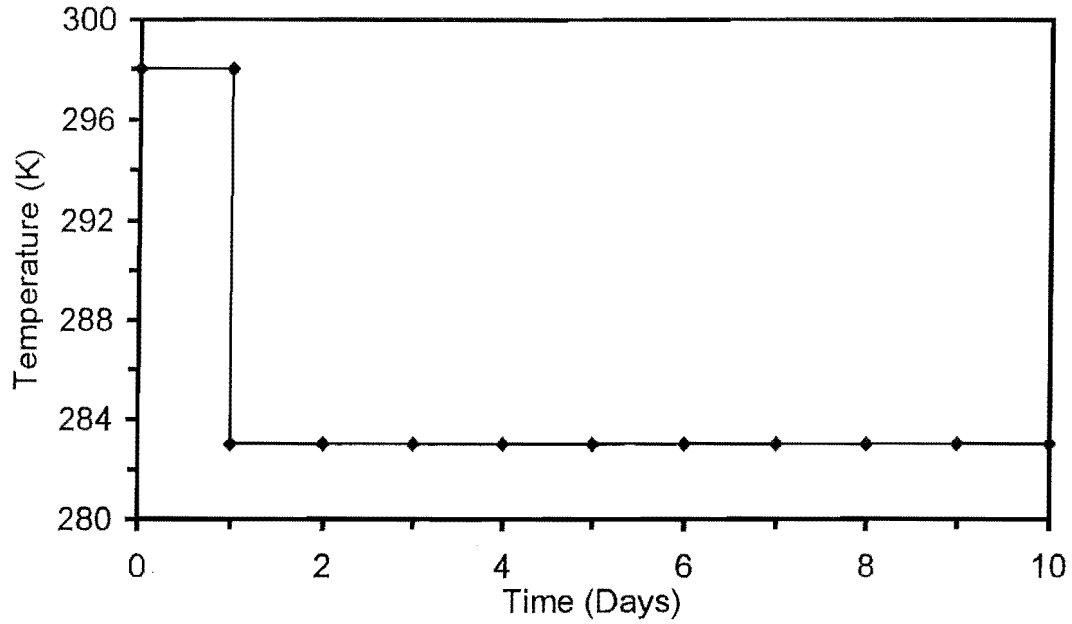

Figure 6.2. Variation of inlet air temperature with time

6.4 Case 6: Performance with Bed Weight as Set Point

A load cell approach was used to regulate the irrigation to maintain the bed weight at a desired set point value. The system dynamics associated with controlling the bed weight (Fig. 6.3) was for a set point of 5,951 g (0.538 m^3/m^3). In order to accentuate the disturbance rejection of this system, the controlled variable and the manipulated variable (water flow) were compared with those of the open loop system. Both open and closed loop systems were subjected to the two external disturbances one day after steady state was reached.

Comparison of the controlled variable from Case 6 (Fig. 6.3) with that of the open loop system indicated a similar bed weight of 5,951 g up to day 1. However, with the introduction of external disturbances on day 1 the two systems displayed a clear difference in bed weight. A rapid decrease in bed weight from 5,951 g to 5,748 g occurred in the open loop system from day 2 to day 8. Moisture was stripped from both systems by greater evaporation from the high mass loading (62 g/m^3h) complemented with a cooler inlet air stream. In the open loop system, the inability of the constant water flux to rapidly redistribute and counteract the drying front manifested itself as a decrease in bed weight. The dynamics in the closed loop scheme consisted of a local minimum at

day 2.5 which was attributed to moisture changes caused by both load and inlet temperature variations. In this case the maximum deviation of the controlled variable from the set point was approximately 10 g. The robustness of this scheme in effectively counteracting moisture variation induced by external disturbances was amply demonstrated by the recovery of bed weight as the system recovered its steady state bed weight of 5,951 g on day 6.

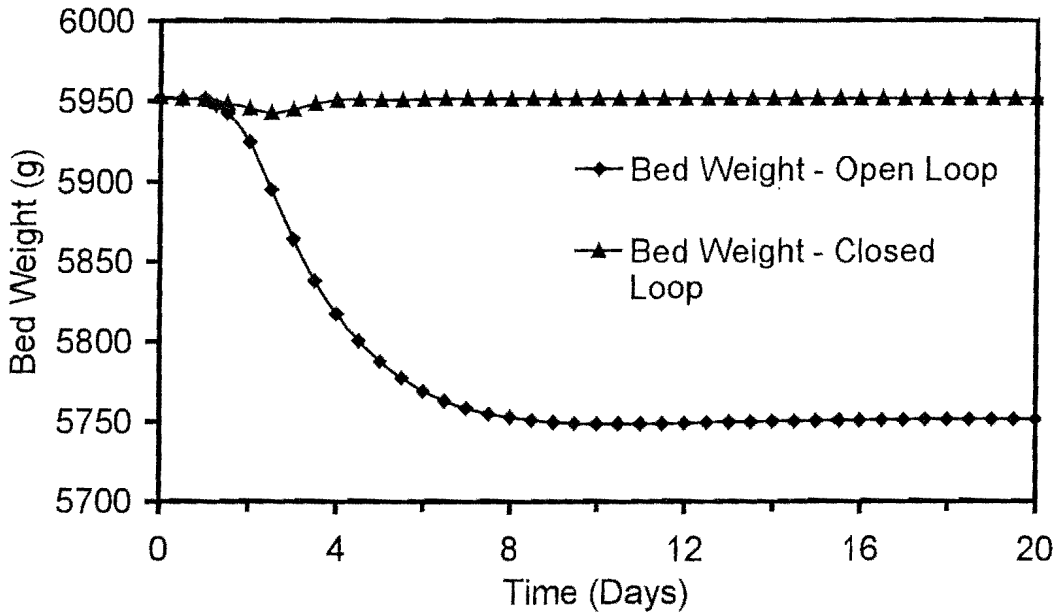

Figure 6.3. The variation of bed weight with time under feedback control/open loop in Case 6.

The removal efficiencies of the two systems initially displayed a similar removal of 96%, but the load change on day 1 caused a drop in the performance of both systems to 84% (Fig. 6.4). However, as stated earlier, the closed loop scheme's ability to overcome drying from the higher loading prevented a further drop and facilitated the maintenance of removal at 84%. On the contrary, the open loop scheme depicted a drop in RE to 73% before steady state was reached with permanent moisture loss from the bed.

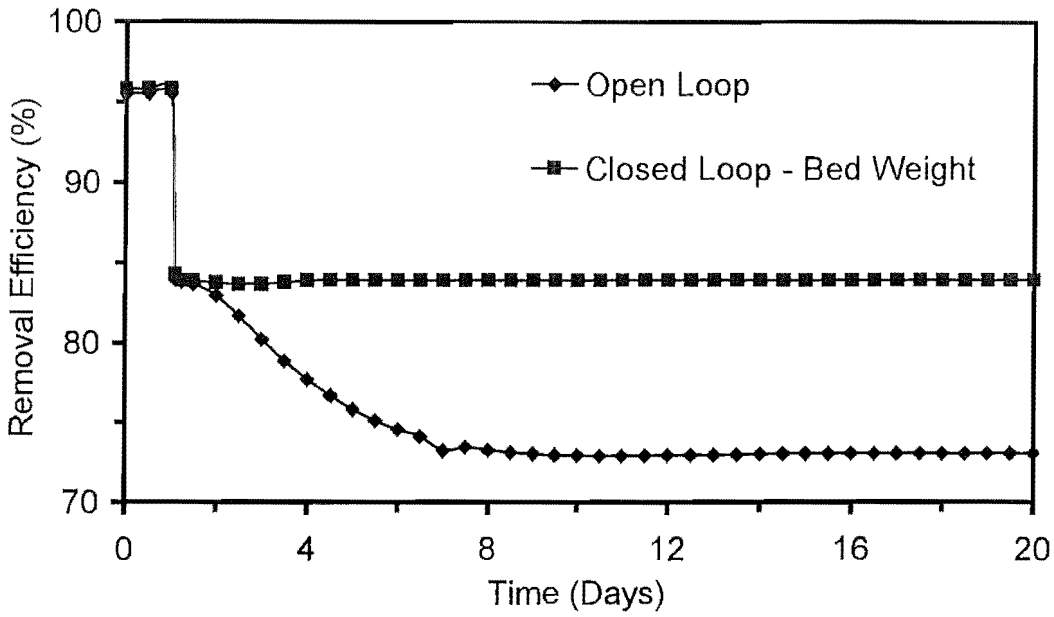

Figure 6.4. The variation of removal efficiency with time under feedback control/open loop in Case 6.

The variations of the water flow rate (manipulated variable) and the leachate rate as a function of time are indicated in Fig. 6.5. As in the case of the controlled variable, flow rate comparisons were also performed on the two schemes to stress the disturbance rejection property. At the onset of the simulation both open and closed loop schemes irrigated the bed with a constant flow rate of 0.158 g/m^2s. The sensitive nature of the controller in the closed loop scheme to the moisture variations induced by the external disturbances was displayed on day 1.5 and onward. In this case the controller action increased the flow rate to a steady state value of 0.25 g/m^2s, which was sufficient to negate the drying effect and hence maintain the bed weight at 5,951 g. The open loop scheme irrigated the bed with a constant flow rate, which was not responsive to the external disturbances and thus, highlighted its drawback and inappropriateness under these conditions. The initial decrease in the leachate rates of both schemes was attributed to the drying in the inlet regions. However the stabilisation of the leachate rate in the closed loop scheme to a value of 0.07 g/m^2s indicated no further propagation of the drying front. Moreover, increased drying of the medium in the open loop scheme resulted in the decrease of leachate rate to 0.009 g/m^2s as steady state was reached on day 12.

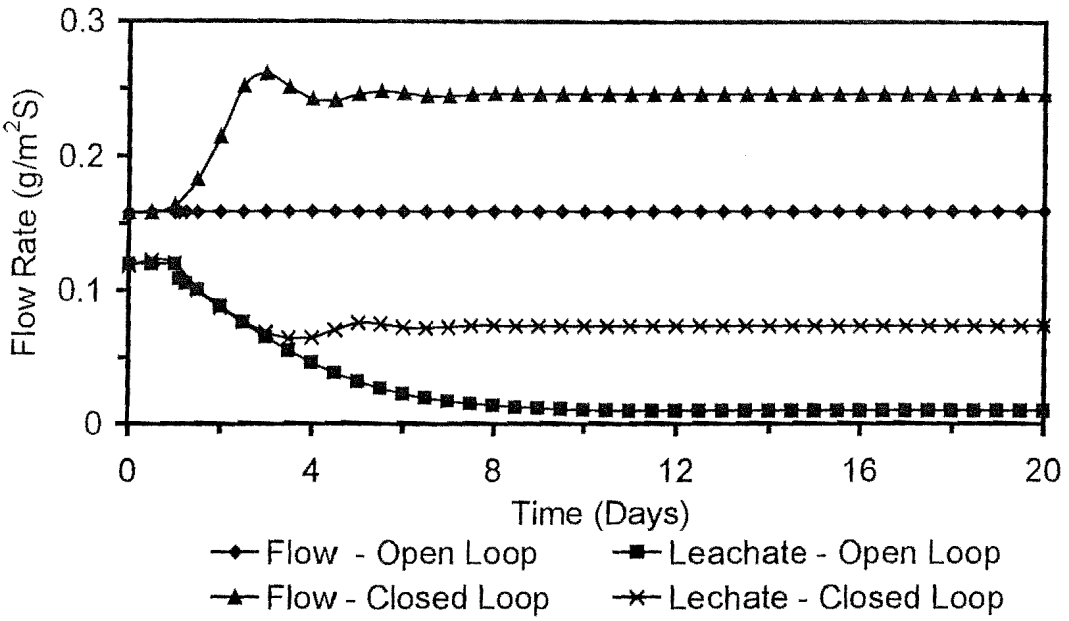

Figure 6.5. The variation of water flow/leachate rate with time under feedback control/open loop in Case 6.

The moisture content profile (Fig. 6.6) on day 0 indicated an average moisture content of 0.538 m^3/m^3, which was on par with that of the open loop scheme. The drop in moisture content in the inlet region on day 0 was due to the fact that the biofilter was operated until steady state was reached. Thus, day 0 referred to the time frame where steady state was reached and from where each profile was plotted. The introduction of a step change in the mass loading from 13 to 62 g/m^3h and a 15 °C drop in the inlet air on day 1 gave rise to a drying front. Hence, as a result on day 2, moisture was stripped from the first 50% of the bed with drying more predominant in the inlet region. In this scenario, the drying caused the controller to increase the water flux, which increased the local moisture content over the top 30-40 cm of the bed. But, propagation of the drying front and further moisture loss in the inlet region was still occurring by day 6. This required the controller to irrigate the bed continually with a higher water flux to effectively halt any further drying. Thus, as steady state was attained on day 6 the inlet region displayed a permanent moisture loss, while the upper regions benefited from a higher local moisture content. The maximum and minimum volumetric water contents attained in the system across the bed length were 0.553 m^3/m^3 and 0.521 m^3/m^3, respectively.

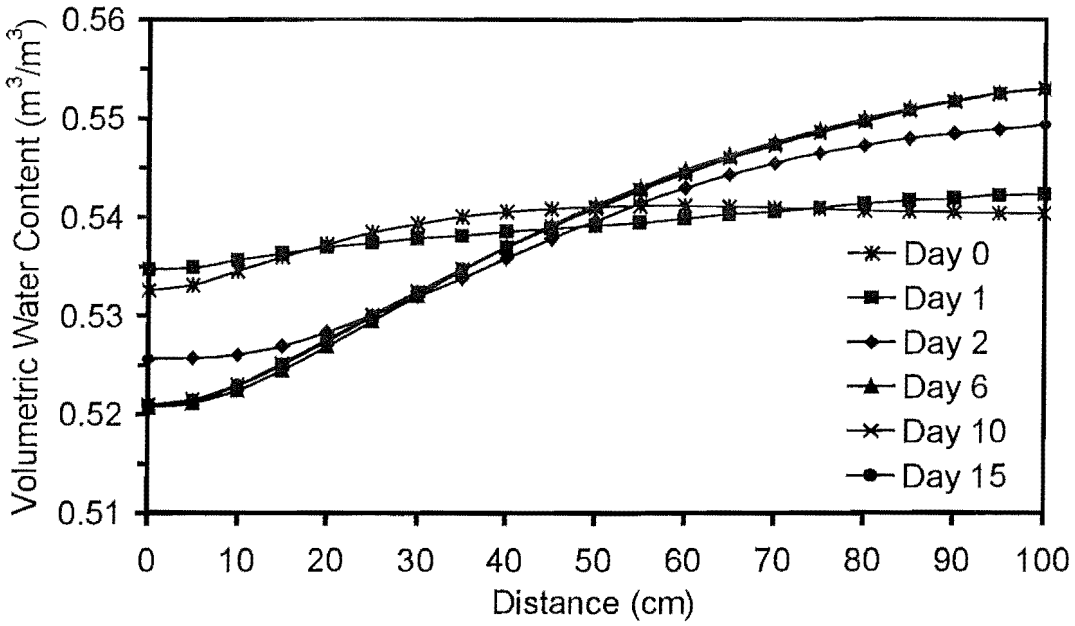

Figure 6.6. The variation of water content along the bed length under feedback control in Case 6

The moisture content profile for the corresponding open loop scheme is provided in Fig. 6.7. In this case a similar moisture distribution pattern to the closed loop scheme was displayed on days 0 and 1. However, the effects of a higher loading and a cooler influent air stream coupled together with an inadequate irrigation rate caused significant drying through out the bed by day 6. The ramification of this increased drying was a decrease in the biological activity across the bed with greater retardation in the first 60% of the column (data not shown). For both schemes, the inlet temperature fluctuation contributed to drying at the initial stages as thermal equilibrium was reached between the air and solid phase. However, the higher mass loading and the resulting exothermic heat release played a more dominant role in the movement of the drying front and the subsequent removal of moisture from the medium.

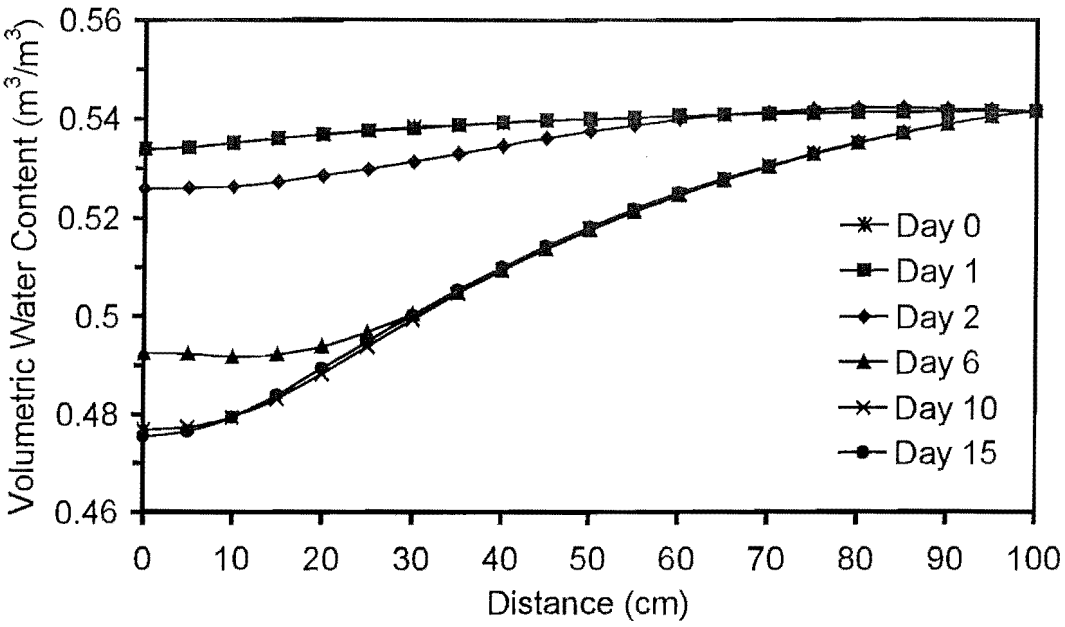

Figure 6.7. The variation of water content along the bed length for the open loop scheme in Case 6

The degradation profile for the closed loop scheme of Case 6 (Fig. 6.8) followed a trend that was consistent with the change in mass loading. The variability in the inlet region of the bed on day 1 was due to the introduction of a higher inlet concentration. The effect of the higher inlet concentration became more pronounced as the concentration front propagated through the bed and gave rise to higher local degradation rates by day 2. Compared to day 2, a slight decrease in the local degradation rates in the air inlet region occurred on day 6, due to a lower moisture content. The concentration profile for the bed (data not shown) displayed a similar type of behaviour as the degradation profile with a final removal efficiency of 84%.

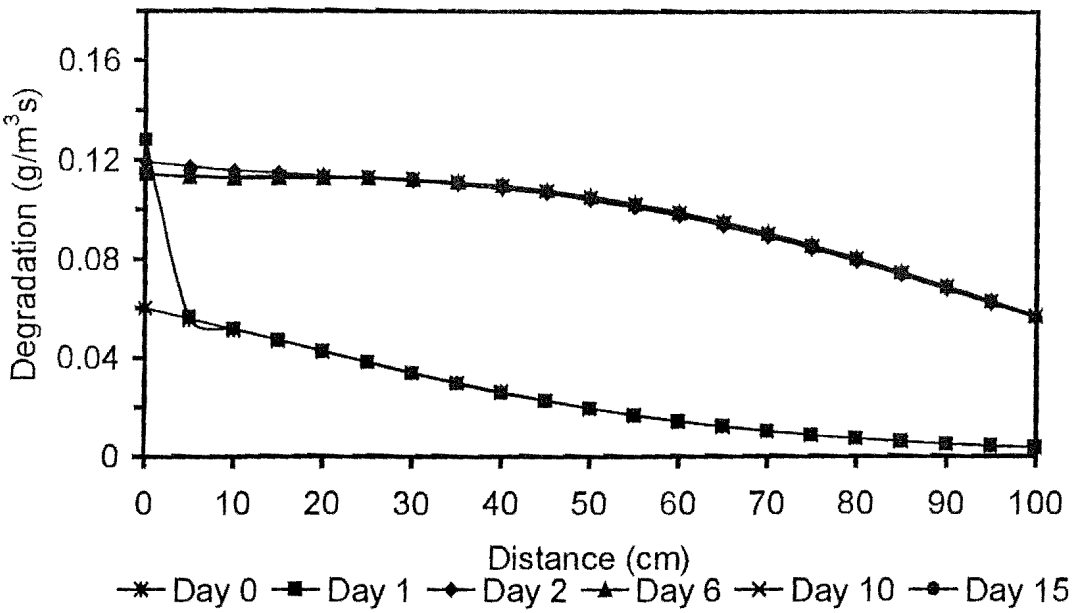

Figure 6.8. Degradation profile along compost bed under feedback control in Case 6

Compared to the insufficient water addition in the constant flow scenario, this closed loop approach ensured adequate irrigation to maintain the process variable at the desired set point in the face of external disturbances. Although both schemes did not recover their initial removal efficiency due to undergoing the load change, the closed loop scheme was able to maintain a steady removal of 84% as opposed to a RE of 73% from the open loop scheme. The leachate flow rate produced was significantly higher in the former scheme. However, it should be stated that the attainment of a similar removal, under a constant flow scheme would have produced leachate rates of greater magnitude. In this case, the system reached a steady state with respect to the key variables on day 10 of the simulation run with a steady state removal of 84%. The system parameters were not rigorously optimised and possibly a lower bed weight could provide adequate removal with even less leachate production or conversely a higher removal efficiency at a higher moisture content.

6.5 Case 7: Performance with Three Point Averaged Moisture Content

A spot measurement technique was used for Case 7. By measuring the bed moisture content over multiple points, the controller was made more sensitive to the spatial moisture distribution rather than an average moisture content in the bed as generated by the total bed weight. The same external disturbances as before were used and the feedback signal was the arithmetic mean of water contents at 5, 50 and 90 cm from the bottom of the column. The system simulated was a biofilter column with upward gas flow with initial and parameter values as stated in Table 6.2.

The values of the controller parameters from Eq. 6.3 for this case are listed in Table 6.3.

Table 6.3. Parameters used in the PI controller for set point using average moisture content

Controller Parameter	Three Point Averaged Moisture Content
K_p	9.74×10^{2} m^3s/m^3cm
τ_c	129,600 s
K_C	4.43×10^{-3} m^3 cm/m^3s
τ_I	129,600 s

As in Case 6, in order to verify the presence of disturbance rejection in the closed loop scheme, both the controlled and the manipulated variables were compared with those of the open loop system. In this case also, external disturbances were introduced one day after steady state had been reached.

This system was simulated for a set point consisting of an average moisture content of 0.538 m^3/m^3 (5,951g). The dynamics associated with the controlled variable are depicted in Fig. 6.9. The controlled variables for the two systems displayed a similar average moisture content of 0.538 m^3/m^3 prior to the introduction of both load and inlet temperature variations on day 1. The two controlled variables started to drift apart after

day 2 as drying induced by external disturbances reduced the local moisture content. The inadequate water addition by the open loop scheme under these circumstances caused the average moisture content in that system to decline to 0.511 m^3/m^3 by day 15. This represented the permanent drying that occurred in this system as steady state was reached (see Fig. 6.7). The effect of moisture loss from the above disturbances was portrayed as a slight decrease in the process variable in the closed loop scheme. However, the dynamics associated with the controlled variable was limited to the time frame of 2-7 days, as controlled water addition was effectively able to raise the average moisture content to the previous value of 0.538 m^3/m^3. This action again reiterated the robustness of closed loop schemes in maintaining the bed moisture in the face of increased moisture stripping mechanisms.

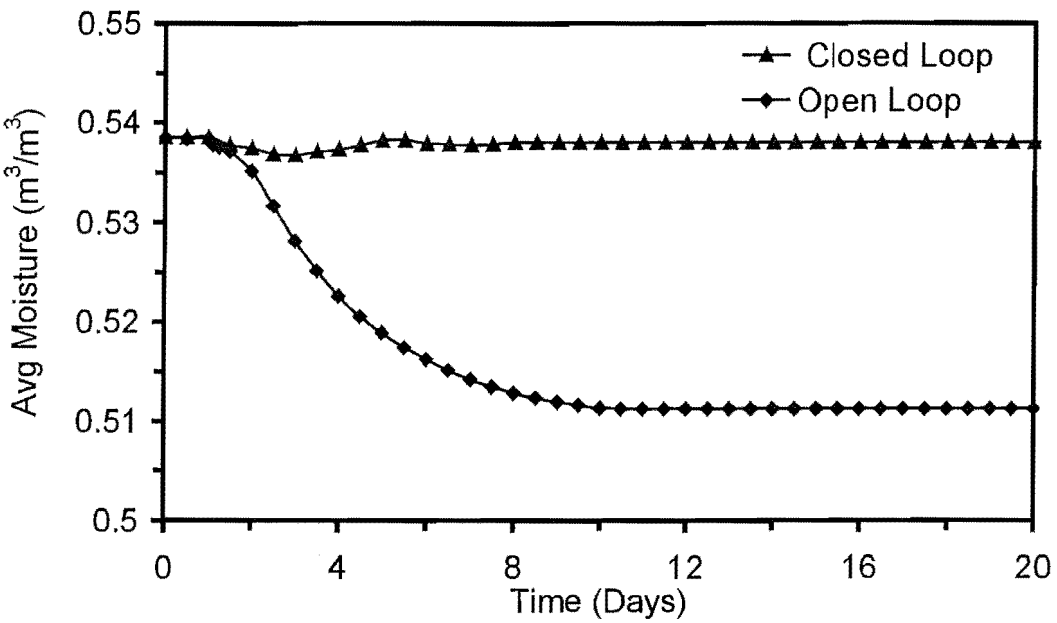

Figure 6.9 The variation of average moisture content with time under feedback control/open loop in Case 7

As in Case 6, the removal efficiency of the two systems was initially 96% (Fig. 6.10). However the decrease in removal in both systems on day 1 to 84% was due to the systems' undergoing the load change. The removal attained under the higher loading could not be sustained in the open loop scheme as retardation of microbial activity from moisture loss caused the removal to decline to 73% as steady state was achieved. But, in

the closed loop scheme, any further drop in removal was prevented by its ability to counteract the drying by irrigating the bed sufficiently.

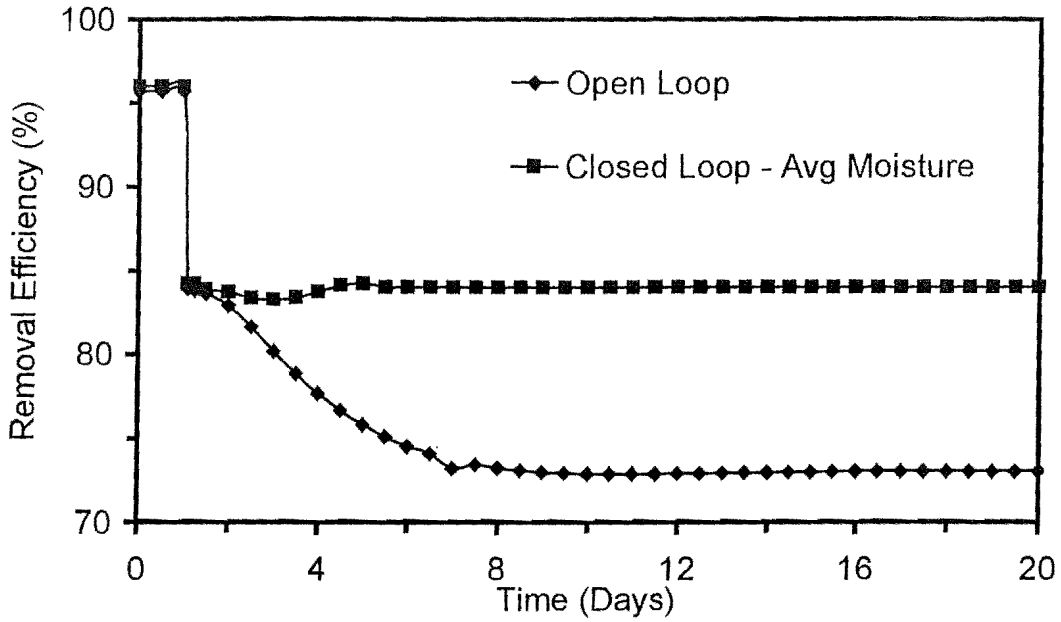

Figure 6.10. The variation of removal efficiency with time under feedback control/open loop in Case 7

As in Case 6, flow rate comparisons (manipulated variable) were also performed for both open and closed loop schemes (Fig. 6.11). The two schemes initially irrigated the bed with a constant flow rate of 0.158 g/m^2s, to maintain the desired set point value. This was however reversed due to the introduction of external disturbances from day 1. In the closed loop scheme, the daily variation of the water flow rate depicted an overall increase from day 1 onwards, as the controller attempted to overcome drying by using a higher water flux.

The oscillations present during days 4-8 were due to the manipulation of the flow rates by the controller as a new steady flow of 0.25 g/m^2s was reached. The transients observed in the flow rate were in accordance with the variations in the controlled variable during the relevant time frames. In comparison the open loop scheme's constant flow rate was insufficient to counter the drying and was reflected as a significant moisture loss in the biofilter (Fig. 6.7). Both schemes displayed decreasing leachate flow rates at the initial stages, which represented moisture loss from evaporation. The local maximum displayed in the closed loop leachate on day 6, was attributed to flow rate variations by the

controller during the above time period. The closed loop scheme attained a steady flow of 0.07 g/m^{2}s as opposed to a lower leachate flow of 0.009 g/m^{2}s in the open loop scheme.

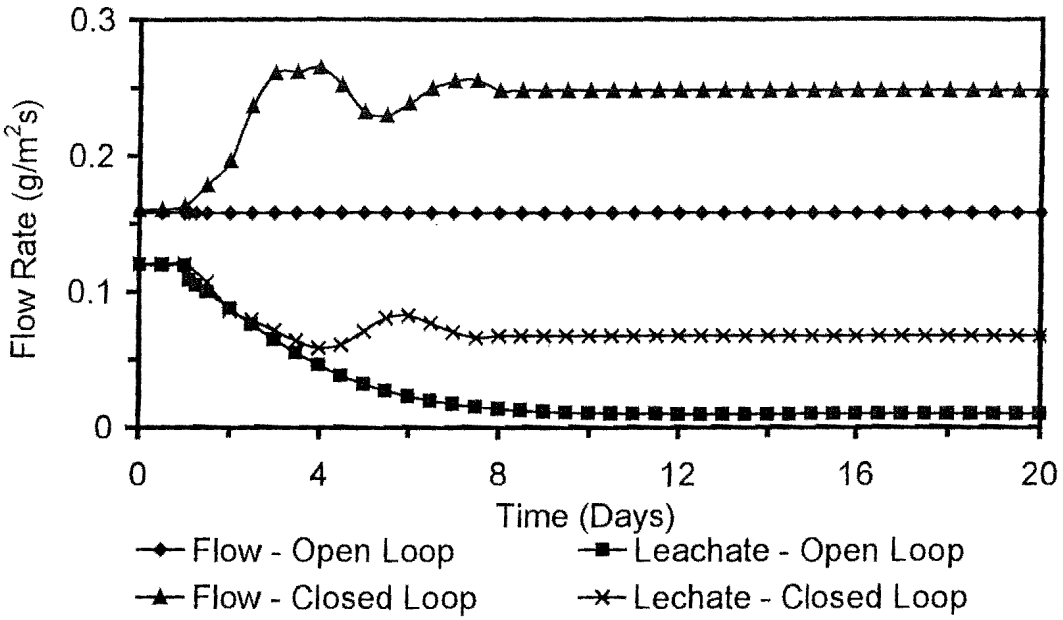

Figure 6.11 The variation of water flow/leachate rate with time under feedback control/open loop in Case 7

In this case too, the attainment of a higher stable leachate rate signified the former scheme's ability to effectively maintain bed moisture when subjected to disturbances and also highlighted the latter scheme's weakness under such conditions.

The moisture content profile (Fig. 6.12) on day 0 indicated an average moisture content of 0.538 m^3/m^3, similar to that of the open loop scheme. Although, this system was also initially operated until steady state was reached, no significant gradients in water content were observed in the inlet region of the column on day 0. This was due to the fact that the local moisture was better regulated, as the controlled variable comprised of three distributed spatial moisture contents. In this case too, day 0 referred to where steady state was reached and from where each profile was plotted. The changes in the mass loading and inlet temperature on day 1, gave rise to a drying front whose effect became more pronounced in the first 40-50% of the bed on day 2. As in Case 6, the moisture removal associated with the drying forced the controller to increase the water flux, which caused an increase in the local moisture content over the top 30-40 cm of the bed. However, by day 6, propagation of the drying front and further moisture loss in the inlet region was

still occurring. Under these conditions, a continuous high water flux was imparted by the controller to effectively prevent any further drying. Although, further drying was prevented, the inlet region did not recover to its initial moisture content as steady state was attained on day 10. A clear gradient in moisture content was observed across the bed with the maximum and minimum volumetric water content attained being 0.553 m^3/m^3 and 0.521 m^3/m^3 respectively.

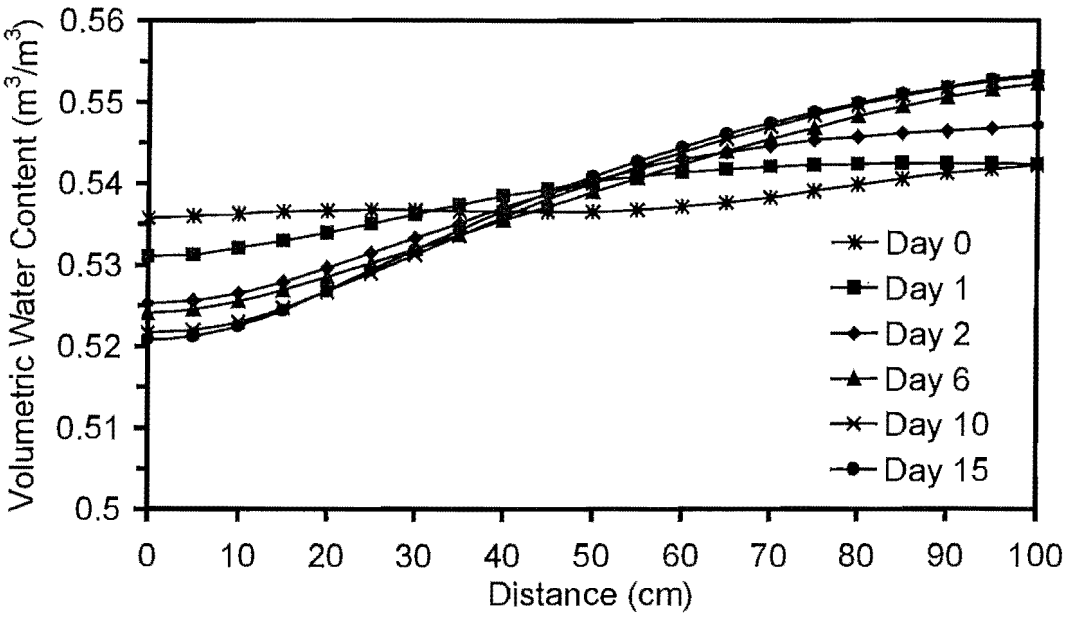

Figure 6.12. The variation of water content along the bed length under feedback control in Case 7

The degradation profile for the bed was quite similar to that observed in Case 6 using the bed weight as set point (data not shown). Initially, the local degradation rates at the air inlet region were affected by the step change in concentration, which however started to influence the activity across the bed as time progressed. A similar pattern of behaviour was reflected in the concentration profile with the final removal attained at 84%. This system also reached a steady state with respect to the key variables on day 10.

The closed loop scheme discussed under Case 7, prevented bed moisture loss when confronted with moisture loss mechanisms such as load increments and cooler inlet air. Compared to the open loop case, although there was sufficient water addition, the leachate production at steady state was considerably higher. However, extensive drying

lowered the leachate production in the open loop scheme. This system with multiple probes could be extended by identifying the optimum locations for the probes or by implementing a true distributed parameter control technique, both of which were beyond the scope of this work.

6.6 Conclusions

Although disturbances on biofilter systems would predominantly be oscillatory in nature, the use of step changes in mass loading and inlet temperature in the current simulations was able to demonstrate the superiority of closed loop irrigation schemes in maintaining bed moisture and removal. Since the removal achieved and leachate produced were identical in the closed loop schemes of Case 6 and Case 7, both schemes could be recommended as accurate and robust irrigation strategies for regulating biofilter moisture. The simulation results lead to the conclusion that incorporation of such schemes in biofilter beds would eliminate media dry-out, particularly under a load change scenario. This would not only prolong the useful life of the organic medium but also ensure consistent performance from the biofilter system. Furthermore, irrigation control strategies based on feedback control could also avoid drawbacks such as high leachate production associated with the open loop irrigation, particularly under external disturbances when high removal efficiencies are required (Case 5-higher water addition). From an industrial perspective, implementation of such schemes would ensure optimum bed performance, which is crucial to satisfying the stringent regulatory standards. This would also alleviate the need for manual sampling of medium moisture along the column length and the subsequent ascertainment of the desired water flow rates as performed under the traditional operation. The simulation model developed here provided a useful tool to implement and evaluate various irrigation strategies. This was achieved by way of greater flexibility in incorporating the various schemes into the base model and the comparatively low simulation time taken to obtain the relevant results.

Chapter 7: Directional Switching

7.1 Introduction

In packed bed biofilters, unidirectional (UD) airflow is normally utilised as it provides various benefits in practice. Thus, in the downflow mode of operation, the moisture control process is often easier, which is of critical importance in biofilter operations. In addition, due to the co-current flow of the air and water, better drainage is provided at the bottom of the biofilter. However, in the treatment of sulphur/chlorinated compounds (Yang & Allen, 1994) the build-up of acids can cause a drop in pH and in such circumstances the upflow mode of operation is preferred because the waste products are more easily washed from the bed. In most cases the actual airflow direction is an initial design criterion and is rarely subject to change during the operational time of a biofilter.

Research work in the past has resulted in a novel concept known as "directional switching" (DS). Under this approach, the inlet feed stream was switched between the top and bottom of the biofilter according to a predetermined frequency. Initial work performed by Kinney *et al.* (1996) and continued by Song *et al.* (1999) attempted to overcome biomass accumulation and reduce biodegradation at high loading using directional switching. In this case a comparison was made for toluene removal between a UD biofilter and a DS biofilter packed with porous silicate pellets and an aerosol moisture supply. The results indicated a retardation of activity in the inlet regions of the former, while uniform degradation was maintained in the latter. The loss of activity and subsequent increase in the pressure drop of the UD biofilter was attributed to the excess biomass build up in the inlet region, which was also confirmed by measuring volatile solids. Switching the airflow at three day intervals resulted in a more sustained and even biomass distribution in the DS biofilter, which was confirmed by measuring the microbial respiratory activity. Subsequent work performed by Song *et al.* (2000) analysed the effect of switching frequency on DS mode of operation. A high RE (> 99%) was recorded for each frequency, although the actual length of the active period depended on the frequency used. Thus, at lower frequencies, prolonged exposure to high concentration caused microbial inhibition, while at high frequencies the retardation was much more subdued as the recovery time was faster.

7.2 Directional Switching for Moisture Control

Directional switching was derived for controlling biomass, although its implication on moisture control was explored recently (Devinny *et al.*, 1999; Striebig, *et al.*, 2001). Experimental work performed by Striebig *et al.* (2001) for the treatment of ethylbenzene using non-irrigated biofilters packed with compost and slow release fertiliser indicated the presence of moisture content gradients and subsequent loss of activity in a UD biofilter (upflow). This decrease in removal efficiency was attributed to the loss of moisture arising from metabolic activity causing evaporative cooling and was confirmed by the close correlation between moisture content and the primary active zone. A higher removal was achieved in the DS biofilter by utilising the condensate from upflow mode in the downward operation. However, due to the non-addition of supplemental water and the related drying effect, continuous operation under DS mode was impractical. Thus, directional switching was recommended only as a means of prolonging the operation time of a biofilter without water addition.

In the current model, since it was assumed that the biofilm was fully developed (no active growth) and stable, operation under high mass loading would not generate biomass clogging and reduced activity. However, as the driving force for the model was the moisture content effect on degradation, the loss of moisture under high loads could lead to reduced local activity and decrease in overall removal efficiency. Thus, using the Case 1 scenario (Chapter 5), directional switching was tested for better moisture distribution and potentially increased local degradation. The removal efficiency obtained was compared to that of upflow/downflow operation under both open and closed loop irrigation control. Simulations were performed for two start-up moisture contents of 0.5 m^3/m^3 and 0.53 m^3/m^3 and switching frequencies of one and three day durations. The parameter values used in the simulations are given in Table 7.1.

Table 7.1 Parameter values in directional switching operation

Parameter	Value	Units
Length	1	m
Diameter	0.05	m
EBRT	1.45	min
Interstitial Gas Velocity	4.7	m/min
Inlet Toluene Concentration	1.5 (400 ppm_v)	g/m^3
Toluene Loading	60	g/m^3h
Irrigation Rate	0.0546	g/m^2s
Inlet Temperature	298	K
Bed Porosity (ε)	0.645	-
Gas Phase Porosity (εS_g)	0.145	-
Initial Moisture Content	0.5	m^3/m^3
Initial Gas Phase Concentration	0	g/m^3
Initial Solid Phase Concentration	0	g/m^3

7.3 Case 8: Performance under Directional Switching

7.3.1 Three Day Switching Frequency

The system was simulated with a constant water flux of 0.0546 g/m^2s with the gas flow upward at the start of simulation. As the three day frequency provided the most stable performance in Song *et al.* (2000), it was decided to alternate the gas flow every three days. The propagation of a drying front in the water content profile was attributed to the exothermic bioreaction and the resulting local temperature rise associated with the high loading of 60 g/m^3h. Furthermore, as in Case 1, the inability of the wetting front to counteract the drying caused further moisture loss. The reversal of airflow direction on day 4 caused the degradation to increase in the water inlet region and was depicted as a minor decrease in the local moisture in that region (Fig. 7.1). Moisture was continuously stripped from the lower regions as convective and evaporative heat from the active upper region warmed up the lower regions of the column. The moisture loss in the lower region continued until dynamic equilibrium was reached around day 19.

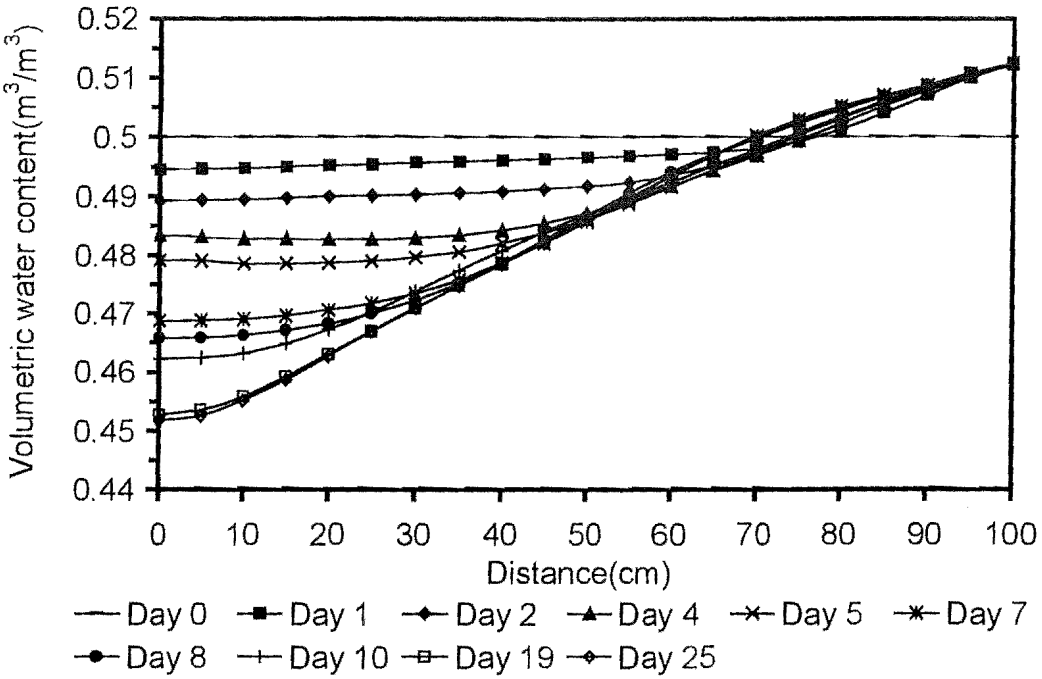

Figure 7.1 Variation of water content along the bed length under directional switching with a three day frequency.

The temperature profile for the bed (Fig.7.2) indicated a reversal of local temperature distribution as airflow direction was switched on day 4. The local temperature rise of 4 °C as a result caused an increase in the absolute humidity of the air and, as thermal equilibrium was reached, moisture was removed from these regions. Furthermore, the permanent drying in the lower region and the subsequent retardation of activity as upward air flow commenced on day 7 was illustrated as a decline in local temperature across the bed. Local temperature drops continued to occur during upflow until moisture equilibrium was reached on day 19. The similar inlet temperature patterns under downward airflow demonstrated a consistent microbial activity in the inlet region, which was attributed to better moisture control.

The degradation profile for the bed (Fig.7.3) during days 1-2 indicated a uniform activity across the bed. However, the reversal of airflow on day 4 caused the active region to shift to the upper regions of the column. The localised drying that occurred in the lower regions during this time was depicted as a reduction in the local activity. The second upflow operation on day 7 saw the transition of the active region to the upper regions of the column.

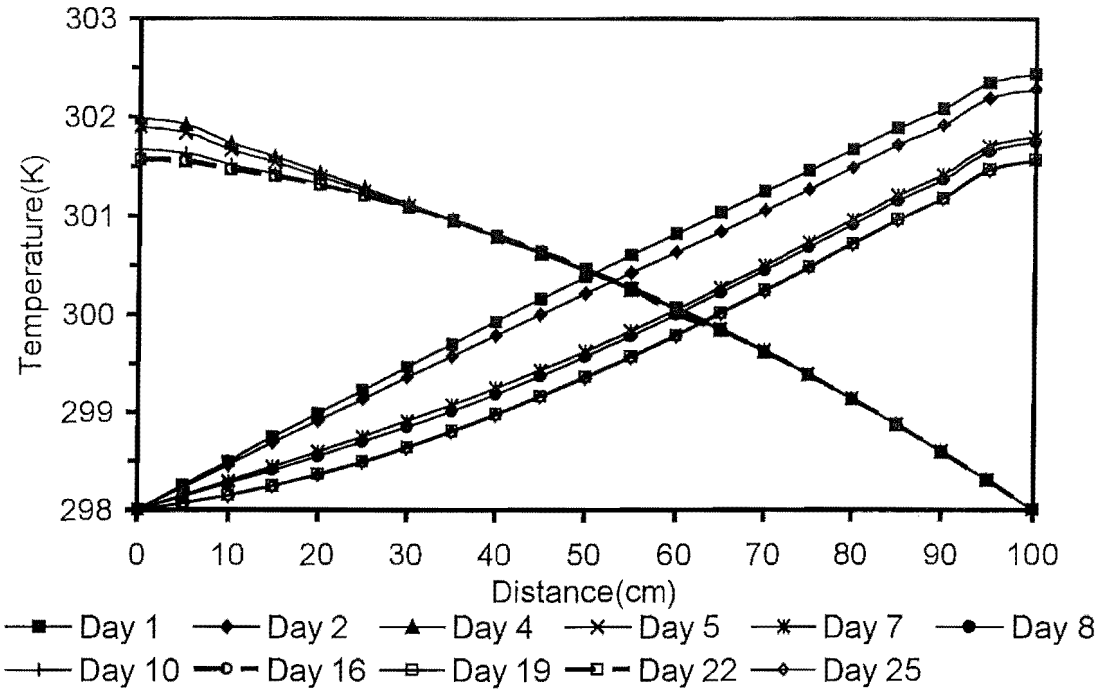

Figure 7.2 Temperature profile along the bed under directional switching with a three day frequency.

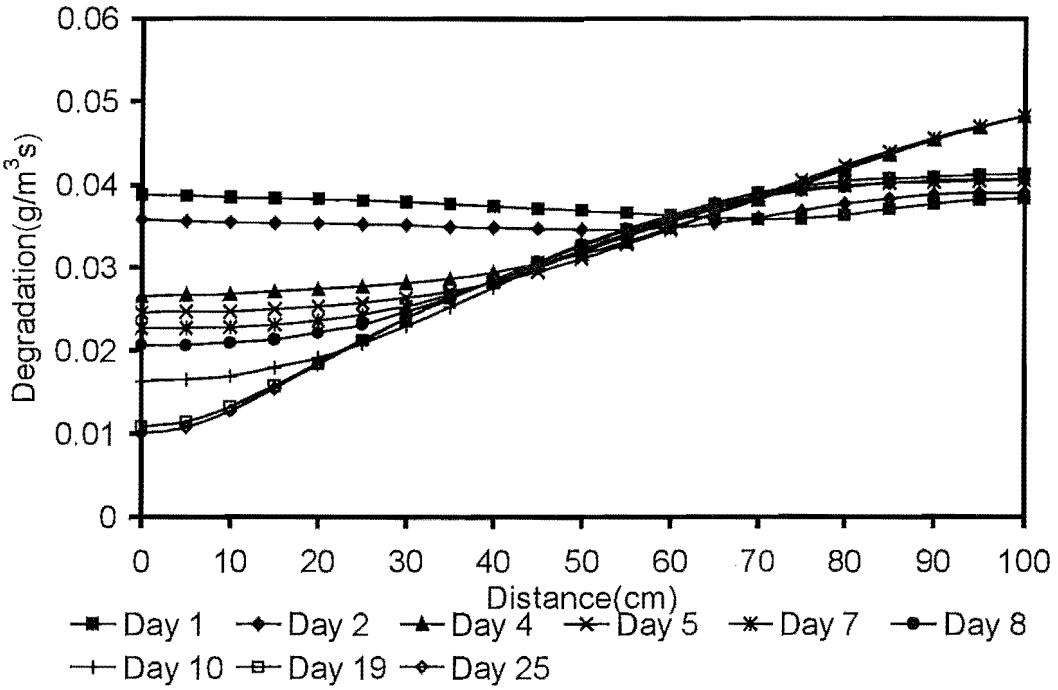

Figure 7.3 Degradation profile of toluene along the bed length under directional switching with a three day frequency.

This retardation of microbial activity in the lower regions was because of the lower steady state moisture contents in this section of the column. The downflow operation on day 10 depicted an unchanged local degradation at the air inlet, although continuous moisture loss from the lower regions caused further loss of activity in this region. Thus, local biological activity at the lower end of the column continued to decrease until steady state was reached on day 19.

The concentration plots for the bed (Fig.7.4) yielded contrasting gas phase concentration profiles for the upward and downward gas flow scenarios. Declining microbial activity related to moisture loss caused the gas phase concentration to increase throughout the column under upward airflow. This resulted in the drop of removal in the upflow cycle from 33% on day 1 to 26.5% on day 19 as steady state was reached. On the contrary, the removal remained fairly uniform under downward flow, although the effect of drying in the lower regions started to impact at the latter stages. A more stable performance occurred under downflow with removal reducing by only 2%, which reiterated its superiority in ensuring better moisture control.

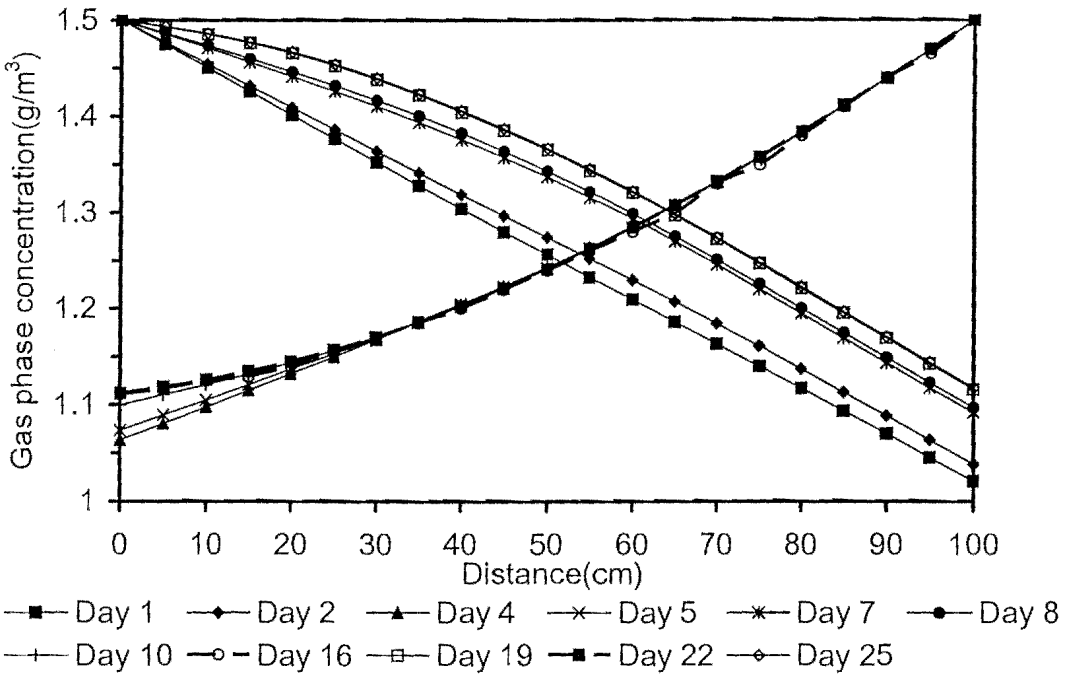

Figure 7.4 Concentration profile of toluene along the bed length under directional switching with a three day frequency.

7.3.2 Comparison of Performance

Comparison of the steady state removal with other forms of operation, for the same organic loading yielded varying results (Fig 7.5). Directional switching (DS) with a three day frequency did not provide a significantly different performance (26.5%) as compared to the upflow mode (26%). However, downflow operation increased the removal to 28%, which was attributed to greater activity arising from higher water contents and higher gas concentrations in the upper regions of the column. Thus, due to better moisture control/distribution, the active region under downflow was concentrated at the water inlet side. This confirmed that downflow mode of operation was more suitable than upflow for high organic loading. However, the best performance under this loading was provided by the system with controlled irrigation using closed loop feedback control. Due to the industrial preference for the load cell approach, the closed loop irrigation scheme used the bed weight as the controlled variable. The closed loop scheme used a set point value of 5720 g (average moisture content 0.51 m^3/m^3), which represented the equilibrium bed moisture content in the beds, under a no load scenario. This system provided a steady state removal efficiency of 35%.

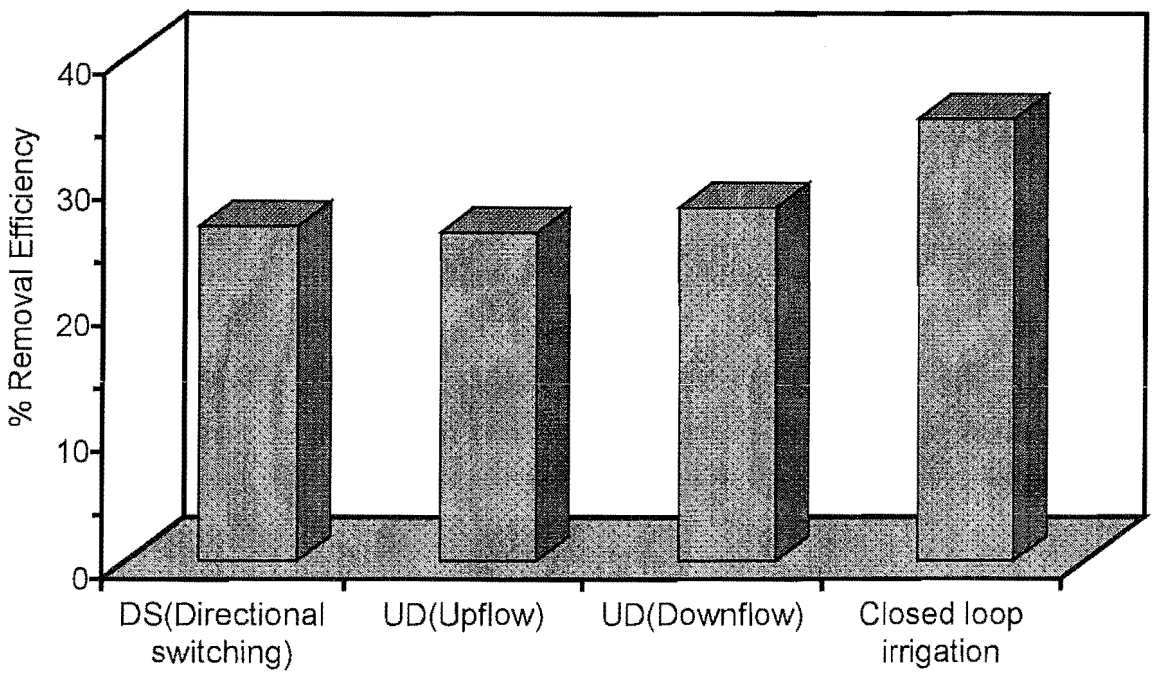

Figure 7.5 Comparison of performance of different operating schemes for a high organic loading

The leachate flow rates produced by the different schemes at steady state provided mixed results (Fig. 7.6). Both the three day directional switching scheme and the upflow scheme produced similar leachate, which was due to a similar moisture distribution pattern in the lower regions of the column. The slightly higher removal in the downflow mode was accompanied by a leachate rate that was greater than that of the DS operation. This was attributed to the condensation that occurred in the initially cooler lower regions of the column. A ten-fold increase in the leachate rate occurred, in the closed loop scheme as compared with the DS mode, as the controller maintained the bed weight at the desired set point value. The higher average moisture content attained at dynamic equilibrium, resulted in the production of this higher leachate. Controlled water addition therefore was capable of ensuring a better moisture distribution and counteracting drying, which resulted in the bulk activity remaining in the inlet region.

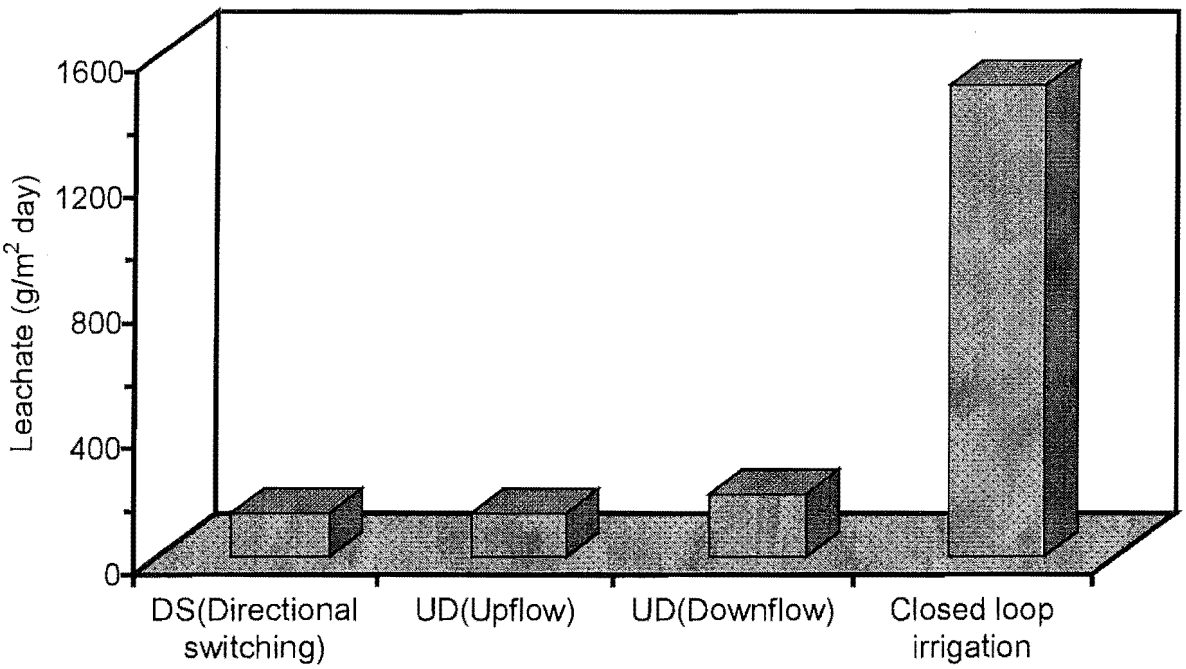

Figure 7.6 Comparison of the leachate rates for different operating schemes under a high organic loading

7.4 Performance of Inlet Regions

The degradation capacity of the inlet sides were compared within and between the operating cycles for a given airflow direction under directional switching. For the purpose of analysis, the inlet region was defined as the first 25% of the column from the air inlet and the biofilter column operated for a period of 12 days with the parameter values listed in Table 7.1. Each upflow and downflow operation comprised of three day cycles. Hence, cycles 1 and 3 were under upward flow while cycles 2 and 4 were under downward flow. For the case of upflow operation, a gradual decline in performance was observed over the cycle 1 (days 1-3) (Fig 7.7). The moisture content profile for the corresponding time indicated a rapid drop in the moisture in the inlet region due to evaporation and slow redistribution of water in the medium. The loss of inlet moisture with directional switching resulted in a 39-41% drop in performance when cycles 1 and 3 were compared on a daily basis.

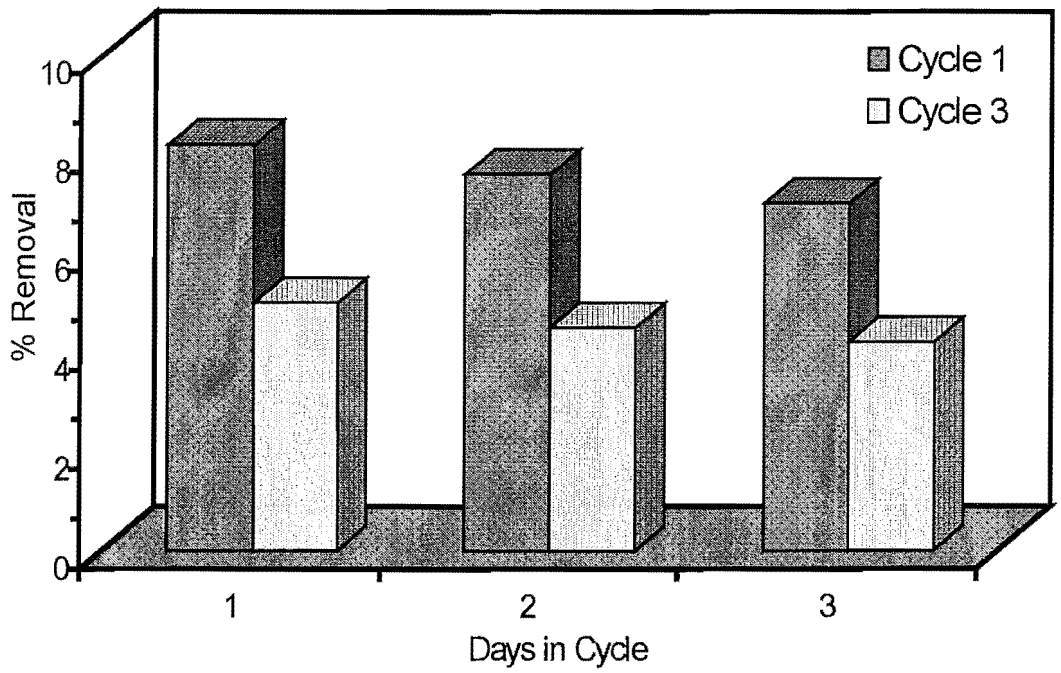

Figure 7.7 Daily comparison of the inlet regions' performance under the upflow cycles of the directionally switched scheme

For cycles 2 and 4 (airflow downwards), the inlet removal was constant and higher than in the opposite direction (Fig. 7.8). The local removal during the cycles did not vary and was primarily linked to the rapid replenishment of moisture to the active region, which as a result

counteracted any moisture loss. Thus, the inlet region under cycles 2 and 4 had a similar moisture distribution pattern and hence similar performance.

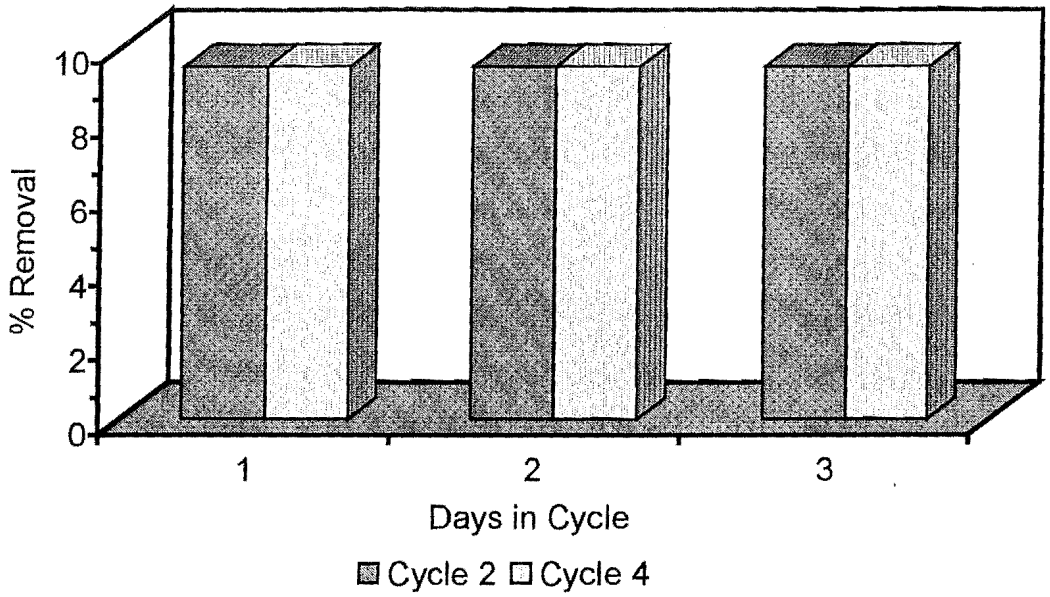

Figure 7.8 Daily comparison of the inlet regions' performance under the downflow cycles of the directionally switched scheme

7.5 Case 9: Frequency Effect on Directionally Switched Biofilters.

The frequency effect of switching the gas flow was determined by reversing the feed stream to the biofilter every day. The moisture content profile (Fig. 7.9) on days 1-2 indicated a slight drop in moisture in the middle of the column, which was due to the development of the temperature profile on day 2. As the flow direction was reversed on day 2 the heat generated from the active region (upper regions) was transferred through convection and evaporation to the lower regions.

This resulted in an initial increase in the local temperatures of the mid regions, which caused the absolute humidity of the oncoming air to increase and resulted in moisture removal from this region. As in Case 8 alternating gas flow resulted in a similar local moisture distribution pattern at the upper regions of the column. Irrespective of the switched airflow direction, the lower regions experienced moisture removal by way of evaporation. However, the drying in the above region was marginally reduced under both frequencies when compared to the UD mode of operation.

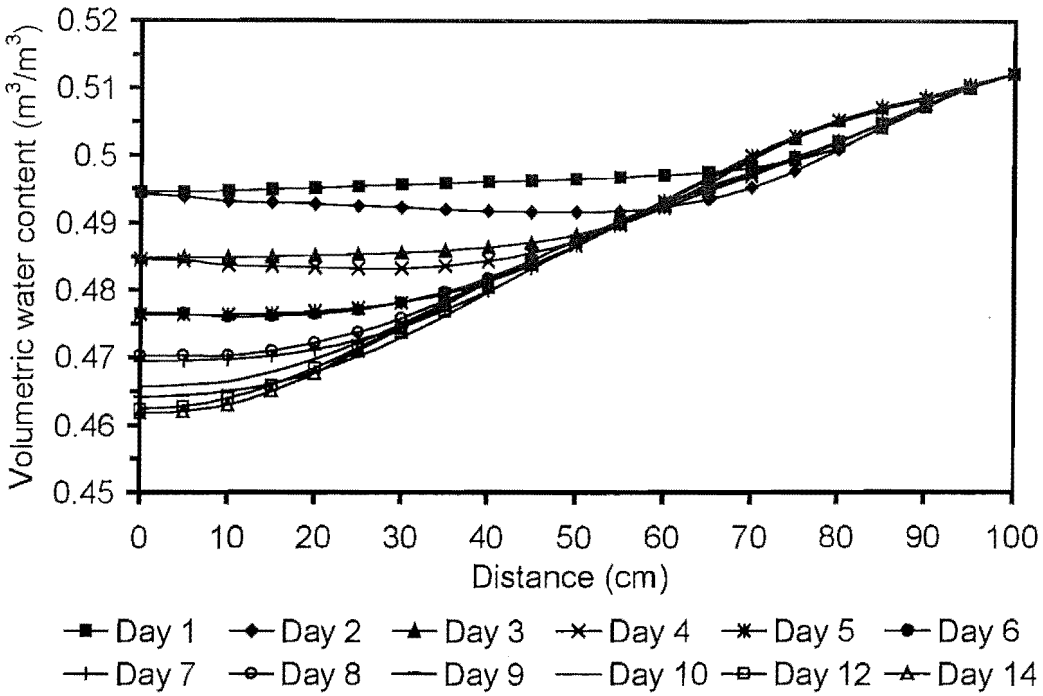

Figure 7.9 Variation of water content along the bed length under directional switching with a one day frequency.

This system reached dynamic equilibrium on day 12 with permanent moisture loss in the lower regions of the column. The concentration profile for the bed (Fig. 7.10) indicated the drying effect on the lower regions of the column by way of an increased local gas phase concentration under both flow directions. Due to better moisture control in the upper region where the bulk activity was concentrated, the gas phase concentration in the upper region remained constant under downflow mode. This system displayed steady state in the upflow direction on day 9 and steady state on day 12 in the downward flow.

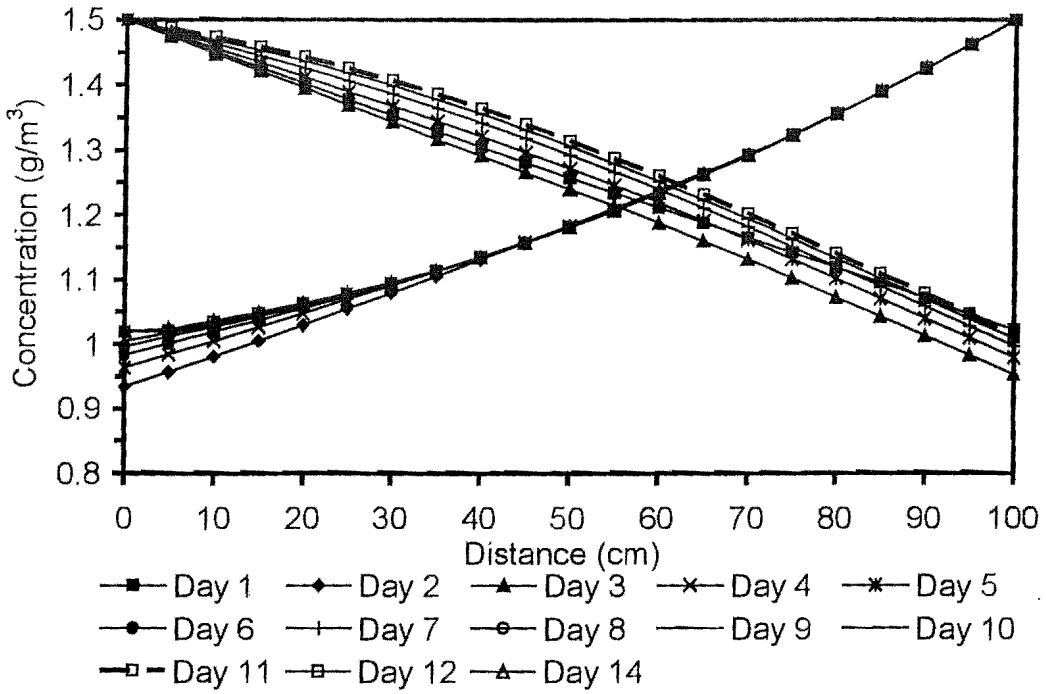

Figure 7.10 Concentration profile of toluene along the bed length under directional switching with a one day frequency

The degradation profile for the bed (Fig. 7.11) indicated a uniform distribution of activity across the bed on day 1. The activity at the air inlet region for the downflow operation was of a higher magnitude due to better moisture control. Continuous moisture loss from the lower regions of the column retarded the local activity and forced the active zone to occur in the upper regions under upflow mode. Compared to downward flow operation, the lower gas phase concentration encountered in the upper regions in this instance forced the degradation in the active zone to be lower.

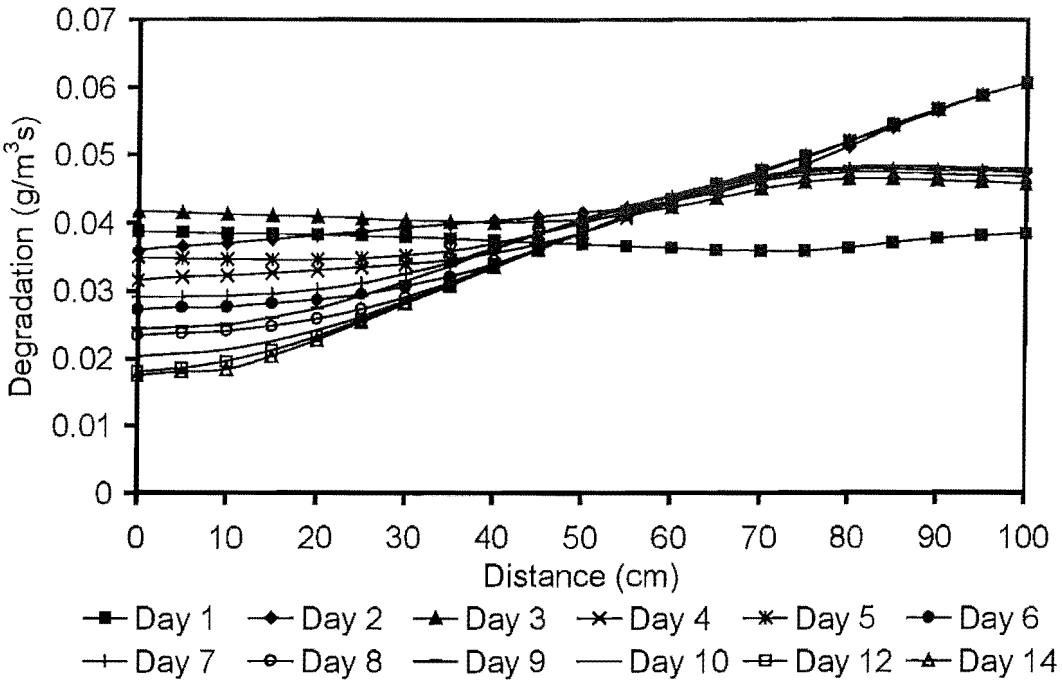

Figure 7.11 Degradation profile of toluene along the bed length under directional switching with a one day frequency.

The system considered provided a steady state RE of 32%, which was higher than the three day switching. Comparison of the moisture content profiles indicated an improved moisture distribution, particularly in the lower regions under the one day frequency. This was attributed to the transfer of the active region more frequently between the water inlet and column bottom, which ensured a lower moisture removal than in either UD (downflow/upflow) operation. The degradation rates of Case 9 were higher when compared to uni-directional downflow operation, which was partially due to a better moisture distribution in the former. The local activity in the upper regions also benefited from the warmer temperatures arising from the upflow operation (300-303 K) as governed by Eq. 3.12. Overall these effects contributed to an increased removal.

Analysis of the inlet region's performance (25% of the column from air inlet) under upflow indicated an initial increase followed by a moisture loss induced steady drop for a 10-day period of operation (Fig 7.12). As stated earlier steady state removal was reached on day 12 in the upflow cycle. However, as stated earlier, due to better moisture control the inlet

region's performance under the downflow mode resulted in a uniform RE of 12%. The value attained was higher than that of Case 8 as the inlet region achieved higher activity due to warmer temperatures from previous upflow operations.

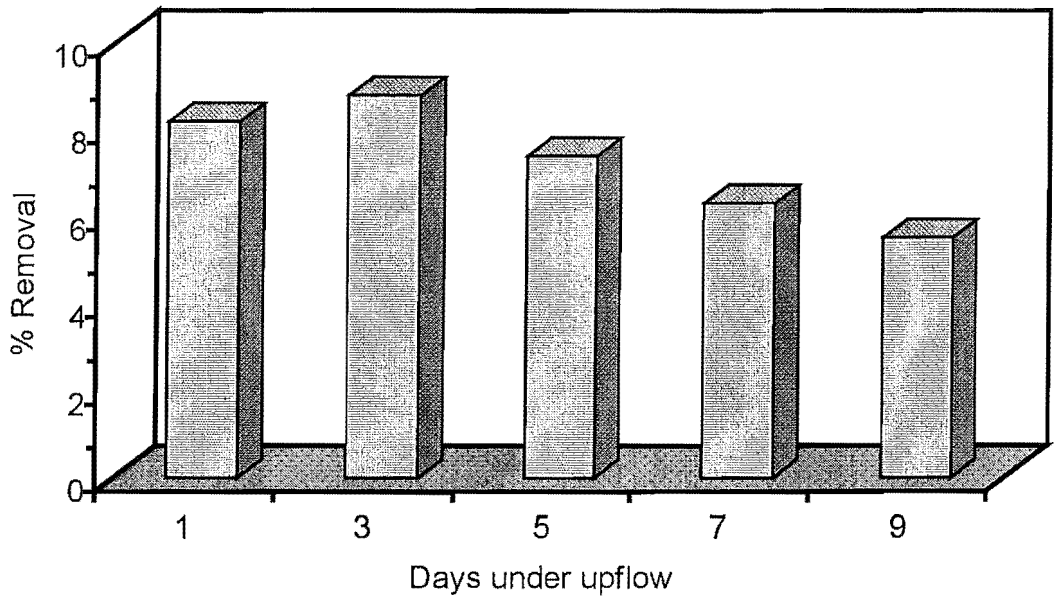

Figure 7.12 Performance of the inlet region under upflow mode during directional switching with a one day frequency

7.6 Case 10: Start up Moisture Effect on Directionally Switched Biofilters

The effect of start up moisture on DS mode was explored by increasing the initial bed moisture content to 0.53 m^3/m^3 and operating the system under the relevant parameter values stipulated in Table 7.1. In this case, the water flow rate was increased to 0.143 g/m^2s to reflect the moisture content at start-up. A three day frequency was selected for the directional switching process. The increase in saturated air temperature from the biological activity caused a drying front to propagate in the water content profile. The inability of the wetting front to redistribute rapidly and counteract the drying further aggravated the moisture loss at the initial stages. The reversal of air flow direction on day 4 caused the bulk degradation to shift to the water inlet region and was depicted as a decrease in local moisture in that region (Fig. 7.13). However, the wetting front subsequently counteracted the drying as indicated by the higher moisture content present in the lower regions when steady state was reached on day 13.

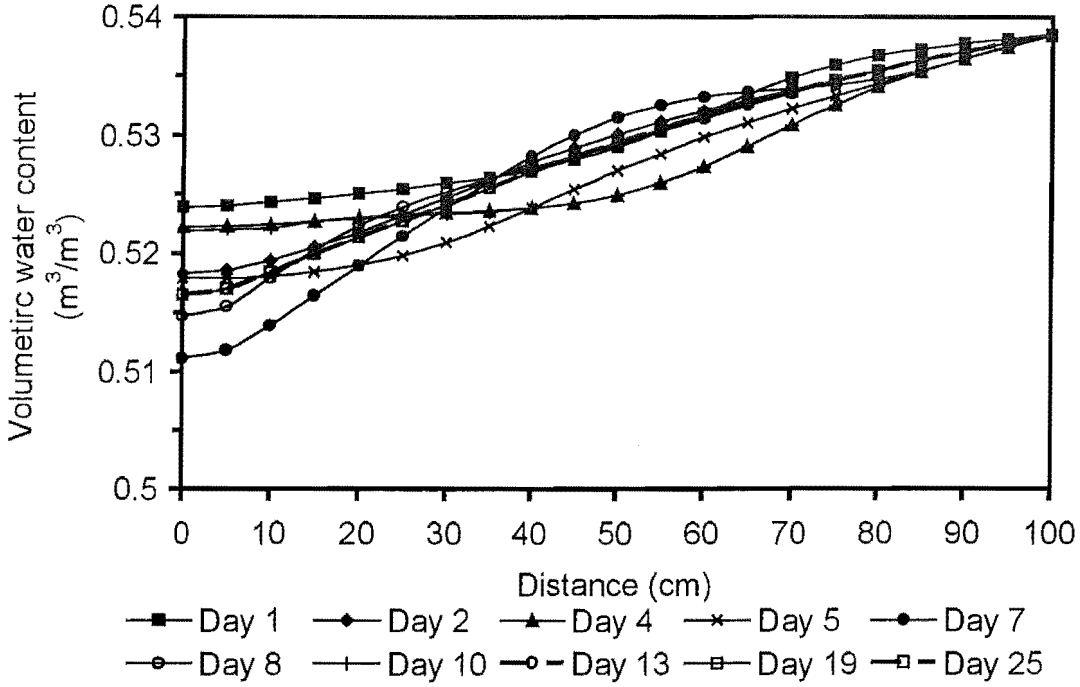

Figure 7.13 Variation of moisture content along the bed length for an initial moisture of 0.53 m^3/m^3, subjected to directional switching with a three day frequency

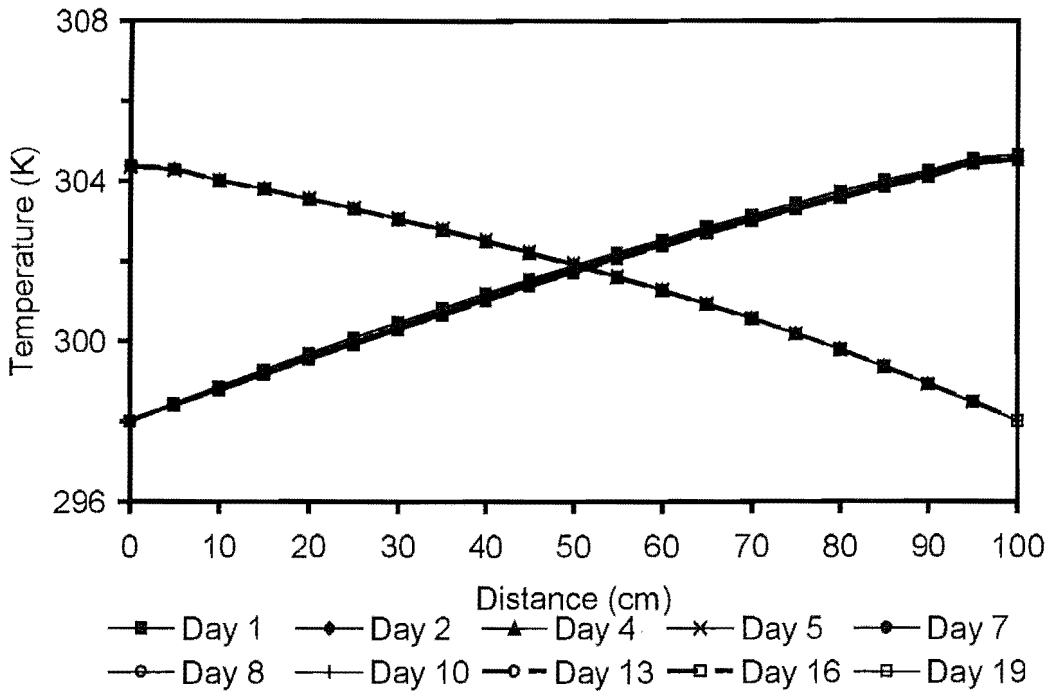

Figure 7.14 Temperature profile along the bed length for an initial moisture of 0.53 m^3/m^3, subjected to directional switching with a three day frequency

Changing the airflow also resulted in an increase in the temperature of the mid regions of the bed (Fig. 7.14). The increase in temperature was associated with the higher metabolic activity arising from a better moisture control in the active region (upper region). The subsequent evaporation caused a drop in moisture content in the mid region. With time the lower regions of the bed attained a higher temperature and the moisture loss mechanism as above was repeated in this region too.

The local moisture loss was not significant enough to cause a drop in activity in the lower regions and hence the gas phase concentration for days 4-5 remained constant (Fig. 7.15). The greater activity present was reflected in the steady state removal efficiency of 50%, which was higher than all previous operations under directional switching.

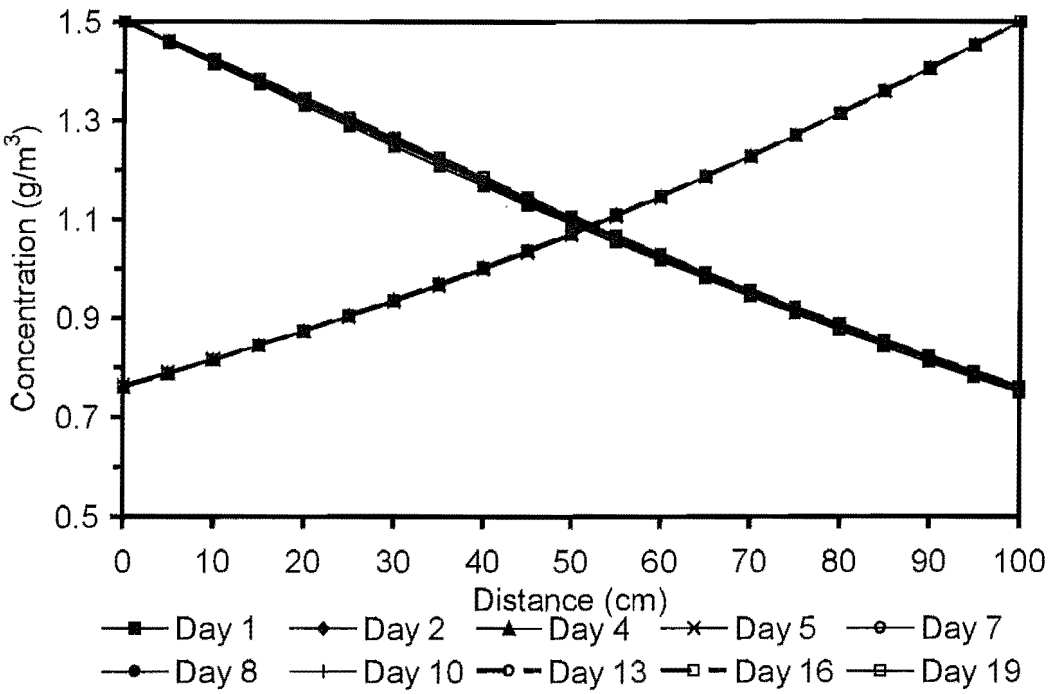

Figure 7.15 Concentration profile along the bed length for an initial moisture of 0.53 m^3/m^3, subjected to directional switching with a three day frequency

Compared to operation at a start-up moisture of 0.5 m^3/m^3 (Case 8 & Case 9), the reversal of airflow on day 7 caused the active region to shift to the lower regions of the column. However, the degradation rates were lower than when compared to days 1-2, due to the lower

water content present (Fig. 7.16). Subsequent water advection was successful in overcoming drying and increasing the local moisture content. This increased the local microbial activity in the lower region around day 8, but was not sufficient enough to be reflected in the concentration profile for days 7-8. As the flow direction was reversed on day 10, this system reverted to a scenario similar to that of day 4 in terms of both the moisture distribution and microbial activity.

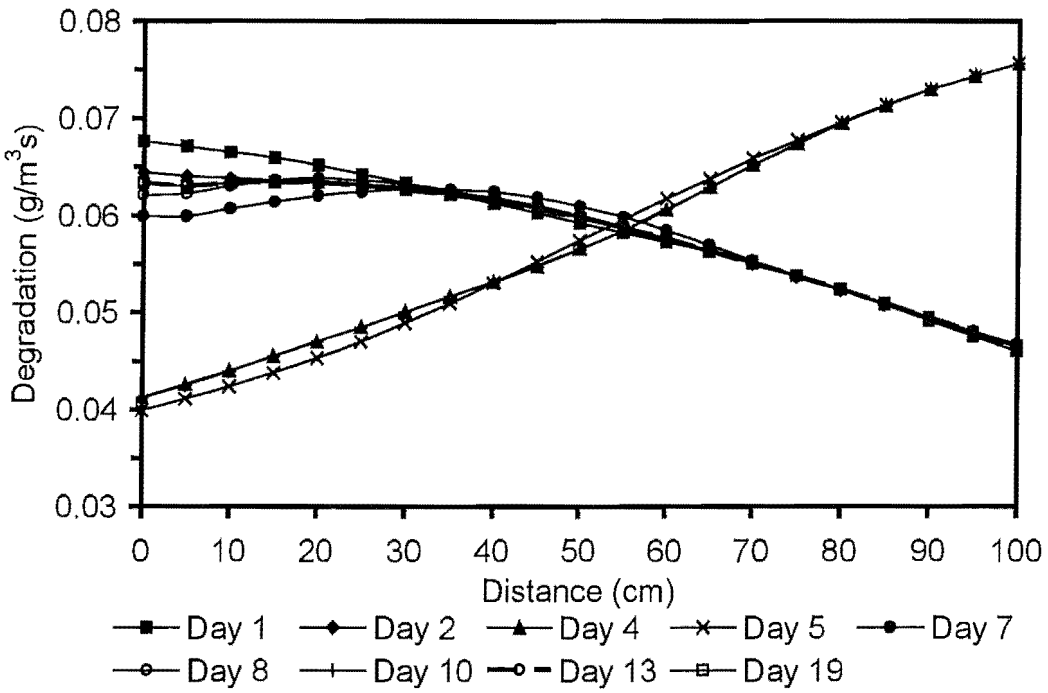

Figure 7.16 Degradation profile along the bed length for an initial moisture of 0.53 m^3/m^3, subjected to directional switching with a 3-day frequency

7.7 Conclusions

In this chapter, directional switching was explored as a potential operating scheme to overcome the media drying caused by high mass loadings. A comparison of the performance of a DS system with a three day frequency with other schemes using constant irrigation, indicated no significant improvement in removal. The removal in the DS scheme was also lower than that achieved with irrigation using feedback control. However, model simulations with a one day frequency provided an improved performance, which implied that for successful DS operation a high switchover rate would be required. The effect of higher initial

moisture content on DS schemes indicated an improved performance from a higher local activity. But, an upflow biofilter operated under the same parameters/initial conditions also provided similar results in terms of both removal and leachate. Thus, it was concluded that, contrary to expectations, directional switching with a three day frequency would not yield a superior performance through better moisture distribution, when treating high mass loadings. Although a higher removal is possible with higher frequencies, practical difficulties pertaining to implementation when compared with the traditional forms of operation could cause such schemes to be rejected at an industrial scale. The analysis performed in this chapter also reiterated the need to implement irrigation strategies based on feedback control, when accurate and robust moisture control is required.

A summary of the different case studies analysed in this work is given in Table 7.2.

Table 7.2 Summary of the case studies

Case #	Toluene Loading (g/m^3h)	Gas Flow Direction	Initial Moisture Content (m^3/m^3)	RE (%)	Water Flux (g/m^2s)	Leachate (g/m^2s)	Feedback Control (Y/N)	External Disturbance (Y/N)
1	60	Upwards	0.5	26	5.46×10^{-2}	1.5×10^{-3}	N	N
2	13	Upwards	0.5	88	5.46×10^{-2}	1.6×10^{-2}	N	N
3	13	Upwards	0.5	97	8.21×10^{-1}	7.8×10^{-1}	N	N
4	13	Downward	0.5	89	5.46×10^{-2}	1.95×10^{-2}	N	N
5	13	Upwards	0.5	88	5.46×10^{-2}	2×10^{-2}	N	Y
6	13-62[a]	Upwards	0.5	84	2.5×10^{-1}	7×10^{-2}	Y	Y
7	13-62[a]	Upwards	0.5	84	2.5×10^{-1}	7×10^{-2}	Y	Y
8	60	Switched (3-Day)	0.5	26.5	5.46×10^{-2}	1.55×10^{-3}	N	N
9	60	Switched (Daily)	0.5	32	5.46×10^{-2}	5.1×10^{-3}	N	N
10	60	Switched (3Day)	0.53	50	1.43×10^{-1}	6×10^{-2}	N	N

a = A step change in mass loading, from 13-62 g/m^3hr was introduced one day after steady state was reached.

Chapter 8: Experimental Results

Introduction

As indicated in the modelling work of chapter 5, the model was found to be quite sensitive to the form of the relationship between water content and microbial activity. This aspect was further highlighted by the high degree of sensitivity indicated by the model to the kinetic parameters in the degradation term. Since the premise of the modelling work was the independent validation of key parameters it was decided to use experimental data obtained from the differential reactor (chapter 4), to investigate the relationship between water content and performance. The goal of this work therefore was to explore the above relationship by rigorously controlling the medium moisture and also to elucidate whether performance was entirely moisture dependent.

8.1 Concentration Profiles

The toluene degradation profiles with acclimatised microorganisms at matric potential values of -6, -16, -26, -36 cm H_2O, indicated a period of constant degradation followed by a non-linear region at lower concentrations. The concentration profile for toluene at matric potential values of -6 and -26 cm H_2O are provided in Fig. 8.1. Similar profiles were observed in other experiments at varying matric potentials (Appendix D).

Similar observations of constant degradation rates followed by reduced rates were made in the degradation of 2,4-dinitrophenol (DNP) using an indigenous microbial consortium (Hess *et al.*, 1996). The constant degradation rate region would support the argument of a biologically limited region of activity controlled by a constant maintenance energy requirement (Pirt, 1975), which was independent of the extracellular substrate concentrations. The use of a maintenance metabolism approach was stressed particularly in batch scale work due to the slow growth rate coupled together with the low concentration present (Andrews, 1984). Maintenance models were also used to describe the mineralisation of toxic substrates in soils (Schmidt *et al.*, 1985b). It was also postulated that maintenance energy contained an additional growth dependent term and its implication was explored using oxygen consumption rates (Pirt, 1982).

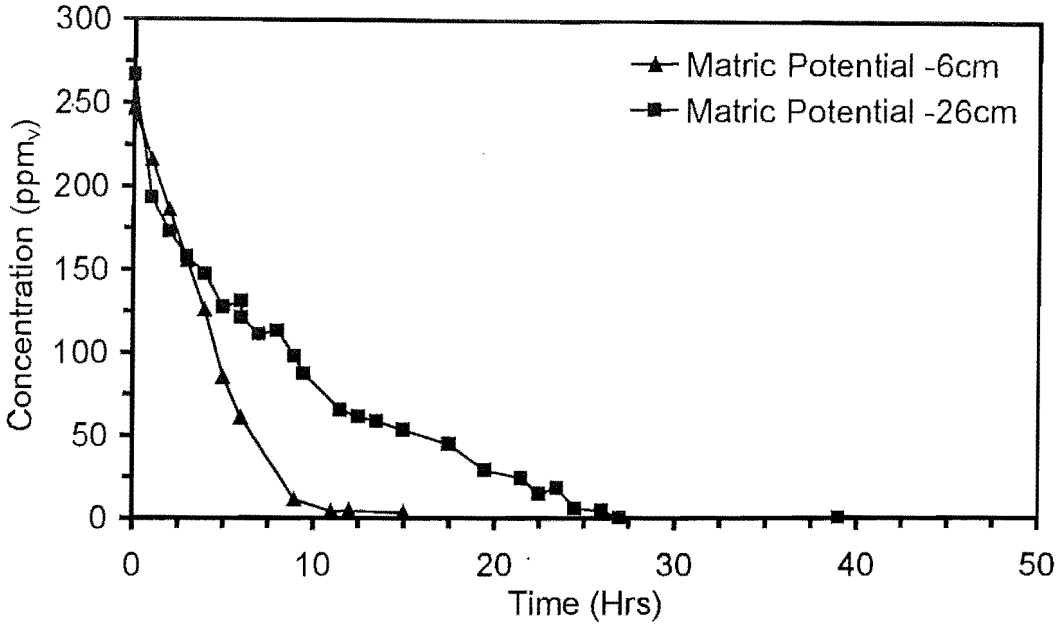

Figure 8.1 Concentration profiles of toluene with time in the batch recycle reactor-using compost at -6 & -26cm H_2O matric potential.

The presence of a nonlinear degradation rate towards the lower end of the concentration profile indicated the possible transition to diffusion or kinetically limited degradation. For a non-indigenous pentachlorophenol (PCP) degrading consortium, mineralisation at low concentration was not adequately described by a maintenance model (Hess *et al.*, 1996) and was attributed to the presence of mass transfer limited metabolism. However, more experiments would be required to differentiate mass transfer and metabolism effects on degradation in this system.

8.2 Water Retention Curve

The water retention curve (WRC) for a porous medium is dependent on the texture and structure and is therefore unique to each medium. The WRC consists of four main regions (Stephens, 1996), is highly non-linear (Hanks, 1992) and is obtained by establishing a series of equilibria between the soil water and bulk water at a known matric potential (Klute, 1986). Due to the presence of hysteresis the WRC consists of both a drying and wetting curve. The wetting curve is mapped by establishing equilibrium in soil samples by wetting from a low water content (residual water content) to natural saturation (Klute, 1986).

In this study, the WRC for compost was generated for a range of matric potentials used along the wetting direction (wetting curve). In this case, static reactors that were uncoupled from the flow system were used to obtain the equilibrium moisture contents corresponding to the matric potentials applied. As discussed earlier, to ensure that the moisture content in the medium was maintained at a constant value, periodic dry weight analysis of reactor compost were performed. The values were subsequently compared to the moisture contents corresponding to the matric potential applied from the water retention curve (WRC).

Literature indicated that ambient temperature has a significant influence on the steady state moisture contents and that the effect tends to be more pronounced in the low water content regions (Hopman *et al.*, 1986a). The temperature effect on the WRC was attributed to a multitude of factors, such as the influence of temperature on the surface tension at the air water interface, entrapped air and the presence of surface-active contaminants, which would produce temperature-surface tension relationships exceeding that of pure water. In Liu *et al.* (1993) a new theory was proposed to elucidate the temperature effect on the WRC, which assumed the water to consist of isolated and continuous water and where the latter parameter would determine the matric potential. Under this approach, the inclusion of a temperature dependence on the isolated water content resulted in an additional temperature dependence on the WRC.

The WRC for Organix compost (Fig. 8.2) was thus obtained at a constant 30 °C. Analysis of the WRC indicated that the slope of the curve increased as water content was reduced. Thus, the trend observed was quite similar to what was observed by Hon (1999) for the WRC generated using a steady state, long column, constant flux method for Organix compost. Hence, the effect of changing matric potential on system performance in terms of moisture content was more pronounced at lower water content values.

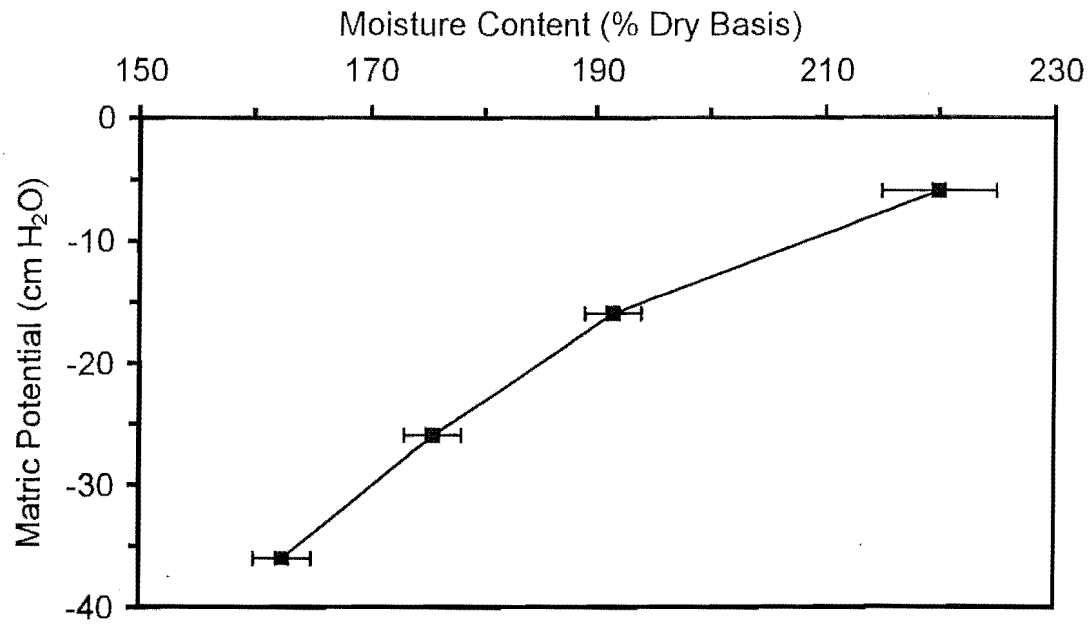

Figure 8.2 Water retention curve for Organix compost (wetting curve).

8.3 Water Content Effects on Degradation

To determine the effect of different moisture contents on biological activity, the elimination capacities from the initial, linear region (biologically-limited) of the concentration profiles (>50 ppm_v) were compared. The higher degradation rates in this region caused greater stress on the moisture content and full-scale bioreactors also tend to operate in this constant rate regime (Cherry & Thompson, 1997). Additionally, in this batch system, degradation at the lower concentrations took extended periods of time and caused practical issues pertaining to monitoring. Elimination capacities (EC) were averaged over two runs. The EC values at the different matric potentials ranged from 24 g/m^3h to 155 g/m^3h and matched the range of values stated in literature for toluene elimination capacity (Devinny *et al.*, 1999; Elmrini *et al.*, 2001)

The EC results were initially generated with increasing media moisture content (wetting curve) (Fig. 8.3). The error bars in Fig. 8.3 indicated the range of the two steady state EC values. The EC was relatively constant between -36 and -16 cm H_2O with some indication of possibly a slightly lower EC at the mid-range matric potential (-26 cm H_2O) value. The EC was markedly higher at the wetter region associated with -6 cm H_2O. The moisture content varied considerably over the range of matric potential generated with -36 cm H_2O corresponding to 1.65 g/g on a dry basis and -6 cm H_2O generating 2.20 g/g

on a dry basis (Fig. 8.2). Although reduced toluene degradation at low water contents was observed in a peat bed (Acuna *et al.*, 1999), this was attributed to a non-homogeneous distribution of moisture. For the current results, moisture changes were adequately counteracted with a robust moisture control strategy.

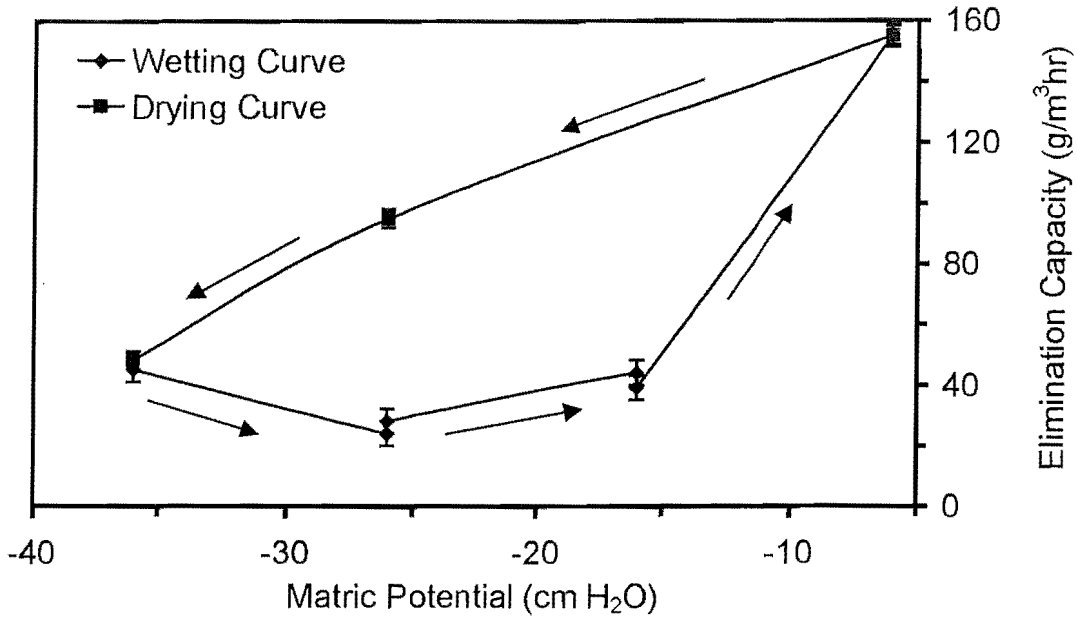

Figure 8.3 Variation of elimination capacity with matric potential for toluene removal by compost in a batch recycle reactor

The batch system developed did not allow careful study of the dynamics of EC changes with matric potential changes. However consistent batch degradation profiles took at least one to two weeks to develop. This time period could not be adequately explained purely by the dynamics of water content change, since separate experiments indicated that moisture content attained equilibrium within two to five days after a change in matric potential. A detailed investigation of these dynamics would require the system to be operated in a continuous mode.

The EC values for the system were also computed at decreasing moisture contents (drying curve). Under this approach the EC dropped in a more steady fashion between -6 cm H_2O and -36 cm H_2O. The elimination capacity at -26 cm H_2O from the drying curve was considerably higher than that at the same matric potential along the wetting curve (95 g/m^3h vs. 24 g/m^3h). The most probable explanation for the EC hysteresis was that

there was a higher moisture content at -26 cm H_2O during the drying cycle. While many porous media display hysteresis in the water retention curve (Klute, 1986), earlier experiments did not show hysteresis in Organix compost (Hon, 1999). If water content hysteresis was the cause for variation at -26 cm H_2O, it would indicate that the physical amount of water and not the inherent matric potential was the controlling mechanism for the variation in EC in Fig. 8.3.

The EC values at -36 cm H_2O along the wetting (initial) and drying curves did not show significant variation. It was possible that hysteresis in moisture content became negligible at this point or that another mechanism was controlling the elimination capacity at the lower water contents. A combination of operation at lower matric potentials (< -36 cm H_2O) and a more detailed water release curve would be required to determine if the EC continues to drop at low matric potentials and if it continues to remain unique, independent of the direction of approach. The lack of variation in EC at -6 cm H_2O is purely an artifact as that was the highest matric potential achieved. The potential of hysteresis in moisture content is the subject of future work.

8.4 Repeatability Tests

Although the apparatus constructed permitted the accurate control of the medium moisture content, it did not guarantee that the observed changes in EC were entirely due to moisture content changes. Other changes that could have influenced the EC include active biomass content, specific biomass activity and metabolic degradation product concentrations. Thus, repeatability tests were performed at matric potential values of -26 and -16 cm H_2O along the wetting direction. These repeats represented the same compost that had experienced a number of batch degradation cycles at different matric potentials prior to returning to the given matric potential.

The EC values yielded in the repeatability runs for the above matric potential values were 28 $\pm$ 2 g/m^3h and 39 $\pm$ 3 g/m^3h respectively. The results obtained thus demonstrated significant repeatability (Fig. 8.3) in terms of the EC at the two matric potentials concerned. These repeatability runs were performed as independent experiments using two separate reactors. The reactor used to obtain EC at -26 cm H_2O matric potential was subjected to 20 batch cycles of one day duration along the drying curve (-6 to -36 cm H_2O) prior to its operation at -26 cm H_2O. Similarly, 12 days of batch runs were

performed along the wetting curve (-36 to -26 cm H_2O) on the reactor used to obtain EC at a matric potential of -16 cm H_2O. Hence, it was concluded that the microbial structure and environmental conditions within compost remained unchanged and that EC changes were due to changes in the physical water content. This was supported by observations made by Cox, *et al.* (1996), where, irrespective of the water activity, styrene degradation by a fungal culture was greatly dependent on the media moisture content. The water activity (a_w) computed for the range of moisture contents (1.65 to 2.20 g/g on a dry basis) presented here was 0.999975-0.999995 (Papendick, 1980) (ignoring osmotic potential contributions), which was sufficient to maintain a bacterial activity (Bohn, 1999). Additionally these results support the argument that the difference in EC along the wetting and drying curve was due to the presence of water content hysteresis in the medium.

The range of matric potentials studied here was certainly not inclusive of conditions seen in biofiltration and the conditions investigated were qualitatively on the wet side. The maximum EC was observed at -6 cm H_2O, but this matric potential could be difficult to maintain over an entire length of a standard biofilter and there could be additional operational issues of pressure drop and leachate production at these water contents. This reactor system should be able to investigate the EC at lower water contents more typical of industrial biofilter operation 40% - 60% wet basis (0.67-1.5 g/g dry basis), which is the subject of future work. However at some point, the low hydraulic conductivity of compost at low matric potentials could make the maintenance of a constant water content over extended periods of time somewhat difficult (Hon, 1999).

8.5 Adsorption Isotherms

The adsorption isotherms generated at 25 °C & 35 °C using microbially inhibited compost depicted the variation of toluene sorption with headspace toluene concentration under equilibrium conditions. The experimental results obtained in this case indicated that in the absence of microbial activity, the compost medium had a significant sorption capacity. But, this is case specific as the actual sorption to gas phase contaminant mass ratio would depend on the gas volume and the amount of solid in the system considered. For the toluene concentration range (0-1000 ppm_v) tested under both temperatures, the equilibrium solid phase concentration of toluene increased linearly as a function of headspace toluene concentration. In this case linear equilibrium isotherms were fitted to both sets of data and the equilibrium coefficient in each case determined using an ordinary least squares algorithm. These results (Fig. 8.4) also indicated the relative influence of temperature effects on the sorption capacity of the bed medium.

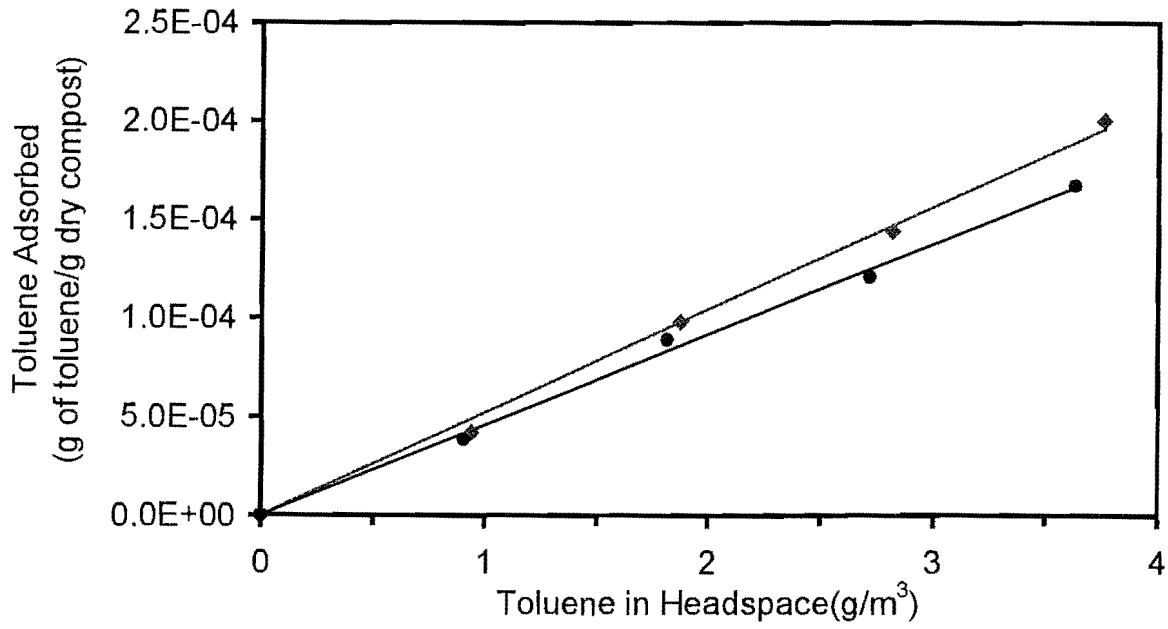

Figure 8.4 Equilibrium isotherms for toluene in compost at 25 °C (♦) and at 35 °C (•)

The isotherm at 25 °C was described by $y = 5.21\times10^{-5}x$ and at 35 °C by $y = 4.57\times10^{-5}x$. Although, the sorption capacity of the bed medium did not vary significantly with temperature, the results indicated that a slight difference did exist in the adsorbed phase concentration particularly at higher headspace concentration values. This was also consistent with the observations made by Apel *et al.* (1994) with regard to gasoline adsorption onto a compost medium. Literature indicated that this phenomenon was attributed to the variation of the equilibrium coefficient with temperature according to an Arrhenius type relationship (Ruthven, 1984). Hence, the two equilibrium coefficients experimentally obtained at 25 °C and 35 °C were fitted to an Arrhenius type model and the relevant parameters obtained by minimising the sum of squares of residuals (SSR) using the solver tool in Excel®. This equilibrium coefficient with the Arrhenius relationship as given below was subsequently used in model simulations.

$$K_{eqm} = k_0 e(-\Delta H / RT) \qquad \text{[Eq. 8.1]}$$

The values obtained were as follows,

$k_0 = 7.43\times10^{-7}$ g of toluene/(g of dry compost)(g/m^3), $\Delta H = -10.5\times10^3$ J/mol.

However, in order to be unit consistent with the model variables, the equilibrium coefficient was converted to be expressed as per volume of compost as given in Eq. 3.18.

For comparison purposes the adsorption data were fitted to a Freundlich model, which also yielded a linear relationship. The equilibrium adsorption coefficient thus obtained at 25 °C amounted to 0.0521 mg/g of dry compost. In this case the adsorbed phase concentration was expressed per g of dry compost to provide consistency in the final results as the moisture content of the compost used could vary from one sample to another. Thus, the value obtained was an order of magnitude smaller than the value (0.459 mg/g dry peat) reported by Acuna *et al.* (1999) and was slightly less than the value (0.0225 mg/g moist material) of Shareefdeen *et al.* (1994). Increased adsorption of toluene had been attributed to the presence organic matter in soil (Fan & Scow, 1993) and hence the higher organic content of peat could contribute to the greater sorption effect observed.

Chapter 9: Conclusions and Recommendations

9.1 Conclusions

A transient biofilter model incorporating the mass and energy balance was developed during this study. An important inclusion was the water balance, which was the main mechanism for coupling the biological heat generation with the heat loss to the environment. The governing equations were derived from first principles and simplifying assumptions. The key assumption in the model was that diffusion in the biofilm was neglected, by treating the biofilm as well mixed and in instantaneous equilibrium with the gas phase. This permitted the degradation within the biofilm to be written directly as a function of the gas phase concentration as in solid-phase catalysis. Under this approach, the overall degradation term contained the uncertainty associated with the biofilm parameters. A LDF (Linear Driving Force) approach was used to model the dynamics in the solid phase, under which the solid phase was treated as consisting of well-mixed layers. A biologically limited scenario was modelled as biofilm dynamics were neglected and mass transfer dynamics consigned to the inert solid phase. The energy balance of the model assumed a pseudohomogeneous structure based on thermal and moisture equilibrium in the system. The water balance of the model consisted of the mixed form of Richards' equation together with experimentally obtained hydraulic properties of compost. Based on the assumptions and structures, a dynamic biofilter model was developed where all parameters could be independently verified without any estimation from column data.

Simulations were performed to determine suitable irrigation strategies for a biofilter system that was subjected to various practical operational conditions. Constant water addition schemes as well as irrigation schemes based on feedback control were implemented and each scheme compared in terms of removal and leachate produced. The effect of changing the airflow direction periodically was also explored in the simulations. A sensitivity analysis was performed to evaluate the influence of model parameters on system performance.

9.1.1 Dynamic Model Simulations

Simulations on high and low mass loading scenarios indicated the importance of moisture on biofilter performance and also that adequate water addition was imperative in maintaining high removal efficiency. Model simulations qualitatively matched the experimental results in literature where available, although no explicit experimental validation was performed. A simulation varying the inlet air temperature indicated the complexity of attempting to maintain a desired moisture content using a constant water addition rate. This demonstrated the need to have a water flux that was sensitive to moisture variations induced by external disturbances and that arbitrary increases in the water flux rate to gain higher removal efficiency would result in greater leachate generation. The effect of airflow direction was explored by simulating systems that contained both upflow and downflow contaminant streams. The resulting comparisons between the airflow directions were supported by experimental observations in literature.

The model was utilised to determine the effect of directional switching for a high mass loading of 60 g/m^3h. The 26.5% removal for the three day directional switching, when compared with conventional operating schemes did not demonstrate any significant improvement, which suggested that the desired increase in moisture was not attained. In contrast, directional switching with a one day frequency yielded a higher removal of 32%, due to a better moisture distribution from the frequent switchover of the active region. The above work necessitated the evaluation of directional switching at higher start-up moisture content. Although this approach did produce an improved removal, it was similar to an upflow biofilter operated under the same moisture content. This work was able to highlight directional switching as a potential operating scheme, particularly when the airflow stream is subjected to high frequency changeovers.

Owing to the inherent weakness of open loop irrigation schemes in maintaining medium moisture and removal, when subjected to disturbances, irrigation strategies based on feedback control that incorporated on-line measurement of moisture content were implemented. Thus two measurements, bed weight and the average of moisture content at three points, which corresponded to bulk moisture measurements using load cells and point measurements using time domain reflectometry or tensiometers were tested using the model. Simulation results were performed for a disturbance rejection scenario that incorporated load variations from 13 g/m^3h to 62 g/m^3h and inlet air temperature

variations from 298 K to 283 K. The outcome of the simulations provided a valuable insight into the performance of automated irrigation schemes in biofilters subjected to external disturbances. The superiority of these schemes over the more traditional direct water addition was amply depicted by the maintenance of a higher removal of 84% as opposed to the 73% removal achieved in the latter, when subjected to the above disturbances. These simulations also demonstrated their capability in maintaining a desired bed moisture content, under externally induced moisture variation.

Although the scheme utilising average moisture content had higher sensitivity to the spatial moisture distribution, the overall results in terms of the 84% removal and 0.07 g/m^2s leachate rate were similar to that of the scheme using bed weight. However, an improved performance would be possible by the placement of probes at optimum positions. The case using bed weight as set point demonstrated that, adequate moisture control could also be achieved through common automated irrigation schemes based on load cell measurements. Optimising the system parameters to provide a sufficient removal with lower leachate could further refine this approach. Overall the simulations performed with the above closed loop irrigation schemes indicated their viability for accurate moisture control and thereby justified to a certain extent the capital expenditure associated with full-scale implementation of such automated schemes.

9.1.2 Water Content Effects on Degradation

As model simulations indicated a high sensitivity of moisture content on degradation, this relationship was experimentally investigated. A novel batch recycle bioreactor was developed, which tightly controlled the moisture content of the packing medium using the suction cell principle. The reactor was used to determine the moisture content effect on toluene degradation in a compost medium between matric potentials of -36 cm and -6 cm H_2O. The concentration profiles for toluene removal demonstrated an initial region deemed to be under maintenance metabolism and a non-linear region indicating a possible movement into mass transfer limited metabolism. A maximum elimination capacity of 155 g/m^3h was observed at the highest water contents in the linear region. However, the distinction of mass transfer and metabolism effects on the above degradation data would require additional experimental analysis.

Degradation data obtained from the bioreactor indicated unique elimination capacity profiles along the wetting and drying curves. The EC was higher at a given matric potential along the drying curve than the wetting curve. The general trend in the data obtained qualitatively matched results in literature. Repeatability runs performed along the wetting curve for matric potential values of -26 cm and -36 cm H_2O indicated that changes in media moisture content were the sole cause for EC changes in the system. This suggested that the difference in EC along the wetting and drying curves was dependent on the physical water content and not the matric potential applied. Thus, the 295% increase in EC (from 24 to 95 g/m^3h) observed at -26 cm H_2O along the drying curve was attributed to the potential of hysteresis in the physical water content. The possible reduction of hysteresis at low water content explained the smaller variation in EC at -36 cm H_2O. Although previous observations did not indicate the presence of water content hysteresis in compost, the potential for hysteresis from the current set-up would be greater as the matric potential was an independent variable. The rigorous maintenance of medium moisture content in this experimental set up was confirmed by performing periodic dry weight analyses of reactor samples and comparing these with the steady state moisture content data. The results indicated that the difference was within the measurement error for dry weight analysis (± 2-5 %).

9.1.3 Sorption Capacity of Compost

Microbially inhibited compost was used in batch scale experiments to determine the sorption isotherm for toluene on compost. The isotherms were generated over a concentration range of 0-1000 ppm_v. The temperature effect on the sorption isotherm was also determined by performing the above experiment at temperatures of 25 °C and 35 °C. Linear isotherms were obtained for the above temperatures in the concentration range tested. The equilibrium coefficient of the isotherm at 25 °C was an order of magnitude lower than that reported in literature for peat. Based on reported comparisons between soil and peat, the lower adsorption capacity suggested a potential limitation of the organic content within compost.

In general the temperature effect on the sorption capacity was more pronounced at the higher headspace concentration values, which qualitatively agreed with observations in literature. This indicated a varying equilibrium coefficient with temperature, which was

subsequently modelled in the form of an Arrhenius type relationship and incorporated into the model.

9.2 Recommendations

The simulation model developed here provided a flexible, yet comprehensive tool to implement and evaluate various biofilter operational schemes under different irrigation strategies. The robustness and the accuracy of the simulations generated were numerically verified. However, it is recommended that the model be experimentally validated, so that its suitability to simulate pilot or full-scale bioreactors could be adequately determined. It is also envisaged that the moisture content - degradation effect, which was experimentally evaluated, be incorporated into the model to facilitate more accurate simulations. Furthermore, the presence of possible hysteresis in water content as concluded in the experimental component needs to be further explored. Future work within the research group will focus on performing independent experiments to determine the existence of separate wetting and drying curves for compost, for a range of matric potential values. If the presence of hysteresis is substantiated, it is suggested that this phenomenon be reflected in the model simulations. This would involve the incorporation of the hysteresis effect in the non-linear, matric potential-conductivity and matric potential-water content relationships.

The reactor configuration developed in this study, with its robust moisture control strategy, could be used as a research tool to determine a comprehensive relationship between moisture content and degradation. In this regard, the reactor should be used to investigate elimination capacities at moisture contents more representative of field scale biofilters. These data would provide a valuable input for optimising both pilot and full-scale biofilter performance, in terms of moisture content. This should be investigated by operating the reactor set-up under continuous mode and obtaining the steady state elimination capacity data as a function of both inlet concentration and moisture content. This form of operation would also facilitate the analysis of EC transients with moisture content changes, which was not possible under the batch system. However, caution must be exercised under a continuous gas flow stream as it could lead to bed medium drying, potential oxygen limitation and transient inlet concentration. Thus, preventive measures should be implemented to overcome the above with particular emphasis placed on the

provision of adequate humidification of inlet air. The experimental set-up used manual gas sampling and analysis, which was tedious and particularly cumbersome when extended runs were performed. With the system configured for continuous flow operation, it is however recommended that a combined GC and auto sampling device be used to monitor the gas phase accurately and conveniently. Temperature within the system though regulated to $30 \pm 0.5^{\circ}C$ could be further improved by using a temperature control unit with a rapid response. It is also recommended that the current heat source consisting of incandescent bulbs be replaced with a heating coil for durable and reliable heat emissions.

The reactor in its current form should also be used to ascertain the effect of other media types and their composition on the degradation rates. This would indicate whether the moisture content-degradation relationship is medium specific or not. Since the system has a rigorous control over the water content applied this would also permit the studying of the implication of trace nutrient additions in a controlled environment. Additional experiments should also be carried out to verify the effects of wetting fluids and medium pH on the degradation rates of various compounds.

References

1. Abumaizar, R.J., Smith, E.H., Kocher, W. Analytical model of dual media biofilter for removal of organic air pollutants, *Journal of Environmental Engineering*, 123(6), 606-614, 1997.
2. Acuna, M.A., Perez, F., Auria, R., Revah, S. Microbiological and Kinetic Aspects of a Biofilter for the Removal of Toluene from Waste Gases, *Biotechnology and Bioengineering*, 63(2), 175-184, 1999.
3. Amanullah, Md., Farooq, S., & Viswanathan, S. Modeling and Simulation of a Biofilter, *Industrial and Engineering Chemistry*, 38, 2765-2774, 1999.
4. Amanullah, Md., Farooq, S., & Viswanathan, S. Equilibrium, kinetics and column dynamics of Methyl Ethyl Ketone Biodegradation, *Industrial and Engineering Chemistry*, 39, 3387-3396, 2000.
5. Andrews, G.F. Parameter Estimation from Batch Culture Date, *Biotechnology and Bioengineering*, 26, 824-825, 1984.
6. Apel, W.A., Kant, W.D., Colwell, F.S., Singleton, B., Lee, B.D., Andrews, G.F., Espinosa, A.M., Johnson, E.G. Removal of Gasoline Vapors from Air Streams by Biofiltration; Chapter 9, in "Emerging Technologies in Hazardous Waste Management IV, ACS Symposium Series". D.W. Tedder and F.G. Pohland, eds. American Chemical Society, Washington. D. C, pp 142-159, 1994.
7. Archer, H.E., Fullerton, R.W. In *Proceedings of the New Zealand Water Supply and Disposal Associations' Annual Conference*, 1992.
8. Auria, R., Aycaguer, A.C., Devinny, J.S. Influence of Water Content on Degrdation Rates for Ethanol in Biofiltration, *Journal of the Air & Waste Management Association*, 48,65-70, 1998.
9. Bailey, J.E., & Ollis, D.F. *Biochemical Engineering Fundamentals*, McGraw-Hil, Inc, USA, 1986.
10. Baltzis, B.C., Androutsopoulou, H. *Proceedings of the Air & Waste Management Association's 87th Annual Meeting & Exhibition*, Paper No 94-RP115B.02, Cincinnati, OH, 1994.

11. Baltzis, B.C. Biofiltration of VOC Vapours, *Biological Treatment of Hazardous Wastes*, John Wiley & Sons. Inc, 119-150, 1997.
12. Bear, J. *Dynamics of Fluids in Porous Media,* American Elsivier Publishing Company, New York, USA, 1972.
13. Bohn, H.L., and Bohn, K.H. Moisture in Biofilters, *Environmental Progress*, 18(3), 156-160, 1999.
14. Bohn, H., Consider Biofiltration for Decontaminating Gases, *Chemical Engineering Progress*, 88(4), 34-40, 1992.
15. Borman, P.C., Bos, A.N., Westerterp, K.R. A Novel Reactor for Determination of Kinetics for Solid Catalysed Gas Reaction, *AIChE Journal*, 40(5), 862-868, 1994.
16. Carberry, J.J. Designing Laboratory Catalytic Reactors, *Industrial and Engineering Chemistry*, 56(11), 39-46, 1964.
17. Cardenas-Gonzalez, B., Ergas, S.J., Switzenbaum, M.S., Characterization of Compost Biofiltration Media, *Journal of the Air & Waste Management Association,* 49, 784-793, 1999.
18. Celia, M.A., Bouloutas, E.T., & Zarba, R.L. A General Mass-Conservative Numerical Solution for the Unsaturated Flow Equation, *Water Resources Research*, 26(7), 1483-1496, 1990.
19. Cherry, R.S., Thompson, D.N. Shift from Growth related to Nutrient-Limited Maintenance kinetics during Biofilter Acclimation, *Biotechnology and Bioengineering*, 56(3), 330-339, 1997.
20. Cook, L.L., Gostomski, P.A., Apel, W.A. Biofiltration of Asphalt Emissions, *Environmental Progress,* 18(3), 178 - 187, 1999.
21. Coulson, J.M & Richardson, J.F. *Chemical Engineering*, 5th edn, Vol 1, Butterworth & Heineman, UK, 1996.
22. Cox, H.H.J., Magielsen, F.J., Doddema, H.J., and Harder, W. Influence of the water content and water activity on styrene degradation by *Exophiala jeanselmei* in biofilters, *Applied Microbiology and Biotechnology*, 45, 851-856, 1996.
23. de Beer, D., Stoodley, P., Lewandowski, Z. Liquid Flow in Heterogeneous Biofilms, *Biotechnology and Bioengineering,* 44, 636-641, 1994

24. de Beer, D., Stoodley, P., Lewandowski, Z. Effects of Biofilm Structures on Oxygen Distribution and Mass Transport, *Biotechnology and Bioengineering*, 43, 1131-1138, 1994.

25. Dabney, J.B., Harman, T.L., *Mastering Simulink 2,* Prentice Hall Inc, USA, 1998.

26. Deshusses, M.A., Hamer, G & Dunn, I.J., Behaviour of Biofilters for Waste Air Biotreatment. 1. Dynamic Model Development, *Environmental Science & Technology,* 29,(4), 1048-1058, 1995.

27. Deshusses, M.A. PhD Dissertation, Swiss Federal Institute of Technology Zurich, Switzerland, 1994.

28. Deshusses, M. Biological waster air treatment in biofilters, *Current Opinion in Biotechnology*, 8,335-339, 1997.

29. Devinny, J.S., Deshusses, M.A., Webster, T.S. *Biofiltration for Air Pollution Control,* Lewis Publication, Boca Raton, 1999.

30. Devinny, J.S., Hodge, D.S. Formation of Acidic and Toxic Intermediates in Overloaded Ethanol Biofilters, Journal of the Air & Waste Management Association, 45, 125-131, 1995

31. Elmrini, H., F. Kerdouss, H. Jorio, M. Heitz. Biofiltration of Air Contaminated with Toluene, *Environmental Technology,* 22, 927-940, 2001.

32. Fan, L.S., Ramos, L., Wisecarver, K.D., Zehner, B.J. Diffusion of Phenol through a Biofilm Grown on Activated Carbon Particles in a Draft- Tube Three Phase Fluidised-Bed Bioreactor, *Biotechnology and Bioengineering,* 35, 279-286, 1990.

33. Fan, S., Scow, K.M. Biodegradation of Trichloroethylene and Toluene by Indigenous Microbial Populations in Soil, *Applied & Environmental Microbiology,* 59(6), 1911-1918, 1993.

34. Ghildyal, N.P., Gowthaman, M.K., Raghava Rao, K.S.M.S and Karanth, N.G. Interaction of transport resistance with biochemical reaction in packed-bed solid-state fermentors: Effect of temperature gradients, *Enzyme and Microbial Technology,* 16, 253-257, 1994.

35. Gostomski, P.A., Sisson, J.B., Cherry, R.S. Water Content Dynamics in Biofiltration: The Role of Humidity and Microbial Heat Generation, *Journal of the Air & Waste Management Association,* 47, 936-944, 1997.

36. Gostomski, P.A. Ench604 Lecture Notes on Biofiltration, University of Canterbury, New Zealand, 2000.

37. Gostomski, P.A., Liaw, L.P. *Proceedings of the Air & Waste Management Association's 94th Annual Meeting & Exhibition,* Paper No 94-RP115B.02, Cincinnati, OH, 1994.

38. Govind, R., Wang, Z. Biofiltration Kinetics for Volatile Organic Compounds (VOC) and Development of a Structure-Biodegradability Relationship, *Proceedings of the Air & Waste Management Association's 90th Annual Meeting & Exhibition,* Paper No 97-RA71C.07, Toronto, Ontario, 1997.

39. Govind, R., Utgikar, V., Zhao, W., Shan, Y., Parvatiyar, M. Development of Novel Biofilters for Treatment of Volatile Organic Compounds, *Proceedings of the IGT Symposium in Gas, Oil and Environmental Biotechnology,* Colorado Springs, CO, 1993.

40. Hanks, R.J., *Applied Soil Physics: Soil Water and Temperature Applications,* 2nd edn. pp 23-99, Springer -Verlag Inc, USA, 1992.

41. Haug, R.T. *The Practical Handbook of Compost Engineering*, Lewis Publishers, Boca Raton, USA, 1993.

42. Havercamp, R., Vauclin, M., Touma, J., Wierenga, P.J., & Vachaud, G. A Comparison of Numerical Simulation Models for One-Dimensional Infiltration, *Soil Science Society of America Journal*, 41, 285-293, 1977.

43. Hess, T.F., Schmidt, S.K., Colores, G.M., Maintenance Energy Model for Microbial Degrdation of Toxic Chemicals in Soil, *Soil Biology & Biochemistry,* 28(7), 907-915, 1996.

44. Hillel, D. *Fundamentals Of Soil Physics*, Academic Press, New York, USA, 1980.

45. Hodge, D.S & Devinny, J.S. Modeling removal of air contaminants by Biofiltration, *Journal Of Environmental Engineering,* 121,(1), 21-31,1995.

46. Hodge, D.S & Devinny, J.S. Biofilter Treatment of Ethanol Vapors, *Environmental Progress,* 13(3), 167-173, 1994.

47. Hodge, D.S & Devinny, J.S., Determination of Transfer Rate Constants And Partition Coefficients for Air Phase Biofilters, *Journal of Environmental Engineering*, 123(6), 577-585, 1997.

48. Hon, A.S.Y. ME Thesis, University of Canterbury, Christchurch, New Zealand, 1999.

49. Hopmans, J.W., Dane, J.H., Temperature Dependence of Soil Hydraulic Properties, *Soil Science Society of America Journal,* 50, 4-9, 1986.

50. Hyman, J.M. *Method of lines solution of partial differential equations,* National Technical Information Service, Springfield, Va, 1977.

51. Hwang, S & Tang, H. Kinetic Behaviour of the Toluene Biofiltration Process, *Journal of the Air & Waste Management Association,* 47, 664-673, 1997.

52. Kinney, K.A., Chang, D.P.Y., Schroeder., Scow, K.M. Performance of a Directionally-Switching Biofilter Treating Toluene Contaminated Air, *Proceedings of the Air & Waste Management Association's 89th Annual Meeting & Exhibition,* Paper No 96-RP87C.05, Nashville, TN, 1996.

53. Klute, A. *Methods of Soil Analysis,* Part 1, Soil Science Society of America, Inc, USA, 1986.

54. Krailas, S. PhD Thesis, University of New South Wales, Sydney, Australia, 2000.

55. Lee, B.D., Apel, W.A., Cook, L.L., and Nichols, K.M. Effect of Bed Medium Moisture on α-Pinene Removal by Biofilters, *Proceedings of the 1996 Conference on Biofiltration (an Air Pollution Control Technology),* Hodge, D.S. and Reynolds F.E., Eds, The Reynolds Group, Tustin, California, 214-223, 1996

56. Leson, G., Winer, A.M. Biofiltration: An Innovative Air Pollution Control Technology for VOC Emissions, *Journal of the Air & Waste Management Association,* 41(8), 1045- 1053, 1991.

57. Liu, H.H., Dane, J.H. Reconciliation between Measured and Theoretical Temperature Effects on Soil Water Retention Curves, *Soil Science Society of America Journal,* 57, 1202-1207, 1993.

58. Luo, J., van Oostrom, A.J. Odour-Control Biofitlers: Design, Operation and Maintenance, *Proceedings of the New Zealand Waste Water Association (NZWWA) conference,* 74-81, 1998.

59. Marshall, T.J & Holmes, J.W. *Soil Physics,* Cambridge University Press, London, England, 1979.

60. Mitchell, D.A., von Meien, O.F. Mathematical Modelling as a Tool to Investigate the Design and Operation of the Zymotis Packed-Bed Bioreactor for Solid-State Fermentation, *Biotechnology and Bioengineering,* 68(2), 127-135, 2000.

61. Mohseni, M & Allen, D.G. Biofiltration of mixtures of hydrophilic and hydrophobic volatile organic compounds, *Chemical Engineering Science*, 55, 1545-1558, 2000.
62. Morari, M., Zafiriou, E. *Robust Process Control*, Prentice Hall: New Jersey, 1989.
63. Mualem, Y. A New Model for Predicting the Hydraulic Conductivity of Unsaturated Porous Media, *Water Resources Research*, 12(3), 513-522, 1976
64. Mysliwiec, M.J., VanderGheynst, J. S., Rashid, M.M., Schroeder, E. D. Dynamic Volume-Averaged Model of Heat and Mass Transport Within a Compost Biofilter: 1. Model Development, *Biotechnology and Bioengineering*, 73(4), 282-294, 2001.
65. Mysliwiec, M.J. PhD Thesis, University of California, Davis, USA, 2000.
66. Necati Ozisik, M., *Finite difference methods in heat transfer*, CRC Press, Boca Raton, 1994.
67. Nielsen, D.R., van Genuchten, M Th., and Biggar, J.W. Water Flow and Solute Transport Processes in the Unsaturated Zone, *Water Resources Research*, 22(9), 89S-108S, 1986.
68. Ogunnaike, B.A. & Harmon Ray, W. *Process Dynamics, Modeling and Control*, Oxford University Press, New York, 1994.
69. Ottengraf, S.P.P & van Den Oever, A.H.C. Kinetic of Organic Compound Removal form Waste Gases with a Biological Filter, *Biotechnology and Bioengineering*, 25, 3089-3102, 1983.
70. Papendick, R.I., Campbell, G.S. *Water Potential Relations in Soil Microbiology*, Soil Science Society of America, 1980.
71. Perry, R.H., Chilton, C.H. *Chemical engineers' handbook*, McGraw-Hill Kogakusha, Tokyo, 1973.
72. Pinnette, J.R., Dwinal, C.A., Giggey, M.D., and Hendry, G.E., Design implications of the Biofilter Heat and Moisture Balance, *Proceedings of the 1996 Conference on Biofiltration (an Air Pollution Control Technology)*, Hodge, D.S. and Reynolds F.E., Eds, The Reynolds Group, Tustin, California, 85-95, 1995.
73. Pirt, S.J. *Principles of Microbe and Cell*, Blackwell Scientific Publications, Oxford, 1975.
74. Pirt, S.J. Maintenance Energy: a General Model for Energy-Limited and Energy-Sufficient Growth, *Archives of Microbiology*, 133, 300-302, 1982.

75. Ruthven, D.M. *Principles of adsorption and adsorption processes separation by Adsorption Processes*, Wiley Interscience publication, New York, 1984.

76. Sangsurasak, P & Mitchell, D. Validation of a Model Describing Two- Dimensional Heat Transfer During Solid - State Fermentation in Packed Bed Bioreactors, *Biotechnology and Bioengineering*, 60(6), 739-749, 1998.

77. Schmidt, S.K., Simkins, S., Alexender, M. Models for the kinetics of biodegradation of organic compounds not supporting growth, *Applied and Environmental Microbiology*, 50, 323-331, 1985.

78. Shareefdeen, Z & Baltzis, B.C. Biofiltration of methanol vapour, *Biotechnology and Bioengineering*, 41, 512-524, 1993.

79. Shareefdeen, Z & Baltzis, B.C. Biological Removal of Hydrophobic Solvent Vapors from Airstreams, *Advances in Bioprocess Engineering*, 397-404, 1994a.

80. Shareefdeen, Z & Baltzis, B.C. Biofiltration of Toluene Vapour Under Steady-State And Transient Conditions, Theory And Experimental Results, *Chemical Engineering Science*, 49, 4347-4360, 1994b.

81. Sleep, B.E & Sykes, J.F. Modeling the Transport of Volatile Organics in Variably Saturated Media, *Water Resources Research*, 25(1), 81-92, 1989.

82. Smith, J.M. *Chemical Engineering Kinetics*, McGraw- Hill, Inc, USA, 1970.

83. Song, J., Park, J., Kinney, K. Effect of Directional Switching Frequency and Slip Feed Operation on Biomass Activity in Vapour-Phase Bioreactors, *Proceedings of the Air & Waste Management Association's 93rd Annual Meeting & Exhibition,* Abstract No 677, Salt Lake City, Utah, 2000.

84. Song, J & Kinney, K. A Method for Enhanced Control of Biomass Activity and Distribution in Biofilters, *Proceedings of the Air & Waste Management Association's 92rd Annual Meeting & Exhibition,* Abstract No 99-253, St Louis, Missouri, 1999.

85. Staple, W.J. Infiltration and Redistribution of Water in Vertical Columns of Loam Soil, *Soil Science Society of America Proceedings*, 30, 553-558, 1966.

86. Stephens, D.B. *Vadose Zone Hydrology*, CRC Press Inc USA, 1996.

87. Striebig, B.A., Young, T., Keun Son, H., Doddema, H.J., and Harder, W. Comparison of Water Content fluctuations in a Unidirectional and Switched - flow Biofilter,

Proceedings of the Air & Waste Management Association's 94th Annual Meeting & Exhibition, Abstract No 183, Orlando, Florida, 2001.

88. Swanson, W.J., Loehr, R.C. Biofiltration: Fundamentals, Design and Operations Prinicples, and Applications, *Journal of Environmental Engineering,* 123(6), 538- 546, 1997.
89. Tang, H., Hwang, S and Hwang, Sz. Waste Gas Treatment in Biofilters, *Journal of the Air & Waste Management Association,* 46, 349-354, 1996.
90. Tang, H., Hwang, S, Transient Behaviour of the Biofilters for Toluene Removal, *Journal of the Air & Waste Management Association,* 47, 1142-1151, 1997.
91. TRC Databases for Chemistry and Engineering-Vapour Pressure, Version 1998-2M. k-5969, 1987.
92. van der Ham, A.G.J & Brouwers, H.J.H., Modeling and experimental investigation of transient, nonequilibrium mass transfer during steam stripping of a nonaqueous phase liquid in unsaturated porous media, *Water Resources Research,* 34(1), 47-54, 1998.
93. van Genuchten, M Th. A Closed-form Equation for Predicting the Hydraulic Conductivity of Unsaturated Soils, *Soil Science Society of America Journal,* 44, 892-898, 1980.
94. van Lith, C., Leson, G., and Michelsen, R., Evaluating Design Options for Biofilters, *Journal of the Air & Waste Management Association,* 47(1), 37-48, 1997.
95. Yang, R. T. *Gas separation by Adsorption Processes,* Imperial College Press, London, 1997.
96. Yang, Y., Allen, E.R., Biofiltration Control of Hydrogen Sulphide-1.Design and Operational Parameters, *Journal of the Air & Waste Management Association,* 44, 863-868, 1994.
97. Webster, T.S., Devinny, J.S., Torres, E.M., and Basrai, S.S. Microbial Ecosystems in Compost and Granular Activated Carbon Biofilters, *Biotechnology and Bioengineering,* 53(3), 296-302, 1997.
98. Whitaker, S. *The Method of Volume Averaging (Theories and Applications of Transport in Porous Media),* Kluwer Academic Publishers, USA, 1999.

99. Wolf, D.C., Dao, T.H., Scott, H.D., and Lavy, T.L. Influence of Sterilization Methods on Selected Soil Microbiological, Physical and Chemical Properties, *Journal of Environmental Quality*, 18, 39-43, 1989.

100. Zaidel, J. & Russo, D. Estimation of Finite Difference Interblock Conductivities for Simulation of Infiltration Into Dry Soils, *Water Resources Research*, 28(9), 2285-2295, 1992.

101. Zarook, S.M., Shaikh, A.A & Ansar, Z. Development, experimental validation and dynamic analysis of a general transient biofilter model, *Chemical Engineering Science*, 52,759-773, 1997

Appendix A: Calculation for Thermal Equilibrium

In the thermal sterilisation of solids/stagnant fluids heat transfer from the surrounding particles and time taken to reach a particular temperature within the particle is investigated. Thus this approach was used in the biofilter bed by assuming compost particles to be spherical in shape and also to be governed by the following transient heat conduction equation (Bailey & Ollis, 1986).

$$\frac{\partial T}{\partial t} = \frac{K}{\rho C_p} \frac{1}{r^2} \frac{\partial}{\partial r}\left(r^2 \frac{\partial T}{\partial r} \right)$$

In Bailey & Ollis (1986) this equation is analytically solved to obtain the temperature distribution for various elapsed non-dimensional time given by,

$$\frac{Kt}{\rho C_p R^2}$$

The application of the above expression for compost particles by Haug (1993) emphasised the fact of increasing the centre temperature to the external surface temperature, as this facilitated the remainder of particle to reach the desired temperature. For this modelling process too a non-dimensional temperature of $\frac{(T - T_o)}{(T_1 - T_o)} = 0.9$ was selected to give an internal temperature close to that of the external surface. In this case the boundary condition at the surface assumed the existence of convective heating coupled together with constant conduction within the solid. Thus from the graph provided non-dimensional time taken for the above condition was found as 0.3. Hence;

$$\frac{Kt}{\rho C_p R^2} = 0.3$$

where, K = thermal conductivity of compost, ρ = particle size density of compost, C_p = specific heat capacity of compost, R = radius of the particle.

In this case a moisture content of 50-60 % (wet basis) (Bohn *et al.*, 1999) along with the following parameters were used in the calculation.

Table 1.3 Parameter values used in equation

Parameter	Value	Source
K	3.77 cal/hr.cm.K	Haug, 1993
ρ	1.89 g/cm^3	Hon, 1999
C_p	0.562 cal/g.K	Haug, 1993

The time taken for a particle of radius R to reach external temperature was therefore given by,

$t = 0.08 R^2$

Thus considering the nominal particle sizes as stipulated in Hon (1999) the time taken ranged from 0.1-2 s. In terms of magnitude analysis the required time would be 1-2 orders of magnitude smaller than typical residence time (EBRT) experienced in biofilters. Thus it could be said that the solid compost particles attain thermal equilibrium instantaneously with respect to the surrounding gas and liquid. Hence the above would justify the assumption of local thermal equilibrium between the three phases.

Appendix B: O_2 Limitation on Batch Operation

	Run 1	Run 2	Run 3	Run 4	Run 5	Run 6	Run 7	Run 8
Toluene volume (m^3)	0.00000195	1.95E-06	1.95E-06	1.95E-06	1.95E-06	1.95E-06	1.95E-06	1.95E-06
Toluene moles	7.84136E-05	7.84E-05	7.84E-05	7.84E-05	7.84E-05	7.84E-05	7.84E-05	7.84E-05
O_2 volume (m^3)	0.001638	0.00162	0.001603	0.001585	0.001568	0.00155	0.001533	0.001515
O_2 moles	0.065867426	0.065162	0.064456	0.06375	0.063045	0.062339	0.061633	0.060927
O_2 consumed (moles)	0.000705722	0.000706	0.000706	0.000706	0.000706	0.000706	0.000706	0.000706
O_2 left (moles)	0.00162045	0.001603	0.001585	0.001568	0.00155	0.001533	0.001515	0.001498

% O_2 (v/v)	20.775	20.55	20.325	20.1	19.875	19.65	19.425	19.2

The above calculation was based on the following,

- Each batch recycle operation (run) was based on an initial gas phase concentration of 250 ppm_v.
- Complete combustion of toluene to CO_2 and H_2O.
- Ideal gas behaviour for oxygen.

Appendix C: Simulink and M-Files

- The Simulink® models used in the dissertation are included in the CD-ROM attached to the back cover.
- The M- files which contained the code to obtain the necessary variable data from a specified matrix in MATLAB workspace after having been transferred from Simulink® using the block parameter: To Workspace are as follows,

- Plotting the spatial moisture content data for a given time

```
t=tout/(24*3600); % represents the time matrix from the time domain
discretisation using ODE 15S
z=linspace(0,100,21);%specifies the spatial discretisation points along the
bed length
a=z';
i=find(t>1);% specifies the required time point in the time domain
n=i(1,1)
c=[p20,p19,p18,p17,p16,p15,p14,p13,p12,p11,p10,p9,p8,p7,p6,p5,p4,p3,p2,p1,p0]
;%matrix comprising of the moisture contents along the bed length
A=c(n,:);% selects the required moisture data for a given time
b=A'
plot(a,c(n,:));
hold on
grid on;
ylabel(' Volumetric water content(m3/m3)');
xlabel('Distance(cm)');
title('Variation of water content along bed depth')
```

- Plotting the spatial gas phase concentration data for a given time

```
t=tout/(24*3600);% represents the time matrix from the time domain
discretisation using ODE 15S
z=linspace(0,100,21); %specifies the spatial discretisation points along the
bed length
a=z'
```

```
i=find(t>1);% specifies the required time point in the time domain
n=i(1,1)
c=[y20,y19,y18,y17,y16,y15,y14,y13,y12,y11,y10,y9,y8,y7,y6,y5,y4,y3,y2,y1,y0]
;%matrix comprising of the concentration along the bed length
A=c(n,:);% selects the required concentration data for a given time
b=A'
plot(a,c(n,:));
grid on;
hold on
ylabel('Exit concentration(g/m3)');
xlabel('Distance(cm)');
title('Concentration profile of Toluene along bed length')
```

- Plotting the spatial temperature data for a given time

```
t=tout/(24*3600);% represents the time matrix from the time domain
discretisation using ODE 15S
z=linspace(0,100,21);%specifies the spatial discretisation points along the
bed length
a=z';
i=find(t>1);% specifies the required time point in the time domain
n=i(1,1)
c=[t20,t19,t18,t17,t16,t15,t14,t13,t12,t11,t10,t9,t8,t7,t6,t5,t4,t3,t2,t1,t0]
;%matrix comprising of the temperatures along the bed length
A=c(n,:);% selects the required temperature data for a given time
b=A'
plot(a,c(n,:));
ylabel('Temperature(k)');
xlabel('Distance(cm)');
title('Temperature profile along the bed')
hold on
grid on;
```

- Plotting the spatial degradation data for a given time

```
t=tout/(24*3600);% represents the time matrix from the time domain
discretisation using ODE 15S
z=linspace(0,100,21);%specifies the spatial discretisation points along the
bed length
a=z';
i=find(t>1);% specifies the required time point in the time domain
n=i(1,1)
c=[d0,d1,d2,d3,d4,d5,d6,d7,d8,d9,d10,d11,d12,d13,d14,d15,d16,d17,d18,d19,d20]
;%matrix comprising the local degradation rates along the bed length
A=c(n,:);% selects the required degradation rate data for a given time
b=A'
plot(a,c(n,:));
ylabel('Degradation(g/m3s)');
xlabel('Distance(cm)');
title('Degradation profile along compost bed')
hold on
grid on;
```

- Plotting the spatial local velocity data for a given time

```
t=tout/(24*3600); % represents the time matrix from the time domain
discretisation using ODE 15S
z=linspace(0,100,21);%specifies the spatial discretisation points along the
bed length
a=z';
i=find(t>24.9);% specifies the required time point in the time domain
n=i(1,1)
u=u0(:,2);% specifies the selection of the 2nd column of velocity matrix at
the bottom of column
u20=5.46*1e-8*ones(size(u1));% specifies the magnitude of the veocity at the
top of column under  a constant flux
c=1e8*[u,u1(:,2),u2(:,2),u3(:,2),u4(:,2),u5(:,2),u6(:,2),u7(:,2),u8(:,2),u9(:
,2),u10(:,2),u11(:,2),u12(:,2),u13(:,2),u14(:,2),u15(:,2),u16(:,2),u17(:,2),u
18(:,2),u19(:,2),u20(:,2)];
%matrix comprising of the local velocities along the bed length

A=c(n,:);% selects the required velocity data for a given time
```

```
b=A'
plot(a,c(n,:));
grid on;
hold on
ylabel(' Liquid velocity(m/s) ');
xlabel('Distance(cm)');
title('Liquid velocity profile along bed depth')
```

- Plotting the variation of bed weight with time

```
t=tout/(24*3600);% represents the time matrix from the time domain
discretisation using ODE 15S
hold on
grid on;
i=find(t>1.8);% specifies the required time point in the time domain
n=i(1,1)
plot(t,bd20(:,2));
ylabel('Bed weight(g)');
xlabel('Time(days)');
title('Feedback control for irrigation')
```

- Transferring of variable data under one flow direction as the initial values for simulation under directional switching

```
t=tout/(24*3600);% represents the time matrix from the time domain
discretisation using ODE 15S
z=linspace(0,100,21);%specifies the spatial discretisation points along the
bed length
A=z';
i=find(t>1);% specifies the required time point in the time domain
n=i(1,1)
% c,t,w,s represent the concentration,temperature,moisture and soild phase
concentration
c=[y0,y1,y2,y3,y4,y5,y6,y7,y8,y9,y10,y11,y12,y13,y14,y15,y16,y17,y18,y19,y20]
;
```

```
t=[t0,t1,t2,t3,t4,t5,t6,t7,t8,t9,t10,t11,t12,t13,t14,t15,t16,t17,t18,t19,t20]
;
w=[p0,p1,p2,p3,p4,p5,p6,p7,p8,p9,p10,p11,p12,p13,p14,p15,p16,p17,p18,p19,p20]
;
s=[q0,q1,q2,q3,q4,q5,q6,q7,q8,q9,q10,q11,q12,q13,q14,q15,q16,q17,q18,q19,q20]
;

%Selection of the relevant variables at the required time values under upIfow
or downflow.

for m=1:21
   C=c(:,m);
   l(m)=C(n,:);
   T=t(:,m);
   A(m)=T(n,:);
   a=A';
   W=w(:,m);
   B(m)=W(n,:);
   b=B;
   S =s(:,m);
   g(m)=S(n,:);
end

%Tracks the concentrations in upflow as initial values for downflow or vice-
versa
f0=l(1,1);f1=l(1,2);f2=l(1,3);f3=l(1,4);f4=l(1,5);f5=l(1,6);f6=l(1,7);f7=l(1,
8);f8=l(1,9);f9=l(1,10);f10=l(1,11);
f11=l(1,12);f12=l(1,13);f13=l(1,14);f14=l(1,15);f15=l(1,16);f16=l(1,17);f17=l
(1,18);f18=l(1,19);f19=l(1,20);

% Tracks the upflow temperature at spatial grid points as initial values for
downflow
a1=a(1,2);a2=a(1,3);a3=a(1,4);a4=a(1,5);a5=a(1,6);a6=a(1,7);a7=a(1,8);a8=a(1,
9);a9=a(1,10);a10=a(1,11);
a11=a(1,12);a12=a(1,13);a13=a(1,14);a14=a(1,15);a15=a(1,16);a16=a(1,17);a17=a
(1,18);a18=a(1,19);a19=a(1,20);
```

```
%Tracks the moisture content values for upflow as initial values for the
downflow or vice-versa
c0=b(1,1);c1=b(1,2);c2=b(1,3);c3=b(1,4);c4=b(1,5);c5=b(1,6);c6=b(1,7);c7=b(1,
8);c8=b(1,9);c9=b(1,10);c10=b(1,11);
c11=b(1,12);c12=b(1,13);c13=b(1,14);c14=b(1,15);c15=b(1,16);c16=b(1,17);c17=b
(1,18);c18=b(1,19);c19=b(1,20);c20=b(1,21);

% Tracks the solid phase concentration in upflow as initial values for
downflow or vice-versa.
h0=g(1,1);h1=g(1,2);h2=g(1,3);h3=g(1,4);h4=g(1,5);h5=g(1,6);h6=g(1,7);h7=g(1,
8);h8=g(1,9);h9=g(1,10);h10=g(1,11);
h11=g(1,12);h12=g(1,13);h13=g(1,14);h14=g(1,15);h15=g(1,16);h16=g(1,17);h17=g
(1,18);h18=g(1,19);h19=g(1,20);h20=g(1,21);
```

Appendix D: Concentration Data from the Differential Reactor

- **Increasing media moisture content (wetting curve)**

1. **Concentration profile and data at -6 cm H_2O matric potential**

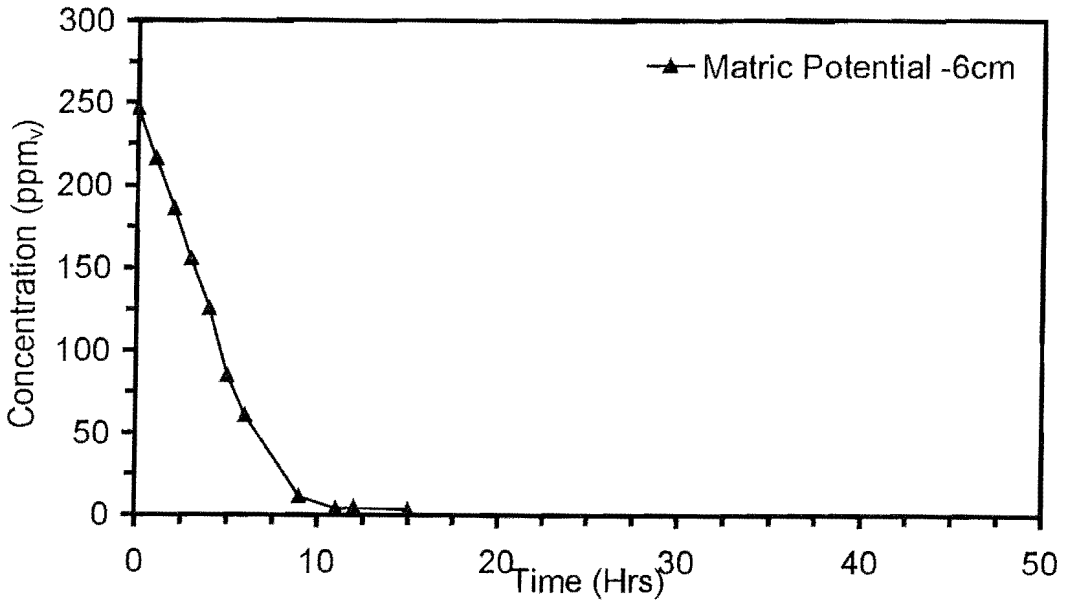

Time (Hours)	Concentration (ppm_v)
0	246.29
1	215.68
2	185.68
3	155.41
4	125.64
5	84.71
6	60.67
9	11.26
11	3.84
12	4.30
15.5	3.1

Sample Calculation for Degradation

As discussed in chapter 8, in calculating the degradation the concentration in the linear region was used. A sample calculation for the degradation at -6 cm H_2O matric potential is given below. All other degradation calculations at different matric potential values used a similar approach.

Reactor volume $= 2.15\times10^{-3}\ m^3$

Reservoir volume $= 0.009\ m^3$

Total volume $= 9.28\times10^{-3}\ m^3$

Temperature = 30 °C

Slope from the linear region of the concentration profile = 32 ppm/h

Degradation rate $= \{(101.3\times 9.28\times32\times10^{-6})/(293\times8.314)\} \times92.14$ g/h

$= 0.0011$ g/h

Weight of wet compost used = 3 g

∴Normalised degradation = 0.0011/3

= 0.000367 g/g wet compost h.

Bulk density of wet compost (60% wet wt) = 440 kg m^{-3}

∴ The Elimination capacity of the system = $0.000367 \times 440 \times 10^3$

= 161 g/m^3h.

2. Concentration profile and data at -16 cm H_2O matric potential

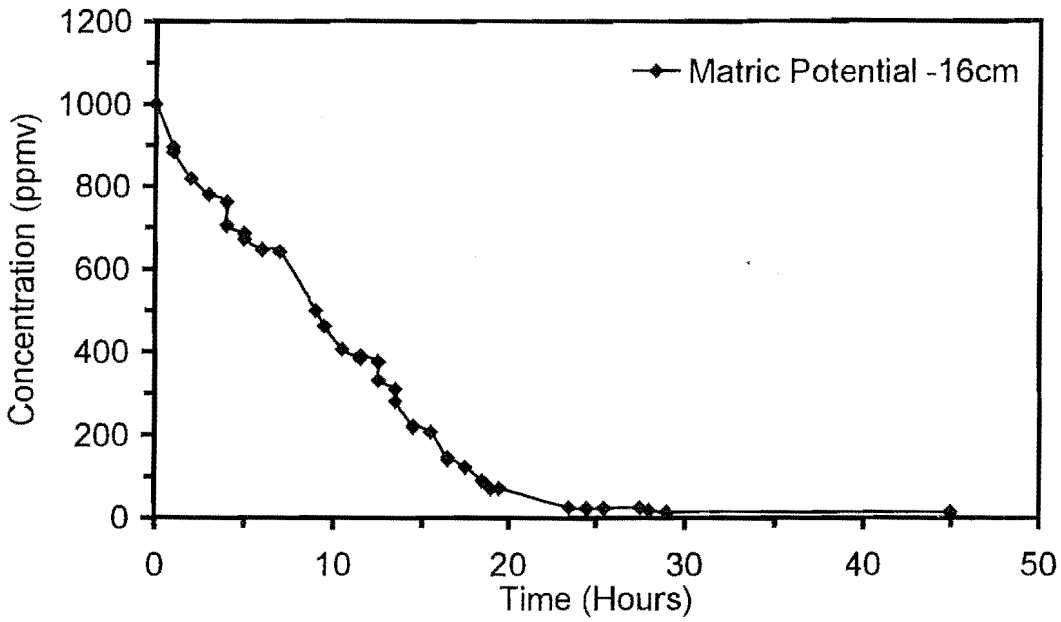

Time (Hours)	Concentration (ppm_v)
0	1000
1	894.28
1	882.36
2	818.3
3	778.06
3	779.93
4	760.51
4	704.55
5	685.50
5	670.61
6	646.5
7	640.45
9	498.27
9.5	461.36
10.5	404.95
11.5	382.75
11.5	388.82
12.5	375.52
12.5	330.20
13.5	308.55
13.5	280.10
14.5	217.66
14.5	221.36
15.5	205.72
16.5	138.84
16.5	144.74
17.5	121.32
18.5	88.245
19	68.28
19.5	70.25
23.5	23.86
24.5	21.24
25.5	23.04
27.5	23.98
28	18.15
29	13.15
45	12.55

3. Concentration profile and data at -26 cm H_2O matric potential

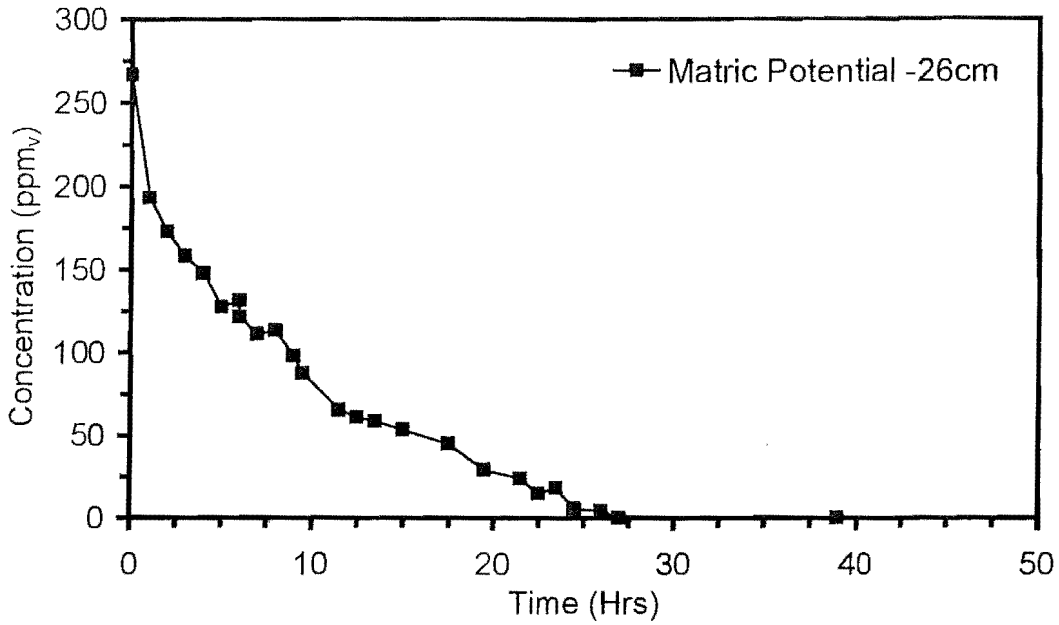

Time (Hours)	Concentration (ppm_v)
0	266.76
1	192.97
2	172.55
3	157.68
4	147.28
5	127.35
6	131.21
6	121.14
7	111.00
8	113.04
9	97.63
9.5	87.30
11.5	65.19
12.5	60.99
13.5	58.44
15	53.17
17.5	44.83
19.5	29.02
21.5	23.96
22.5	14.80
23.5	18.26
24.5	5.72
26	4.35
27	0
39	0

4. Concentration profile and data at -36 cm H_2O matric potential

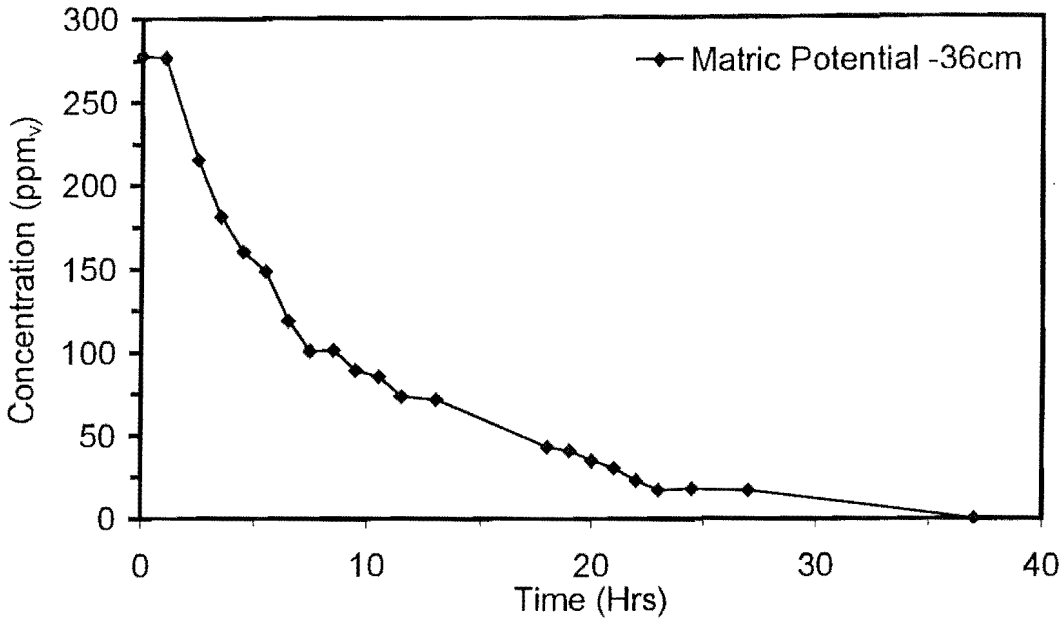

Time (Hours)	Concentration (ppm$_v$)
0	277.64
1	276.41
2.5	215.20
3.5	181.31
4.5	160.48
5.5	148.38
6.5	118.81
7.5	100.65
8.5	101.27
9.5	89.19
10.5	85.34
11.5	73.42
13	71.59

18	42.81
19	40.75
20	34.78
21	30.58
22	22.81
23	17.1
24.5	17.75
27	17.1
37	0

- **Decreasing media moisture content (drying curve)**

In ascertaining the degradation rates for decreasing moisture content only the linear regions of the concentration profiles were monitored and recorded, as this section was explicitly uses used for computational purposes. Also as stated in chapter 8 the non-linear region in this batch experiment took extended periods of time to evolve and caused practical difficulties in monitoring in terms of the time and technical constraints.

5. Concentration profile and data at -26 cm H_2O matric potential

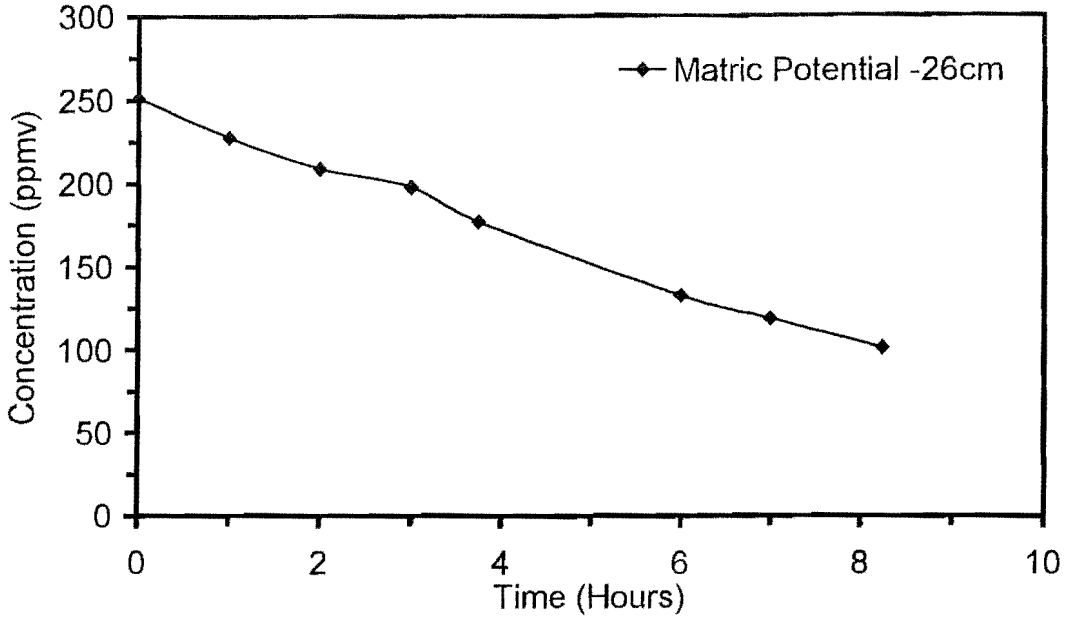

Time (Hours)	Concentration (ppm_v)
0	251
1	227
2	209
3	197
3.75	177
6	132
7	119
8.25	101

6. Concentration profile and data at -36 cm H_2O matric potential

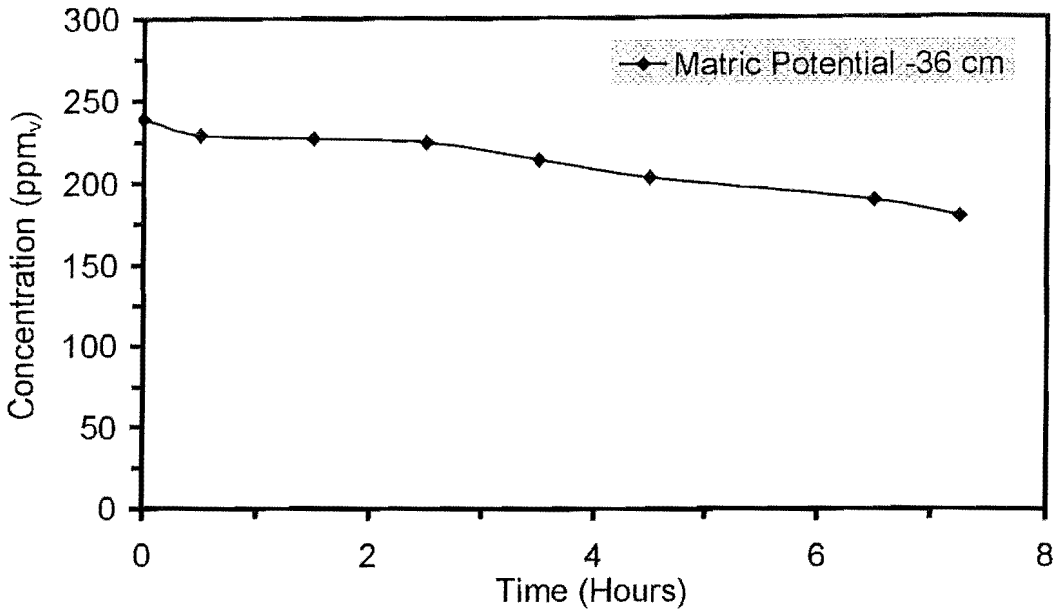

Time (Hours)	Concentration (ppm$_v$)
0	238.83
0.5	229.28
1.5	226.88
2.5	224.44
3.5	213.99
4.5	202.84
6.5	189.19
7.25	179.32

- **Repeatability Runs**

As stated in chapter 8 repeatability runs were performed for matric potential values of -26 & -36 cm H_2O along the wetting direction. In this case too only the linear region of the concentration profile was obtained, as focus was concentrated on this particular region.

7. Concentration profile and data at -26 cm H_2O matric potential

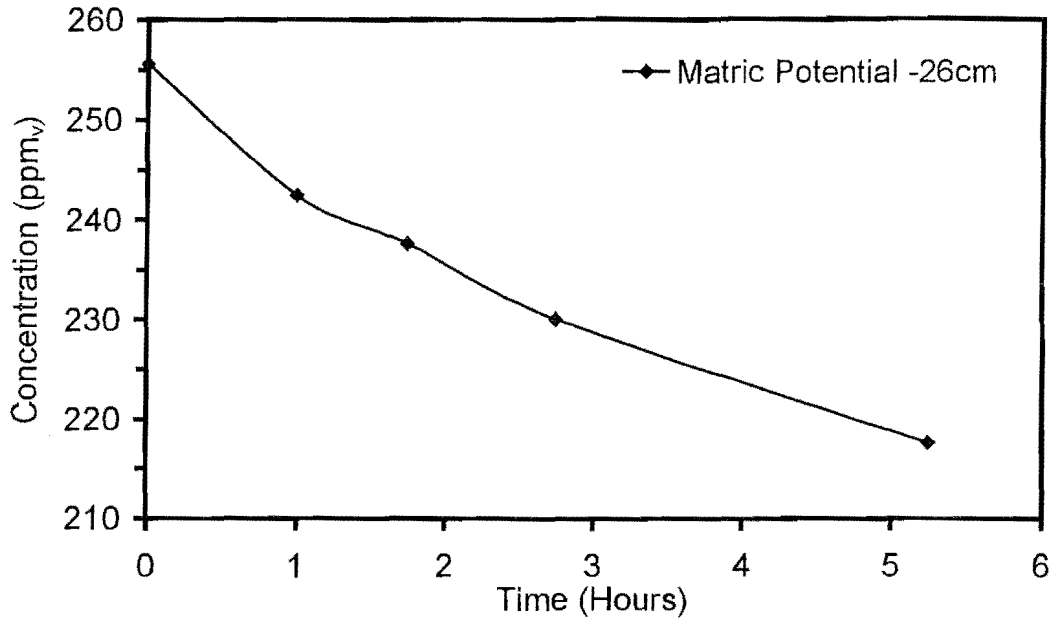

Time (Hours)	Concentration (ppm$_v$)
0.00	256
1.00	242
1.75	238
2.75	230
5.25	218

8. Concentration profile and data at -16 cm H_2O matric potential

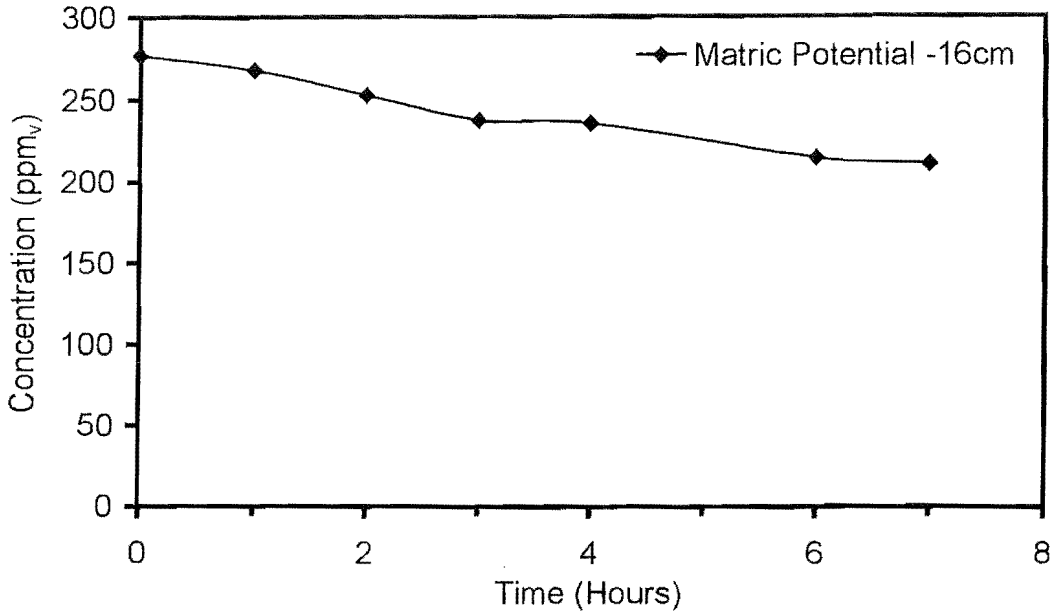

Time (Hours)	Concentration (ppm$_v$)
0	276.85
1	267.74
2	252.54
3	237.28
4	235.39
6	214.17
7	210.56